

**CHARACTERIZATION OF MEMBERS OF TYPE IV  
AND TYPE IIC OF HUMAN P-TYPE ATPASE**

by

Angela Yen-Chun Liou

B.Sc., The University of British Columbia, 2011

A THESIS SUBMITTED IN PARTIAL FULFILLMENT OF  
THE REQUIREMENTS FOR THE DEGREE OF

MASTER OF SCIENCE

in

The Faculty of Graduate and Postdoctoral Studies  
(Biochemistry and Molecular Biology)

THE UNIVERSITY OF BRITISH COLUMBIA  
(Vancouver)

July 2017

© Angela Yen-Chun Liou, 2017

## Abstract

P-type ATPases comprise a superfamily of proteins that play vital roles in the human body and can cause severe diseases if their functions are impaired. P<sub>4</sub>-ATPases or type 4 of P-type ATPases are implicated in the ATP-dependent flipping of phospholipids across cell membranes. This generates and maintains transverse phospholipid asymmetry, a property important for biological processes including vesicle trafficking. ATP9A is a P<sub>4</sub>-ATPase that remains poorly characterized despite its high expression in brain and testis. Interestingly, loss of Neo1p, the yeast ortholog of ATP9A, is lethal. The first part of this study investigates the functional properties and cellular localization of ATP9A. Human ATP9A was expressed in HEK293T cells and characterized using biochemical and cell-based approaches. ATP9A exhibited little if any phospholipid-dependent ATPase activity, but underwent hydroxylamine-sensitive phosphorylation, a characteristic feature of the P-type ATPase reaction cycle. A monoclonal antibody to ATP9A was generated for analysis of ATP9A in cells and brain tissues by western blotting and immunofluorescence microscopy. In transfected HEK293T cells ATP9A localized to perinuclear and peripheral punctate structures possibly related to the endocytic pathway. Our findings suggest that ATP9A undergoes autophosphorylation, but fails to dephosphorylate, possibly due to lack of an accessory protein or a specific substrate. Further studies on endogenous ATP9A should provide further insight into its physiological function and possible role in human disease.

On the other hand, Na<sup>+</sup>/K<sup>+</sup>-ATPase (NKA) belongs to type 2C of P-type ATPases and establishes Na<sup>+</sup> and K<sup>+</sup> gradients across cell membranes. NKA has been shown to interact with retinoschisin (RS1), an adhesion protein essential for normal retinal structure and function.

Mutations in the gene encoding RS1 cause a macular degeneration disorder called X-linked retinoschisis (XLRS). RS1 is thought to be anchored to the membranes of photoreceptor and bipolar cells through interaction with the  $\alpha 3$  and  $\beta 2$  isoforms of NKA. The second part aims to characterize the RS1-NKA complex by generating monoclonal antibodies specific for the components. Indeed, immunoaffinity purification of NKA $\beta 2$  from bovine retinal membranes co-immunoprecipitated the  $\alpha 3$  subunit and RS1. Tandem affinity purification of the native protein complexes should enhance understanding of the molecular and cellular mechanisms underlying XLRS.

## Lay Summary

$P_4$ -ATPases are proteins that transport phospholipids from the outer to the inner layer of cell membranes to generate a strikingly imbalanced, asymmetric lipid distribution in membranes. In humans, defective  $P_4$ -ATPases have been linked to Alzheimer's disease, spread of colorectal cancer, and liver disorders. ATP9A is a human  $P_4$ -ATPase that has remained mysterious. Intriguingly, loss of its yeast counterpart called Neo1p is lethal. This thesis aims to help us understand the role of ATP9A in mammalian cells and disease. The second part focuses on  $Na^+/K^+$ -ATPase (NKA), a protein that moves  $Na^+$  and  $K^+$  ions across most cell membranes. The interaction between NKA and another protein called retinoschisin (RS1) is thought to be important for maintaining healthy retina function. This thesis also studies such interactions in order to understand how non-functional RS1 leads to a macular degeneration disorder called X-linked retinoschisis.

## Preface

The experiments conducted in this thesis were designed through collaborative discussions between myself and my supervisor, Dr. Robert Molday. Design of oligonucleotides and preparation of materials used in the experiments were carried out by myself except for those described below. Common laboratory reagents, such as DH5 $\alpha$  competent cells and Coomassie blue stain, were collaboratively prepared by members of the Molday Lab. CDC50A and ATP8A2 with a C-terminal 1D4 tag were cloned into pcDNA3 vector by Dr. Jonathan Coleman. 1D4-tagged human ATP9B was constructed by Ms. Karen Chang. Rho 1D4 and CDC50A-7F4 monoclonal antibodies were prepared by Ms. Theresa Hii. Generation of ATP9A-10D1 monoclonal antibody was a collaborative effort between myself and Ms. Theresa Hii.

The second part of this study presented in Chapter 3 was a continuation of the collaborative work performed by Ms. Laurie Molday, Mr. Winco Wu, and Dr. Martin Bush as described in their publications. Constructs containing 1D4-tagged cDNA of rat Na<sup>+</sup>/K<sup>+</sup>-ATPase  $\alpha$ 3 and bovine Na<sup>+</sup>/K<sup>+</sup>-ATPase  $\beta$ 2 were cloned by Ms. Laurie Molday. The rod outer segment (ROS) membranes were prepared previously by past members of the Molday Lab. The western blots of ROS and retinal membranes used in screening for monoclonal antibodies against Na<sup>+</sup>/K<sup>+</sup>-ATPase  $\beta$ 2 were prepared collaboratively by myself and Ms. Theresa Hii.

I performed all the other experimental work, analyzed the data for presentation, and wrote this thesis. The first draft of this thesis was revised by Dr. Robert Molday. The animal work described in Chapter 2 and 3 was covered by the UBC Animal Care Committee certificate number A15-0173, and I have completed the Canadian Council on Animal Care/National Institutional Animal User Training Program with certificate number 7943-16.

## Table of Contents

<b>Abstract</b> .....	<b>ii</b>
<b>Lay Summary</b> .....	<b>iv</b>
<b>Preface</b> .....	<b>v</b>
<b>Table of Contents</b> .....	<b>vi</b>
<b>List of Tables</b> .....	<b>ix</b>
<b>List of Figures</b> .....	<b>x</b>
<b>List of Abbreviations</b> .....	<b>xi</b>
<b>Acknowledgements</b> .....	<b>xiv</b>
<b>Chapter 1: Introduction</b> .....	<b>1</b>
1.1 Membrane Asymmetry.....	1
1.2 P-type ATPases.....	4
1.3 P <sub>4</sub> -ATPases.....	6
1.3.1 CDC50—Accessory Subunit.....	11
1.3.2 Class 1a.....	12
1.3.3 Class 1b.....	13
1.3.4 Class 2.....	14
1.3.5 Class 5.....	15
1.3.6 Class 6.....	16
1.4 Distribution in Cells.....	16
1.5 Roles in Cell Physiology.....	17
1.6 Roles in Diseases.....	19
1.7 Na <sup>+</sup> /K <sup>+</sup> -ATPase.....	21
1.8 Thesis Investigation.....	23
<b>Chapter 2: Characterization of ATP9A, a member of the P<sub>4</sub>-ATPase family</b> .....	<b>24</b>
2.1 Introduction.....	24
2.2 Materials and Methods.....	24
2.2.1 Materials.....	24
2.2.2 DNA constructs.....	26

2.2.3 Cell culture and transfection .....	26
2.2.4 Immunofluorescence imaging.....	27
2.2.5 Immunoaffinity purification from HEK293T cells.....	27
2.2.6 ATPase activity assay.....	28
2.2.7 Luminescent ATPase activity assay .....	29
2.2.8 Phosphorylation assay.....	29
2.2.9 Cell surface labeling assay .....	30
2.2.10 In-cell based assay.....	31
2.2.11 Generation of monoclonal antibodies against ATP9A.....	32
2.2.12 Expression and purification of GST fusion proteins from <i>E. coli</i> .....	32
2.2.13 Gene expression by RT-PCR.....	33
2.2.14 Isolation of HEK293T membranes .....	33
2.2.15 Isolation of mouse cortical membranes .....	34
2.2.16 Immunoprecipitation from mouse cortex membranes .....	35
2.2.17 SDS-PAGE and western blots .....	35
2.2.18 Statistical Analysis.....	36
2.3 Results.....	36
2.3.1 Expression and subcellular localization of human ATP9A wildtype and mutants.....	36
2.3.2 Immunoaffinity purification of ATP9A.....	38
2.3.3 ATPase activity.....	41
2.3.4 Phosphorylation assay.....	43
2.3.5 Biotinylation and cell-based flippase assay.....	44
2.3.6 Characterization of the in-house monoclonal antibody ATP9A-10D1.....	48
2.3.7 ATP9A tissue expression.....	51
2.3.8 Comparison of ATP9A-10D1 and the commercial antibody 3G2 .....	53
2.4 Discussion .....	55
<b>Chapter 3: Characterization of Na<sup>+</sup>/K<sup>+</sup>-ATPase (NKA) interactions with retinoschisin (RS1) in retina .....</b>	<b>61</b>

3.1 Introduction .....	61
3.2 Materials and Methods.....	64
3.2.1 Materials .....	64
3.2.2 DNA constructs .....	64
3.2.3 Immunoprecipitation of 1D4-tagged NKA $\beta$ 2 expressed in HEK293T .....	65
3.2.4 Generation of monoclonal antibodies against NKA $\beta$ 2 .....	65
3.2.5 Expression and purification of GST fusion proteins from <i>E. coli</i> .....	66
3.2.6 Isolation of bovine retinal membranes .....	66
3.2.7 Immunoprecipitation of NKA $\beta$ 2 from bovine retinal membranes.....	67
3.2.8 SDS-PAGE and western blot.....	67
3.3 Results.....	68
3.3.1 Expression of NKA $\beta$ 2 in HEK293T and in bovine retina .....	68
3.3.2 Purification of GST-NKA $\beta$ 2 <sub>1-28</sub> peptide from <i>E. coli</i> .....	70
3.3.3 Characterization of the in-house monoclonal antibody NKA $\beta$ 2-9G9 .....	71
3.3.4 Co-immunoprecipitation of the RS1-NKA complex from bovine retina .....	73
3.4 Discussion.....	75
<b>Chapter 4: Conclusion and future directions.....</b>	<b>78</b>
<b>References.....</b>	<b>81</b>

## List of Tables

Table 1.1 Summary of the human P4-ATPases.....	8
--	---

## List of Figures

Figure 1.1 Lipid asymmetry in biological membranes. ....	3
Figure 1.2 P-type ATPase superfamily and human P4-ATPase family .....	5
Figure 1.3 Domain structure, topology, and proposed mechanism of P4-ATPases.....	10
Figure 2.1 Expression and subcellular distribution of ATP9A expressed in HEK293T cells. ....	39
Figure 2.2 Purification of ATP8A2 and ATP9A from transfected HEK293T cells.....	40
Figure 2.3 ATP9A shows minimal lipid-activated ATPase activity.....	42
Figure 2.4 ATP9A binds to ATP and forms an aspartyl-phosphoenzyme, which is sensitive to hydroxylamine.....	43
(Cont.) Figure 2.5 ATP8A2 shows typical flippase activity towards PS, while ATP9A is not activated by PS, PE or PC, despite both P <sub>4</sub> -ATPases get trafficked to the cell surface.....	47
Figure 2.6 Characterization of ATP9A-10D1 monoclonal antibody.....	50
Figure 2.7 Expression and immunoprecipitation of Atp9a in mouse tissues. ....	52
Figure 2.8 Comparison of ATP9A-10D1 and the commercial antibody 3G2.....	54
Figure 3.1 3-D reconstruction of RS1 and schematic representation of the RS1-NKA-SARM1 complex. ....	63
Figure 3.2 Expression of NKAβ2 in transfected HEK293T cells and bovine retina.....	69
Figure 3.3 Purification of GST-NKAβ2 <sub>1-28</sub> from <i>E. coli</i> .....	70
Figure 3.4 Characterization of the in-house NKAβ2-9G9 antibody.....	72
Figure 3.5 Co-immunoprecipitation of RS1-NKA from bovine retina.....	74

## List of Abbreviations

ABC	ATP-binding cassette
ADP	Adenosine diphosphate
ATP	Adenosine-5'-triphosphate
bp	Base pair
BRIC	Benign recurrent intrahepatic cholestasis
BSA	Bovine serum albumin
NBD-PC	1-oleoyl-2-{6-[7-nitro-2- <i>l</i> ,3-benzoxadiazol-4-yl)amino]hexanoyl}- <i>sn</i> -glycero-3-phosphocholine
NBD-PE	1-oleoyl-2-{6-[7-nitro-2- <i>l</i> ,3-benzoxadiazol-4-yl)amino]hexanoyl}- <i>sn</i> -glycero-3-phosphoethanolamine
NBD-PS	1-oleoyl-2-{6-[7-nitro-2- <i>l</i> ,3-benzoxadiazol-4-yl)amino]hexanoyl}- <i>sn</i> -glycero-3-phosphoserine
cDNA	Complementary deoxyribonucleic acid
CHAPS	3-[(3-cholamidopropyl)dimethylammonio]-1-propanesulfonic acid
Chol	Cholesterol
DAPI	4',6-diamidino-2-phenylindole
DMEM	Dulbecco's modified Eagle's medium
DOPC	1,2-dioleoyl- <i>sn</i> -glycero-3-phosphatidylcholine
DOPE	1,2-dioleoyl- <i>sn</i> -glycero-3-phosphatidylethanolamine
DOPS	1,2-dioleoyl- <i>sn</i> -glycero-3-phosphatidylserine
DTT	Dithiothreitol
EDTA	Ethylenediaminetetraacetic acid
EM	Electron microscopy
ER	Endoplasmic reticulum
FACS	Fluorescence-activated cell sorting

GAPDH	Glyceraldehyde 3-phosphate dehydrogenase
GST	Glutathione S-transferase
HEK	Human embryonic kidney
HEPES	4-(2-hydroxyethyl)-1-piperazineethanesulfonic acid
IF	Immunofluorescence
IPTG	Isopropyl $\beta$ -D-1-thiogalactopyranoside
kDa	Kilodalton
mAb	Monoclonal antibody
MS	Mass spectrometry
NBD	7-nitrobenz-2-oxa-1,3-diazol-4-yl
NKA	$\text{Na}^+/\text{K}^+$ -ATPase
OGP	<i>n</i> -octyl- $\beta$ -d-glucopyranoside
PA	Phosphatidic acid
pAB	Polyclonal antibody
PAGE	Polyacrylamide gel electrophoresis
PBS	Phosphate buffered saline
PC	Phosphatidylcholine
PCR	Polymerase chain reaction
PE	Phosphatidylethanolamine
PFIC	Progressive familial intrahepatic cholestasis
PI	Phosphatidylinositol
PM	Plasma membrane
PS	Phosphatidylserine
PVDF	Polyvinylidene fluoride
ROS	Rod outer segment
RS1	Retinoschisin

RT-PCR	Reverse transcription-polymerase chain reaction
SARM1	Sterile alpha and TIR motif-containing protein 1
SDS	Sodium dodecyl sulfate
SFM	Serum free media
SM	Sphingomyelin
SPM	Standard phosphorylation medium
<i>wl/wl</i>	Homozygous <i>Wabblers-lethal (wl)</i> mutant mouse strain
XLRS	X-linked retinoschisis

## **Acknowledgements**

I would like to express my sincere gratitude to my supervisor, Dr. Robert Molday, for the opportunity to work in his laboratory and to take on this thesis project. Dr. Molday has consistently provided insightful feedback on my progress with his expertise in membrane biochemistry and encouraged me to explore all possibilities throughout my studies and establish my own research territory with his guidance. I would also like to thank my committee members, Dr. Masayuki Numata and Dr. Elizabeth Conibear, for their inspiring discussion and valuable input during the meetings.

I greatly appreciate all the past and present members of the Molday Lab who have made my experience and journey as a graduate student so much more enjoyable and fulfilling. Thank you especially to Ms. Laurie Molday, Ms. Theresa Hii, Ms. Karen Chang, Dr. Madhavan Chalat and Mr. Fabian Garces, for teaching and mentoring me on laboratory techniques and skills and for engaging me in intriguing scientific conversations.

I would also like to express my deepest gratitude to my dearest family for their unconditional love and support. To my parents, Gregory and Alice Liou, thank you for always having faith in me and instilling the values of hard-work and self-disciplines which have been the driving force behind my degree completion. To my brother, Anthony Liou, thank you for always being there for me through thick and thin and for your words of optimism and wisdom.

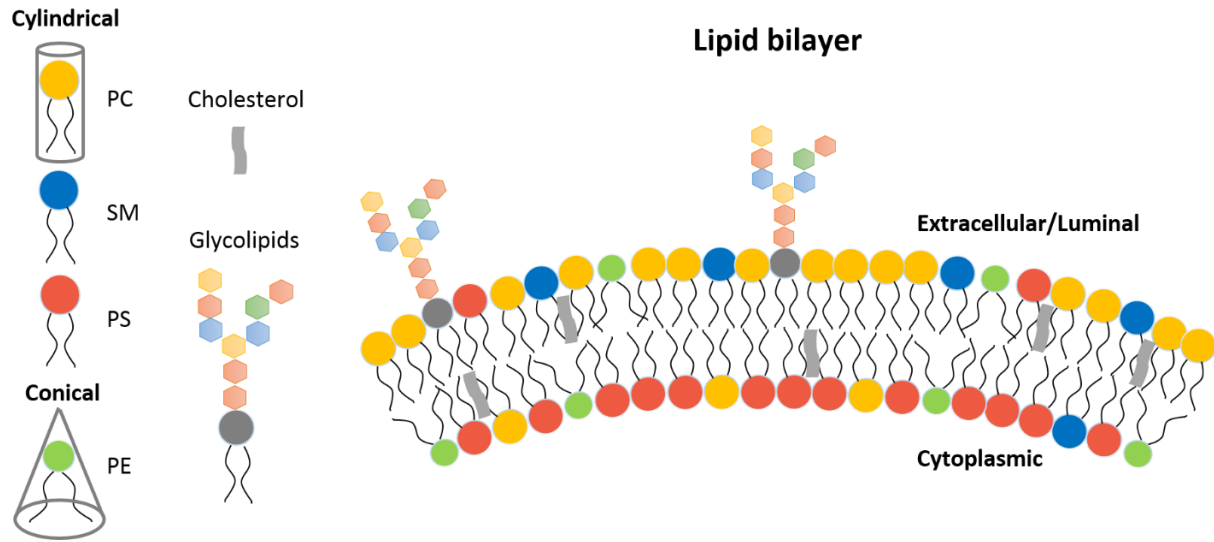
## **Chapter 1: Introduction**

### **1.1 Membrane Asymmetry**

Biological membranes are organized into lipid bilayers that are mainly comprised of amphiphilic phospholipids. The hydrophobic barriers prevent ions and soluble proteins from freely diffusing across the membranes and reaching incorrect destinations. Translocation of phospholipids between the two leaflets of lipid bilayer generates a strikingly imbalanced, asymmetric lipid composition (Andersen et al., 2016). In the plasma membrane, phosphatidylserine (PS) and phosphatidylethanolamine (PE) are enriched in the cytoplasmic leaflet, whereas phosphatidylcholine (PC), sphingomyelin (SM) and glycolipids are predominantly localized to the extracellular or luminal leaflet (Figure 1.1) (Bretscher, 1972; Devaux, 1991; Gordesky & Marinetti, 1973). Membranes of other subcellular compartments including the trans-Golgi network (TGN), endosomes and vesicles also share a similar asymmetry in lipid distribution. Lipid molecules have intrinsic shapes depending on the size of their head groups and their fatty acyl chain composition, such as the length and saturation (van Meer & de Kroon, 2011). For examples, phosphatidylcholine and phosphatidylserine are cylindrical, and phosphatidylethanolamine is conical. As it is the most entropically favourable when their hydrophobic acyl chains are sequestered away from water and their large polar heads in contact with water molecules, phospholipids assemble into a bilayer that adopts the spontaneous curvature of the local lipids. Therefore, membrane asymmetry is crucial for determining and maintaining cellular and organellar shape and has been implicated in various important biological processes, such as vesicle trafficking, phagocytosis, apoptosis, membrane protein

regulation, cellular signalling and lipid homeostasis (Coleman et al., 2013; Lopez-Marques et al., 2014).

Unlike cholesterol and other major lipids of the plasma membrane that can move freely between the two leaflets, phospholipids have a very slow intrinsic rate of transverse diffusion, taking time from hours to weeks (Sharom, 2011). Translocation of their hydrophilic head groups through the hydrophobic interior of native membranes is very energetically unfavorable and thus mechanisms must exist to achieve this movement efficiently. Three major classes of proteins have been identified to transport phospholipids across cellular membranes: P<sub>4</sub>-ATPases, ABC transporters, and scramblases (Coleman et al., 2013; Andersen et al., 2016). P<sub>4</sub>-ATPases are a family of the P-type ATPases that act as ATP-dependent biological pumps to move ions and lipids across biological membranes. They are found only in eukaryotes and have been recently identified as flippases which transport or “flip” phospholipids inward from the exoplasmic to the cytoplasmic leaflet. ATP binding cassette or ABC transporters also utilize energy from ATP hydrolysis to transport a wide variety of substrates across membranes. Many are known to export or “flop” phospholipids from the cytoplasmic to the exoplasmic leaflet, except for ABCA4 which is the only eukaryotic ABC transporter that acts as flippase. Scramblases don't require metabolic energy to facilitate the spontaneous, bi-directional transport of various phospholipids and other membrane lipids. They disrupt the asymmetry generated by P<sub>4</sub>-ATPases and ABC transporters and have been implicated in maintaining membrane integrity of the endoplasmic reticulum (ER) and facilitating blood coagulation and the removal of apoptotic cells in the plasma membrane (Williamson, 2015).

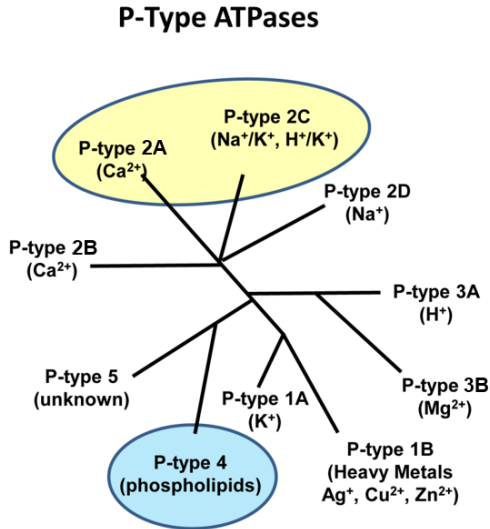
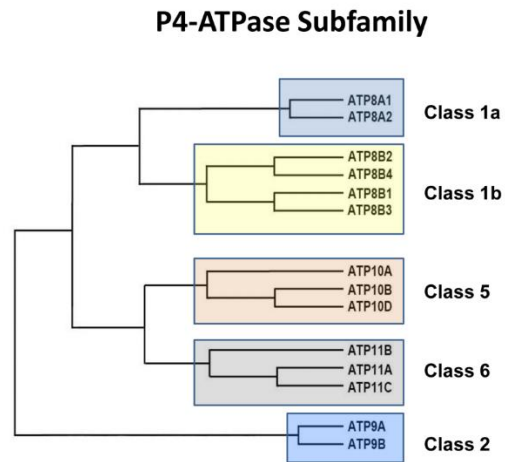


**Figure 1.1 Lipid asymmetry in biological membranes.**

Membranes are made up of a lipid bilayer mainly comprised of amphiphilic phospholipids. The lipid composition between the two leaflets is asymmetric: the cytoplasmic side is concentrated with phosphatidylserine and phosphatidylethanolamine, whereas the extracellular or luminal side is enriched in phosphatidylcholine, sphingomyelin and glycolipids. This lipid asymmetry enables the membrane bilayer to adopt the spontaneous curvature of the local lipids.

## 1.2 P-type ATPases

P-type ATPases comprise a superfamily of integral membrane transporters found in all kingdoms of life (Bublitz et al., 2011). They are distinguished from other types of transporter ATPases by the formation of a phosphorylated intermediate at an invariant aspartic acid residue during the catalytic cycle. Based on sequence similarity and substrate specificity, P-type ATPases are organized into five classes (type 1, 2, 3, 4, 5) with further subfamilies (Figure 1.2A) (Kühlbrandt, 2004). Type 1-ATPases are presumably the most ancient and simplest bacterial ion pumps; type 1A transport  $K^+$  and type 1B transport heavy metal ions such as  $Cu^+$ ,  $Ag^+$ ,  $Zn^{2+}$ ,  $Cd^{2+}$  or  $Pb^{2+}$ . Type 2 and 3 are the best characterized P-type ATPases and they establish crucial electrochemical gradients across cellular membranes. Type 2A consists of the sarcoendoplasmic reticulum  $Ca^{2+}$  ATPases (SERCA) and the secretory pathway  $Ca^{2+}$  ATPases, type 2B contains the plasma-membrane  $Ca^{2+}$  ATPases, and type 2C includes the  $Na^+/K^+$  ATPases (NKA) and the gastric  $H^+/K^+$  ATPase. Type 3A are  $H^+$  pumps that maintain an intracellular pH of 6.6 against an extracellular pH of 3.5 and type 3B are bacterial  $Mg^{2+}$  pumps. Distinct from the other members, type 4 only exists in eukaryotes and have been shown to transport phospholipids. The substrate specificity of type 5 is still unknown, but they have been predicted to be involved in the endosomal-lysosomal system (Andersen et al., 2016).

**A****B**

**Figure 1.2 P-type ATPase superfamily and human P4-ATPase family**

(A) P-type ATPases are grouped into five families based on their sequences and substrate specificity. Type 2B and 2C contain the most famous and extensively studied sarcoendoplasmic reticulum Ca<sup>2+</sup>-ATPase and Na<sup>+</sup>/K<sup>+</sup>-ATPase. Type 4-ATPases only exist in eukaryotes and have been recently identified to transport phospholipids across membranes. (B) In humans, there are 14 P<sub>4</sub>-ATPases divided into five classes according to their sequence similarity.

### 1.3 P<sub>4</sub>-ATPases

In yeast (*Saccharomyces cerevisiae*), there are five Type 4-ATPases, or P<sub>4</sub>-ATPases (Drs2p, Neo1p, Dnf1p, Dnf2p, Dnf3p). In contrast, the human genome contains 14 P<sub>4</sub>-ATPases that are classified into five subfamilies based on sequence similarity (Figure 1.2B) (Table 1.1): Class 1a (ATP8A1, ATP8A2); Class 1b (ATP8B1, ATP8B2, ATP8B3, ATP8B4); Class 2 (ATP9A, ATP9B); Class 5 (ATP10A, ATP10B, ATP10D); and Class 6 (ATP11A, ATP11B, ATP11C) (Table 1.1) (Paulusma & Elferink, 2010; van der Mark et al., 2013).

#### Structural and Functional Domains

Based on amino acid sequence alignment with other P-type ATPases whose crystal structures have been extensively characterized, P<sub>4</sub>-ATPases are similarly composed of four distinct functional and structural domains: a membrane-embedded domain (M, membrane) and three cytoplasmic domains (N, nucleotide binding; P, phosphorylation; A, actuator) (Figure 1.3A) (Andersen et al., 2016). The M domain contains 10 transmembrane segments (M1-M10) that serve as the pathway through which lipid substrates are translocated. Recent studies suggest that M1–M6 form a structural unit that is highly flexible during the catalytic cycle to allow for the transport of phospholipids across membranes, whereas M7-M10 are more rigid and support the transport domain (Morth et al., 2011; Baldrige & Graham, 2012; Vestergaard et al., 2014). The N domain binds ATP and functions as a built-in kinase that phosphorylates the P domain. The P domain contains an aspartic acid (Asp, D) within the conserved DKTG motif that undergoes transient phosphorylation. The A domain contains the signature DGET motif (TGES in Ca<sup>2+</sup>-ATPase and Na<sup>+</sup>/K<sup>+</sup>-ATPase) in which the glutamic acid (Glu, E) acts as an intrinsic phosphatase that dephosphorylates the Asp residue. P<sub>4</sub>-ATPases also have regulatory domains that are

involved in modulating the transport activity and targeting these flippases to specific subcellular membranes. These domains can exist in either the N-terminus, the C-terminus, or both, and they may act as auto-inhibitors that suppress activity by interacting with the rest of the transporter molecule or as protein targeting signals (Takatsu et al., 2011a; Zhou et al., 2013).

### **Catalytic Cycle**

The proposed flippase mechanism of P<sub>4</sub>-ATPases is deduced from the well-established mechanism of the type 2 ATPases, including Ca<sup>2+</sup>- and Na<sup>+</sup>/K<sup>+</sup>-ATPase, based on the conserved functional motifs and similar domain structures. Like the P<sub>2</sub>-ATPases and other P-type ATPases, P<sub>4</sub>-ATPases are phosphorylated by ATP at the conserved aspartate in the P domain in a vanadate-sensitive manner, and they are named “P-type” due to the presence of the phosphorylated intermediate (Figure 1.3B) (Ding et al., 2000; Lenoir et al., 2009; Bryde et al., 2010; Coleman et al., 2012). Detailed examination of the catalytic cycle of ATP8A2 showed that the phosphoenzyme exists in E1P and E2P states, and the dephosphorylation of E2P is activated by the specific substrates PS and PE, but not by PC (Coleman et al., 2012). Crystal structures of the P<sub>2</sub>-ATPases have demonstrated that the conserved glutamate in the A domain rotates to move into the correct position for catalyzing the hydrolysis of the aspartyl-phosphate while the binding of the ion substrate induces some conformational changes (Palmgren & Nissen, 2011; Toyoshima, 2009). Dephosphorylation in P<sub>4</sub>-ATPases is expected to arise from similar structural changes. Correspondingly, a mutation of the conserved A-domain glutamate residue in ATP8A2 blocks the dephosphorylation normally induced by PS (Coleman et al., 2012).

**Table 1.1 Summary of the human P<sub>4</sub>-ATPases.**

The 14 members of human P<sub>4</sub>-ATPases and their known  $\beta$  subunits, substrates, tissue expression and association with disease and disorder are summarized. Modified from Anderson et al., 2016.

Class	Human P <sub>4</sub> -ATPase	$\beta$ -subunit	Substrate	Expression	Pathophysiology	References
Class 1a	ATP8A1	CDC50A	PS > PE	Ubiquitous, high in skeletal muscle, thyroid, spinal cord	Defective hippocampus-dependent learning (mice)	Levano et al., 2012; Kato et al., 2013; Lee et al., 2015
	ATP8A2	CDC50A	PS > PE	Brain, retina, testis, spinal cord	Cerebellar Ataxia, Mental Retardation and Disequilibrium Syndrome (CAMRQ) (humans)  Neurological, spinal, axonal degeneration;  Retinal degeneration; hearing loss (mice)	Coleman et al., 2009; Onat et al., 2012; Zhu et al., 2012; Vestergaard, et al., 2014; Coleman et al., 2014
Class 1b	ATP8B1	CDC50A, CDC50B	PC (PS?)	Ubiquitous, high in small intestine, pancreas	Progressive Familial Intrahepatic Cholestasis (PFIC); Benign Recurrent Intrahepatic Cholestasis (BRIC) (human)  Intrahepatic cholestasis, hearing loss (mice)	Bull et al., 1998; Eppens et al., 2001; Paulusma et al., 2006; Folmer et al., 2009b; Stapelbroek et al., 2009; Takatsu et al., 2014
	ATP8B2	CDC50A, CDC50B	PC	Ubiquitous	Unknown	Takatsu et al., 2014
	ATP8B3	Unknown	PS?	Testis	Impaired sperm-egg interactions	Wang et al., 2004; Gong et al., 2009
	ATP8B4	CDC50A, CDC50B?	Unknown	Moderate levels throughout brain	Alzheimer's disease?	Li et al., 2008; van der Velden et al., 2010
	ATP8B5			only in mice		

Class	Human P4-ATPase	$\beta$ -subunit	Substrate	Expression	Pathophysiology	References
Class 2	ATP9A	Unknown	Unknown	Ubiquitous, high in brain, pancreas	Unknown	Halleck et al., 1998; Takatsu et al., 2011b; Ansari et al., 2015
	ATP9B	Unknown	Unknown	Ubiquitous, high in testis	Unknown	Halleck et al., 1998; Takatsu et al., 2011b
Class 5	ATP10A	CDC50A	PC	High in brain, pancreas, kidney, lung	Angelman syndrome, obesity, type 2 diabetes	Dhar et al., 2004, 2006; Naito et al., 2015
	ATP10B	CDC50A	Unknown	Low expression, brain	Unknown	
	ATP10D	CDC50A	Unknown	High in placenta, low kidney, undetectable in other major organs	Obesity; hyperinsulinemia	Flamant et al., 2003; Takatsu et al., 2011b
Class 6	ATP11A	CDC50A	PS > PE	Ubiquitous, moderate levels in liver, skeletal muscle, ovary	Marker for metastasis in Colorectal cancer (human)	Miyoshi et al., 2010; Takatsu et al., 2014
	ATP11B	CDC50A	PS > PE	Ubiquitous, high in kidney, testis, ovary	Unknown	
	ATP11C	CDC50A	PS > PE	Ubiquitous, high in liver, pancreas, heart	Impaired B lymphocyte differentiation, cholestasis, hepatocarcinoma; anemia, aberrant erythrocyte shape (mice)	Siggs et al., 2011b; Takatsu et al., 2014; Yabas et al., 2014

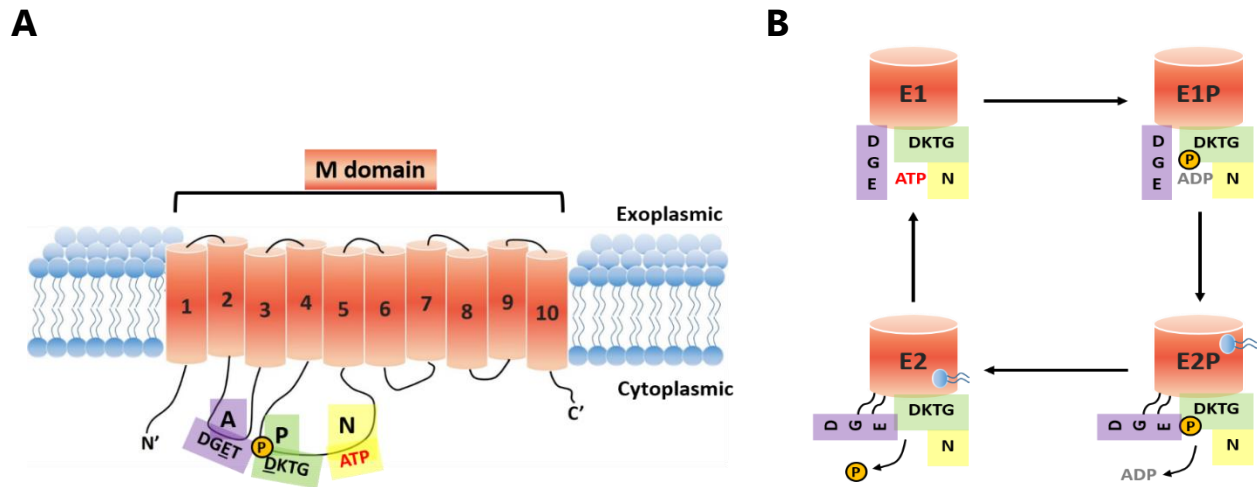


**Figure 1.3 Domain structure, topology, and proposed mechanism of P4-ATPases.**

(A) P4-ATPase is composed of four distinct domains: membrane (M), nucleotide-binding (N), phosphorylation (P), and actuator (A) domain. (B) P-type ATPases undergo four conformational states during the reaction cycle. Binding of ATP and phosphorylation of the P domain convert E1 to E1P. Upon binding of the phospholipid substrate during E1P to E2P transition, the A domain rotates and moves into a position for catalyzing dephosphorylation, which in turn drives the translocation of the lipid through the membrane to the cytoplasmic leaflet. The enzyme is converted back to E1 as the A domain returns to its starting position.

### 1.3.1 CDC50—Accessory Subunit

P<sub>4</sub>-ATPases except for ATP9A and ATP9B are known to associate with an accessory or β-subunit belonging to the CDC50/LEM3 family. There are only three CDC50 proteins (CDC50A, CDC50B, and CDC50C) in humans and three in yeast (Cdc50p, Lem3p, and Crf1p), suggesting that some P<sub>4</sub>-ATPases can bind to the same CDC50 protein to form a heteromeric complex (Andersen et al., 2016). The interaction of various P<sub>4</sub>-ATPases with specific β-subunits has been examined primarily by heterologous co-expression and co-immunoprecipitation. P<sub>4</sub>-ATPases including ATP8A1, ATP8A2, ATP10A, ATP10B, ATP10D, ATP11A, ATP11B, and ATP11C associate with CDC50A. Some, such as ATP8B1, ATP8B2 and ATP8B4, can bind to either CDC50A or CDC50B. Although CDC50/LEM3 family of proteins are evolutionarily conserved in eukaryotes, mouse Cdc50c mRNA is predominantly detected in testes while the CDC50C gene in humans is truncated and likely results in a non-functional transcript (Osada et al., 2007; Xu & Ding, 2007). CDC50C has not been found to associate with any P<sub>4</sub>-ATPases to date. In addition to employing exogenous co-expression of P<sub>4</sub>-ATPases and the β-subunits, studies on physiologically relevant cells and tissues are important to further confirm the presence and function of such native protein complexes.

CDC50 proteins are small membrane glycoproteins composed of two transmembrane helices interconnected by a large glycosylated exoplasmic domain containing three or more N-linked oligosaccharide chains, which confer stability to the protein structure, and short cytoplasmic N- and C-terminus (Coleman & Molday, 2011; García-Sánchez et al., 2014). They typically appear as a broad band at a molecular weight of approximately 50 kDa on SDS-PAGE gels due to their highly heterogeneous glycosylated chains. Both the membrane and exoplasmic

domains of CDC50 are required for forming a functionally active complex with the P<sub>4</sub>-ATPase (Coleman & Molday, 2011). Interactions between these  $\alpha$  and  $\beta$  subunits are crucial for the correct assembly and folding for the protein complexes to exit the ER. However, CDC50 proteins are not directly involved in subcellular targeting of P<sub>4</sub>-ATPases to their preferred membranes (López-Marqués et al., 2010).

Besides serving as molecular chaperones, CDC50 proteins are also suggested to actively participate in the ATP-dependent phospholipid transport in several ways. In the absence of CDC50 expression, ATP8B1 and ATP8B2 cannot undergo phosphorylation at the catalytically important Asp residue (Bryde et al., 2010). The affinity of yeast Drs2p for its  $\beta$ -subunit Cdc50p fluctuates during the catalytic cycle, with the strongest interaction observed when Drs2p is in the E2P state with a bound phospholipid substrate (Lenoir et al., 2009). Furthermore, generation of a high-affinity phospholipid binding site may require CDC50-induced conformational changes in the M domain of P<sub>4</sub>-ATPases, analogous to the role of the  $\beta$ -subunit in the Na<sup>+</sup>/K<sup>+</sup>-ATPase (Käthi Geering, 2001; Puts & Holthuis, 2009). Alternatively, CDC50 proteins may help complete the phospholipid translocation pathway by contributing two additional helices to the M domain, in which case the flipping would occur at the interface between a P<sub>4</sub>-ATPase and its CDC50  $\beta$ -subunit (Coleman et al., 2009; Puts & Holthuis, 2009; Zhou & Graham, 2009).

### **1.3.2 Class 1a**

The first evidence that indicated P<sub>4</sub>-ATPases are phospholipid transporters came from studies on the yeast Drs2p, which was shown to be involved in flipping fluorescent NBD-labeled analogs of PS across the plasma membranes (Tang et al., 1996). ATP8A1, an ortholog of Drs2p, was the first mammalian P<sub>4</sub>-ATPase cloned and it expresses in a wide variety of tissues (Mouro et

al., 1999). Studies on ATP8A1 knockout mice demonstrated that, despite apparently normal brain morphology, the hippocampal cells devoid of Atp8a1 exhibit a significant increase in PS-externalization and the mice display hyperactivity and pronounced hippocampus-dependent learning disabilities (Levano et al., 2012). ATP8A1 has been shown to bind to CDC50A and possibly also to CDC50B, which leads to varying specific ATPase activities and substrate specificities depending on availability of the appropriate  $\beta$ -subunits in the experimental materials and conditions (Bryde et al., 2010; Paterson et al., 2006; van der Velden et al., 2010). ATP8A2 shares 67% sequence similarity with ATP8A1 and is highly expressed in specific tissues including the retina, brain, and testis (Coleman et al., 2009; Cacciagli et al., 2010). In the retina, it localizes to the outer segment disc membranes of both rod and cone photoreceptor cells and co-purifies with CDC50A (Coleman & Molday, 2011). The ATPase activity of the purified complex from photoreceptors is strongly activated by PS and to a lesser extent by PE. Reconstituted ATP8A2 in liposomes showed a specific flippase activity towards PS (Coleman et al., 2009; Coleman & Molday, 2011). ATP8A2 was further shown to rescue endosomal defects in ATP8A1-depleted cells in a flippase-dependent manner, suggesting that ATP8A1 and ATP8A2 share overlapping transport activities (Lee et al., 2015).

### **1.3.3 Class 1b**

ATP8B1 was the first  $P_4$ -ATPase identified to be associated with human disease (van der Mark et al., 2013). ATP8B1 is expressed in many tissues, including the liver, pancreas, stomach, bladder, small intestine, and prostate and is localized to the apical membrane of many epithelial cells, such as the canalicular membrane of hepatocytes (van der Mark et al., 2013). Initial observations using UPS-1 cells, a Chinese hamster ovary (CHO) mutant cell line that has

impaired non-endocytic uptake of NBD-PS, showed that ATP8B1 relocalizes from the endoplasmic reticulum (ER) to the plasma membrane and exhibits a dramatic increase in the translocation of NBD-PS only upon binding with CDC50 proteins (Paulusma et al., 2008). But in a more recent study, ATP8B1 was reported to transport primarily PC, and the NBD-PC uptake mediated by ATP8B1 was abolished by co-expression of ABCB4, an ABC transporter that “flops” PC to the extracellular leaflet of the plasma membranes (Takatsu et al., 2014). The same study also suggested that ATP8B2, like ATP8B1, transports PC. ATP8B3 has been implicated as a PS flippase according to cell-based studies (Gong et al., 2009; Wang et al., 2004). ATP8B5 exists in mice but not in humans, and it has been implicated to flip PE and PC and to play a crucial role in spermatogenesis (Xu et al., 2009). However, the substrate specificity of these other ATP8B members have yet to be investigated with biochemical approaches.

#### **1.3.4 Class 2**

ATP9A and ATP9B and their yeast ortholog Neo1p are the only  $P_4$ -ATPases that do not associate with CDC50 proteins or require such interactions for exiting the ER to reach their destination membranes (Takatsu et al., 2011b). Studies using overexpression in HeLa cells revealed that ATP9A localizes to the trans-Golgi network (TGN) and early/recycling endosomes, whereas ATP9B localizes exclusively to the TGN. In addition, the N-terminal cytoplasmic regions of ATP9A and ATP9B were shown to contain subcellular localization signals using chimeric constructs generated by swapping the N-terminal segments (Takatsu et al., 2011b). ATP9A is highly expressed in the brain and pancreas, whereas ATP9B is more ubiquitously expressed. ATP9A is also expressed in human and rat pancreatic islets and is particularly concentrated in the plasma membranes from membrane fractionation studies (Ansari et al., 2015). Another study

showed that ATP9A is expressed in rat liver and enriched in the microsomal and mitochondrial membranes (Chaubey et al., 2016).

Neo1p is the only yeast  $P_4$ -ATPase that is lethal when it's genetically deleted, indicating that it is involved in some fundamental cellular processes (Prezant et al., 1996). Neo1p localizes to endosomes and Golgi, where it appears to play a role in endosomal membrane trafficking (Barbosa et al., 2010; Hua et al., 2002; Wicky et al., 2004). Recent studies suggested that Neo1p primarily establishes PE asymmetry and is also important for PS asymmetry in budding yeast (Takar et al., 2016). Furthermore, a genome-wide screen for regulators of Neo1p at endosomes proposed that the flippase activity of Neo1p may be required at the site of vesicle formation (Dalton et al., 2017). Investigations with siRNA knock-down of ATP9A in HeLa cells showed impaired recycling of transferrin, which is enriched in PS-positive endosomes (Tanaka et al., 2016). However, the function of ATP9A and ATP9B remains poorly characterized. It is not known yet whether they require an associated protein for activity and whether they transport phospholipids across membranes.

### **1.3.5 Class 5**

Members of the ATP10 subfamily are the least biochemically characterized  $P_4$ -ATPases (Coleman et al., 2013). Their C-terminal regions are generally longer with an unknown function. ATP10A is abundant in the brain, testis and lung; ATP10B has a low expression in brain; and ATP10D expression is high in placenta and low in kidney while undetected in other major tissues (Andersen et al., 2016). Exit from the ER and localization of ATP10A and ATP10D to the plasma membrane and ATP10B to late endosomes require an interaction with CDC50A (Naito et al., 2015). Exogenously expressed ATP10A in HeLa cells showed a significant increase in the specific

uptake of fluorescent NBD-PC but not other lipids (Naito et al., 2015). Cells expressing a dephosphorylation-deficient mutant of ATP10A did not show such an increase in NBD-PC internalization. The substrate specificities of ATP10B and ATP10D have not yet been determined.

### **1.3.6 Class 6**

ATP11A, ATP11B and ATP11C appear to be ubiquitously expressed in the body and only bind CDC50A as the  $\beta$ -subunit (Andersen et al., 2016; Takatsu et al., 2011b). The substrate specificity of ATP11A and ATP11C has also been reported (Takatsu et al., 2014). These P<sub>4</sub>-ATPases flip PS as their main substrate, confirming earlier results showing that ATP11C is involved in PS translocation into B-lymphocytes and other immune cells (Segawa et al., 2014; Yabas et al., 2016, 2011).

### **1.4 Distribution in Cells**

The subcellular distribution of P<sub>4</sub>-ATPases has been studied mainly by immunofluorescence microscopy and flow cytometry analysis of the transport of fluorescently labeled phospholipids in cells overexpressing the protein complexes. ATP8B1, ATP8B2, ATP8B4, ATP10A, ATP10D, ATP11A, and ATP11C primarily localize to the plasma membrane upon binding with their  $\beta$ -subunits to transport phospholipid substrates from the extracellular to the cytoplasmic leaflet (Naito et al., 2015; Takatsu et al., 2011b; van der Velden et al., 2010). ATP8A1, ATP8A2, ATP10B, and ATP11B are predominantly confined to the Golgi and recycling endosomal membranes (Coleman & Molday, 2011; Takatsu et al., 2011b; Lee et al., 2015). However, some studies showed that many of these P<sub>4</sub>-ATPases, such as ATP8A1 and ATP8A2, are also present in the plasma membrane (Segawa et al., 2016; Soupene & Kuypers, 2006). Therefore, P<sub>4</sub>-ATPases likely undergo dynamic trafficking between the Golgi/recycling endosomal system and the cell

surface, but preferentially localize to either destination membrane depending on the specific P<sub>4</sub>-ATPase.

### **1.5 Roles in Cell Physiology**

P<sub>4</sub>-ATPases play a critical role in many fundamental cellular processes associated with the plasma membrane and intracellular membranes. The main function of P<sub>4</sub>-ATPases is to generate and maintain phospholipid asymmetry between the two leaflets of membranes. P<sub>4</sub>-ATPases that act as a PS flippase, including ATP8 and ATP11 subfamilies, ensure that the extracellular leaflet of the plasma membrane is devoid of PS, since this phospholipid serves as an “eat me” signal on the apoptotic cell surface for phagocytosis (Segawa et al., 2014). Studies on ATP11C knockout mice demonstrated a critical role of ATP11C in establishing PS asymmetry during erythropoiesis, an important process for generating normal mature erythrocytes (Yabas et al., 2014). PS internalization mediated by ATP11C has also been shown to be essential for differentiation of B lymphocytes (Siggs et al., 2011a; Yabas et al., 2011). P<sub>4</sub>-ATPases specific for PS and PE also ensure that the cytoplasmic leaflet is highly enriched in these phospholipids, which interact with various membrane-bound cytoskeletal components, enzymes and adaptor proteins to allow for processes such as vesicle trafficking, cell signaling pathways, enzyme regulation and lipid metabolism (Huang et al., 2011; Lee et al., 2015; Newton & Keranen, 1994). For example, the high levels of PS and PE in the cytoplasmic leaflet of erythrocytes may be important for the association of the spectrin-ankyrin cytoskeletal network with the plasma membrane for maintaining normal cellular shape (Machnicka et al., 2014).

The function of P<sub>4</sub>-ATPases to establish phospholipid asymmetry in intracellular membranes is most fundamental to vesicle trafficking in cells. The majority of membrane lipids

are synthesized on the cytoplasmic side of the ER and redistributed symmetrically across the membranes by scramblases. Vesicles bearing the membrane lipids and proteins pinch off from the ER and fuse with the Golgi complex, where lipid asymmetry is induced by the action of flippases and floppases. Studies on the yeast Drs2p have provided the most evidence for the role of P<sub>4</sub>-ATPases in vesicle trafficking (Sebastian et al., 2012). Drs2p is localized to the trans-Golgi network (TGN) where it flips PS and PE from the luminal leaflet to the cytoplasmic leaflet to generate phospholipid asymmetry. The resulting membrane curvature and anionic phospholipid composition in the cytoplasmic leaflet recruits the Arf GTPase-activating protein Gcs1 and clathrin coat proteins for the vesicular transport between the TGN and early endosomes (Xu, Baldrige, Chi, Burd, & Graham, 2013).

Mammalian P<sub>4</sub>-ATPases have also been implicated in vesicle budding and trafficking although the mechanism remains poorly understood. Silencing the expression of ATP8A2 reduces neurite outgrowth in PC12 cells, and mutations in mouse *Atp8a2* disturb axonal transport of phosphorylated neurofilaments in the lumbar motor neurons, suggesting that this P<sub>4</sub>-ATPase plays a role in vesicle trafficking required for neurite extension (Xu et al., 2012; Zhu et al., 2012). *Atp8a2*-knockout mice also show a strikingly shorter photoreceptor outer segments, suggesting that a decrease in vesicle trafficking between the inner and outer segments results from the lack of ATP8A2 (Coleman et al., 2014). ATP8A1-mediated PS transport is important in the recruitment of the membrane fission protein EHD1 to the cytoplasmic leaflet of recycling endosomes (Lee et al., 2015). More recently, ATP9A has been shown to play a role in the recycling pathway from endosomes to the plasma membrane in HeLa cells (Tanaka et al., 2016).

However, whether ATP9A functions as a phospholipid transporter to maintain membrane asymmetry is yet to be demonstrated.

## 1.6 Roles in Diseases

To date, deficiencies in at least two P<sub>4</sub>-ATPases, ATP8B1 and ATP8A2, are directly associated with severe human disease. Mutations in *Atp8a2* were identified to cause the neurodegenerative disease and axonal degeneration in the central and peripheral nervous system in the *wobbler-lethal (wl)* mice (Zhu et al., 2012). These mutant mice display retarded growth and life span shorter than four months. Mice deficient in ATP8A2 display defects in visual and auditory function and degeneration of photoreceptor and spiral ganglion cells (Coleman et al., 2014).

A mutated ATP8A2 was detected in a patient with severe mental retardation and hypotonia, or low muscle tone (Cacciagli et al., 2010). However, screening of 37 other patients with a similar phenotype did not identify similar mutations in *ATP8A2*. Furthermore, a recessive missense mutation in *ATP8A2* (I376M) was found to cause a rare neurodegenerative disease known as cerebellar ataxia, mental retardation and disequilibrium syndrome (CAMRQ) in three members of a consanguineous family (Onat et al., 2012). This missense mutation was confirmed by biochemical characterization to result in the loss of PS flippase activity in ATP8A2. Collectively, these results indicate that functional ATP8A2 is essential in many neuronal cells and that mutations in *ATP8A2* may be a risk factor for neurodegenerative diseases.

Mutations in *ATP8B1* cause benign recurrent intrahepatic cholestasis type 1 (BRIC1) and the more severe progressive familial intrahepatic cholestasis type 1 (PFIC1) (Bull et al., 1998). Both liver disorders have an early onset and are characterized by impaired bile flow or

cholestasis. Patients affected with PFIC1 and BRIC1 patients can also develop extrahepatic disease, such as hearing loss and pneumonia (Ray et al., 2010; Stapelbroek et al., 2009). ATP8B1 localizes to the canalicular membrane of hepatocytes where it is thought to catalyze the flipping of PS to maintain membrane integrity (Folmer et al., 2009b). Loss of ATP8B1 in rat hepatocytes does not alter ABCB4 expression and localization to the canalicular membrane but results in reduced bile salt excretion, defective bile canalicular membrane structure and accumulated PS in the canalicular lumen (Cai et al., 2009). The disease-causing missense mutations have been found to affect the stability of ATP8B1 and reduce the interaction with its  $\beta$ -subunit CDC50A (Folmer et al., 2009b). In addition, the mutant proteins are not properly targeted to the canalicular membrane in WIF-B cells. The underlying mechanism of ATP8B1-linked cholestasis is still unclear, but it has been proposed that an elevated PS level in the luminal leaflet of canalicular membrane resulted from lack of ATP8B1 causes an abnormal lipid packing (Folmer et al., 2009a). This in turn renders the outer leaflet more susceptible to bile salt-mediated extraction of phospholipids and cholesterol, thereby reducing the activity of ABCB11, a principal bile salt exporter that is also associated with PFIC2 (Strautnieks et al., 1998). However, the recent findings that suggest ATP8B1 is a PC flippase point to an alternative model where the disrupted PC transport to the inner leaflet of canalicular membrane due to the loss of functional ATP8B1 could compromise the membrane stability to bile salts. Further studies are necessary to elucidate the pathogenesis of cholestasis associated with ATP8B1.

The pathophysiological functions of other  $P_4$ -ATPases are much less investigated (van der Mark et al., 2013). A significant association between the ATP8B4 locus on chromosome 15 and Alzheimer's disease has been reported (Li et al., 2008). One of the single-nucleotide

polymorphisms (SNPs) was found to localize close to the *ATP8B4* gene, suggesting that mutations in *ATP8B4* may predispose to Alzheimer's disease (Li et al., 2008). *ATP10A* and *ATP10D* have been associated with obesity and hyperinsulinemia. *ATP10A* is likely involved in the control of insulin-stimulated glucose uptake in mouse adipose tissue and a risk factor for type 2 diabetes in African American population (Dhar et al., 2006, 2004). Imprinting mutations and deletions in *ATP10A* have also been linked to Angelman syndrome, a form of autism spectrum disorder (Hogart et al., 2008; Meguro et al., 2001). *ATP11A* has been reported as a predictive marker for metastasis in colorectal cancer (CRC) (Miyoshi et al., 2010). CRC tissue displayed significantly elevated levels of *ATP11A* mRNA when compared to control tissue and affected patients showed a reduction in disease-free survival rates. How *ATP11A* activity involves in metastasis in CRC is yet to be determined. The X-linked *Atp11c* mutant mice have been shown to exhibit abnormal characteristics including loss in B cell development, unconjugated hypercholanemia, conjugated hyperbilirubinemia, hepatocellular carcinoma, anemia and dystocia (Siggs et al., 2011a,b; Yabas et al., 2011). Whether *ATP11C* deficiency leads to similarly diverse phenotypes in human is presently unknown.

### **1.7 Na<sup>+</sup>/K<sup>+</sup>-ATPase**

Na<sup>+</sup>/K<sup>+</sup>-ATPase (NKA) belongs to type 2C of the P-type ATPases and is found on the cell membrane of essentially all eukaryotic cells. NKA is an integral membrane protein that utilizes energy from ATP hydrolysis to transport three Na<sup>+</sup> out of the cell in exchange for two K<sup>+</sup> in, thereby generating and maintaining low intracellular Na<sup>+</sup> and high internal K<sup>+</sup> concentrations (Blanco & Mercer, 1998). It exists as a heterodimeric complex composed of a catalytic  $\alpha$  subunit and a  $\beta$  subunit that modulates the assembly, membrane targeting, and functional properties of

the complex (Blanco & Mercer, 1998). There are four well-characterized  $\alpha$  subunit isoforms ( $\alpha 1$ ,  $\alpha 2$ ,  $\alpha 3$ ,  $\alpha 4$ ) and three  $\beta$  subunit isoforms ( $\beta 1$ ,  $\beta 2$ ,  $\beta 3$ ). The  $\alpha 1$  and  $\beta 1$  isoforms are found in nearly all cells and likely have a housekeeping role (Elmira Tokhtaeva et al., 2012). In contrast, the other isoforms of NKA exhibit a tissue-specific expression pattern. The  $\alpha 2$  isoform is mainly expressed in muscle and nervous system; the  $\alpha 3$  isoform is abundant in neuronal tissues; and  $\alpha 4$  is exclusively expressed in testis. The  $\beta 2$  isoform predominates in brain and muscle, and  $\beta 3$  is present in lung, testis, skeletal muscle, and liver (Elmira Tokhtaeva et al., 2012).

While transfection studies indicate that each of the four  $\alpha$  subunits can interact with each of the three  $\beta$  subunits and form a functional complex, other studies using selective co-immunoprecipitation suggest that there is preferential binding between certain  $\alpha$  and  $\beta$  isoforms for assembly. For example,  $\alpha 1\beta 1$  is known to be the principal isoform of NKA in kidney (Jørgensen, 1986). In the retina, all  $\alpha$  and  $\beta$  isoforms except for  $\alpha 4$  have been localized and extensively examined for their expression in specific cell populations (Wetzel et al., 1999).  $\alpha 3\beta 2$  has been reported to be enriched in photoreceptor and bipolar cells and distributed in the inner segment, outer nuclear and outer plexiform layers, and inner nuclear layer. Besides its function as an ion pump,  $\alpha 3\beta 2$  has also been found to interact with retinoschisin (RS1), a membrane-associated protein suggested to help maintain the cellular and synaptic structure of the retina (Molday et al., 2007). Mutations in the gene encoding RS1 lead to an early-onset macular degeneration disorder called X-linked retinoschisis (XLRS) (Sauer et al., 1997). A detailed investigation of the interactions between RS1 and these isoforms of NKA will contribute to the understanding of the normal retinal function and organization as well as the pathogenesis of

XLRS. Otherwise, much remains unknown about the roles of particular  $\alpha/\beta$  heterodimers in the specific organs and tissues.

## **1.8 Thesis Investigation**

Among the 14 members of human  $P_4$ -ATPases, ATP9A and ATP9B of the ATP9 subfamily have remained poorly studied in terms of function and association with human diseases despite their ubiquitous and particularly high expression in brain and testis, respectively (Halleck et al., 1998; Takatsu et al., 2011b). Interestingly, overexpression of their yeast homolog Neo1p was found to confer neomycin resistance in yeast and deletion of the *NEO1* gene alone is lethal (Hua et al., 2002; Prezant et al., 1996). To date, it has yet to be determined whether ATP9A and ATP9B exhibit ATP-dependent phospholipid flippase activity and if so, which phospholipids serve as substrates and by what mechanism.

Chapter 2 of the current thesis investigates the function of mammalian ATP9A as well as its role in cellular physiology and human disease. These intriguing questions were pursued by using emerging biochemical and molecular biological methodologies.

Chapter 3 of the project describes characterization of the functional complex of retinoschisin (RS1) and  $Na^+/K^+$ -ATPase (NKA) from native retinal tissues by using monoclonal antibodies specific for RS1 and the NKA subunits  $\alpha 3$  and  $\beta 2$ .

Lastly, Chapter 4 provides a conclusion of the studies and discusses the future aspects of this research project.

## **Chapter 2: Characterization of ATP9A, a member of the P<sub>4</sub>-ATPase family**

### **2.1 Introduction**

The yeast ortholog of the human ATP9 subfamily, Neo1p, has long been known to be the only yeast P<sub>4</sub>-ATPase that is lethal when it is genetically knocked out (Prezant et al., 1996). Several studies demonstrated its role in membrane trafficking in the endomembrane system (Barbosa et al., 2010; Hua et al., 2002; Wicky et al., 2004), and others suggested that Neo1p is important for establishing PS and PE asymmetry (Takar et al., 2016). The fact that Neo1p is essential for the survival of yeast cells indicates that these P<sub>4</sub>-ATPases are involved in some fundamental cellular functions. However, to date there is no direct evidence to show whether Neo1p and ATP9A are phospholipid transporters.

In this chapter, we have investigated the subcellular localization and functional properties of human ATP9A expressed in human cell lines. We have also characterized an in-house monoclonal antibody specific to ATP9A and examined the expression of ATP9A in various mouse tissues.

### **2.2 Materials and Methods**

#### **2.2.1 Materials**

Oligonucleotides were ordered from Integrated DNA Technologies (Coralville, IA). 1 kb Plus DNA Ladder were purchased from Invitrogen (Carlsbad, CA), and Phusion® High-Fidelity DNA Polymerase, *Taq* polymerase, Antarctic phosphatase, T4 DNA ligase, and restriction enzymes were from New England Biolabs (Ipswich, MA). Polyethylenimine was obtained from Polysciences (Warrington, PA), 40% acrylamide solution was from Bio-Rad Laboratories

(Hercules, CA), and protein standards were from Bio-Rad Laboratories or FroggaBio (Ontario, Canada).

1,2-dioleoyl-*sn*-glycero-3-phosphocholine (DOPC), 1,2-dioleoyl-*sn*-glycero-3-phosphoserine (DOPS), 1,2-dioleoyl-*sn*-glycero-3-phosphoethanolamine (DOPE), brain polar lipids (porcine) (BPL), L- $\alpha$ -phosphatidylinositol (bovine, liver) (PI), 1,2-dioleoyl-*sn*-glycero-3-phosphate (PA), 1,2-dioleoyl-*sn*-glycero-3-phosphoglycerol (PG), sphingomyelin (porcine, brain) (SM), cholesterol (bovine, wool) (Chol), 1-oleoyl-2-{6-[(7-nitro-2-1,3-benzoxadiazol-4-yl)amino]hexanoyl}-*sn*-glycero-3-phosphocholine (NBD-PC), 1-oleoyl-2-{6-[(7-nitro-2-1,3-benzoxadiazol-4-yl)amino]hexanoyl}-*sn*-glycero-3-phosphoethanolamine (NBD-PE), and 1-oleoyl-2-{6-[(7-nitro-2-1,3-benzoxadiazol-4-yl)amino]hexanoyl}-*sn*-glycero-3-phosphoserine (NBD-PS) were purchased from Avanti Polar Lipids (Alabaster, AL). ATP and octyl- $\beta$ -D-glucopyranoside (OGP) were purchased from Sigma-Aldrich (St. Louis, MO), CHAPS was from Anatrace (Maumee, OH) and Protease Arrest was from G-Biosciences (St. Louis, MO).

Synthetic 1D4 peptide was obtained from Celtek Peptides (Franklin, TN), and the Rho 1D4 antibody was from UBC University-Industry Liaison Office (UBC-UILO, Vancouver, BC). Radioactive [ $\gamma$ -<sup>32</sup>P]-ATP was ordered from PerkinElmer (Waltham, MA). Sulfo-NHS-LC-Biotin was purchased from ProteoChem (Hurricane, UT) and streptavidin agarose resin was from Thermo Fischer Scientific (Waltham, MA). ATP9A-3G2 (WH0010079M2) monoclonal antibody was purchased from Sigma-Aldrich,  $\beta$ -actin (ab8227) polyclonal antibody was from Abcam (Cambridge, UK).

### **2.2.2 DNA constructs**

Human ATP9A cDNA clone was purchased from OriGene (Rockville, MD) and subcloned into pcDNA3 vector (Invitrogen-Thermo Fischer Scientific) with a 1D4 tag (TETSQVAPA) in the C-terminus using BamHI and EcoRV restriction sites introduced by PCR. The 1D4-tagged ATP9A construct was used as a template for generating E195Q, E195A, D391N, and D391A mutants using PCR. pcDNA3 plasmids containing bovine ATP8A2 wildtype or E198Q mutant with a C-terminal 1D4 tag and bovine CDC50A without a tag were generated as previously described (Coleman et al., 2009; Coleman et al., 2012). Human ATP9B cDNA clone was obtained by reverse transcription polymerase chain reaction (RT-PCR) of HEK293T cell total RNA extract and subcloned into pcDNA3 vector with a C-terminal 1D4 tag using BamHI and EcoRV. Human ATP8B1 cDNA with a C-terminal 1D4 tag was purchased from GeneCopoeia (Rockville, MD).

### **2.2.3 Cell culture and transfection**

HEK293T cells were maintained in DMEM (Sigma) supplemented with 8% bovine growth serum (Thermo Fisher Scientific), 100 units/mL penicillin, 100 µg/mL streptomycin, 25 µg/mL amphotericin B, and 2 mM L-glutamine (Gibco-Thermo Fisher Scientific). For transfection in 100 mm TC-treated dish, HEK293T cells were grown to ~50% confluence and 20 µg of wildtype or mutant ATP9A plasmid was transfected with the calcium phosphate method (Chen & Okayama, 1987) or with polyethylenimine (Longo et al., 2013). For ATP8A2 over-expression, 10 µg of ATP8A2 and 10 µg of CDC50A plasmids were co-transfected in HEK293T cells whereas 5 µg of each were co-transfected in HeLa cells. Transfection in 60 mm TC dishes or 6-well TC plates with glass coverslips was scaled according to the surface area ratio to that of 100 mm dishes.

#### **2.2.4 Immunofluorescence imaging**

Cells grown on poly-L-lysine-coated glass coverslips placed in 6-well TC plates were harvested at 48 hr post-transfection by fixing with 4% paraformaldehyde in 100 mM phosphate buffer (PB), pH 7.4, for 15 min at room temperature. After blocking and permeabilization with 10% normal goat serum (NGS) and 0.2% Triton X-100 in PB for 15 min, cells were incubated with primary antibody solution containing 10% NGS and 0.1% Triton X-100 in PB for 2 hr. Cells were labeled with Rho 1D4 antibody (diluted 1:100) and, in the case of double labeling, with rabbit polyclonal anti-calnexin antibody. After washing, cells were incubated with Alexa Fluor® 488-conjugated goat anti-mouse, Alexa Fluor® 594-conjugated goat anti-rabbit secondary antibodies (Invitrogen, diluted 1:1000), and 4',6-diamidino-2-phenylindole (DAPI) (diluted 1:1000) for 1 hr. Cells were washed and coverslips were mounted on glass slides with mowiol mounting solution for imaging. Fluorescence images were acquired using 63x/1.40 Oil DIC objectives on a Zeiss LSM 700 confocal microscope (Oberkochen, Germany).

#### **2.2.5 Immunoaffinity purification from HEK293T cells**

Purified Rho 1D4 monoclonal antibody was coupled to CNBr-activated Sepharose 2B at a concentration of 2 mg of protein/mL of beads as described previously (Cuatrecasas, 1970; Molday et al., 1990). At 48 hr post-transfection, cells were harvested from TC dishes and solubilized in buffer A containing 50 mM HEPES-NaOH, pH 7.5, 150 mM NaCl, 5 mM MgCl<sub>2</sub>, 1 mM DTT, 20 mM CHAPS, 0.5 mg/mL DOPC, and 1X Protease Arrest, by stirring at 4°C for 30 min. After cell lysis, the insoluble fraction was removed by centrifugation at 40,000 rpm at 4°C for 10 min with a TLA-110 rotor in the Optima Ultracentrifuge. The soluble fraction was then incubated with Rho 1D4-Sepharose 2B beads pre-washed with 10 column volumes of buffer B containing

50 mM HEPES-NaOH, pH 7.5, 150 mM NaCl, 5 mM MgCl<sub>2</sub>, 1 mM DTT, 10 mM CHAPS, 0.5 mg/mL DOPC at 4°C for 2 hr. For luminescent ATPase activity assay and phosphorylation assay, buffer B contains 0.75% OGP instead of CHAPS. After binding, the beads were transferred into an Ultrafree-MC-HV centrifugal filter (Millipore, Billerica, MA) and washed six times with 500 µL of buffer B. The bound proteins were eluted with 0.4 mg/mL 1D4 peptide in buffer B with gentle agitation at 17°C for 30 min twice. In cases where ATP9A-10D1-conjugated Sepharose 2B was used as immunoaffinity column, the bound proteins were eluted at room temperature with freshly prepared 4% sodium dodecyl sulfate (SDS) in buffer A without DTT and CHAPS. Concentration of the purified proteins was quantified from Coomassie blue-stained SDS-polyacrylamide gels with bovine serum albumin (BSA) standards with known concentrations.

### **2.2.6 ATPase activity assay**

Typically, 20 ng of purified ATP8A2 or ATP9A was assayed for ATPase activity in 25 µL of buffer C containing 50 mM HEPES-NaOH, pH 7.5, 150 mM NaCl, 12.5 mM MgCl<sub>2</sub>, 1 mM DTT, 10 mM CHAPS, 5 mM ATP, and 2.5 mg/mL lipid as indicated. The reaction was incubated at 37°C for 30 min and then terminated by adding 25 µL of 12% SDS. The concentration of phosphate was determined using a colourimetric method as previously described (Chifflet et al., 1988; González-Romo et al., 1992; Coleman et al., 2009). The reaction was mixed with 75 µL of solution D containing 6% ascorbic acid and 1% ammonium molybdate in 1 N HCl for 10 min, followed by the addition of 120 µL of solution E containing 2% sodium citrate, 2% sodium meta-arsenite, and 2% acetic acid. The amount of phosphate released in the reaction was then measured with the absorbance at 850 nm in a microplate reader by comparing to the absorbance values of

known phosphate concentrations plotted as a standard curve. All data points were performed in triplicate, and each experiment was repeated at least three times independently.

### **2.2.7 Luminescent ATPase activity assay**

Typically, 200 ng of purified ATP8A2 or ATP9A was reconstituted into liposomes in one volume of reconstitution buffer containing 25 mM HEPES-NaOH, pH 7.5, 150 mM NaCl, 0.5 mM EDTA, 1 mM DTT, 10% glycerol, 1% OGP, and 2.5 mg/mL BPL by incubating on ice for 30 min, resting at room temperature for 5 min, and gently stirring at 4°C for 5 min. Proteins in the mixed lipid/detergent micelles were dialyzed against 2 L of dialysis buffer containing 50 mM HEPES-NaOH, pH 7.5, 150 mM NaCl, 5 mM MgCl<sub>2</sub>, 1 mM DTT, and 10% glycerol with three buffer changes at 4°C overnight. ATPase activity of the reconstituted proteins were determined using ADP-Glo™ Kinase Assay (Promega, Madison, WI) following instructions in the manufacturer's manual.

### **2.2.8 Phosphorylation assay**

Purified ATP8A2 or ATP9A proteins were reconstituted as described for the Luminescent ATPase Activity Assay. Typically, 50 ng of proteins were phosphorylated in 100 µL of standard phosphorylation medium (SPM) containing 50 mM HEPES-NaOH, pH 7.5, 150 mM NaCl, 1 mM DTT, 1 mM MgCl<sub>2</sub>, and 3.3 µM [ $\gamma$ -<sup>32</sup>P]-ATP with constant manual mixing at 0°C for 15 min. The reaction was quenched by vortex-mixing with 2 volumes of 25% (w/v) trichloroacetic acid (TCA) containing 100 mM H<sub>3</sub>PO<sub>4</sub>, followed by centrifugation at 25,000 rpm at 4°C for 10 min in a TLA-55 rotor to remove the supernatant. For samples without hydroxylamine (HA) treatment, the TCA-precipitated proteins were dissolved in freshly prepared sample buffer containing 250 mM phosphate buffer, pH 6.0, 10% glycerol, 0.1% (w/v) bromophenol blue, 5%  $\beta$ -mercaptoethanol

(BME), and 10% SDS. For samples with HA treatment, the precipitated proteins were thoroughly mixed and incubated with 60 mM HA at room temperature for 15 min, followed by centrifugation and dissolving with sample buffer. The samples were then run on a 5% SDS-polyacrylamide gel at pH 6.0 at room temperature for 2 hr, and the gel was fixed in 10% acetic acid for 15 min with gentle agitation and dried onto a filter paper under vacuum before putting into an enhanced chemiluminescence (ECL) cassette at -80°C overnight. The radioactivity was then detected by developing autoradiography films.

### **2.2.9 Cell surface labeling assay**

At 48 hr post-transfection, cells cultured in 60 mm TC dishes were washed with ice-cold Dulbecco's Phosphate-Buffered Saline (DPBS) (Sigma-Aldrich) three times, resuspended in 200  $\mu$ L per dish of 2.5 mg/mL biotin in DPBS, and incubated on ice for 30 min with constant manual mixing. Biotinylation reaction was quenched by adding ice-cold buffer containing 200 mM glycine and 25 mM Tris in DPBS. Cells were washed with ice-cold DPBS and resuspended in 300  $\mu$ L DPBS before added dropwise to buffer A for solubilization at 4°C for 30 min as described in for immunoaffinity purification. After centrifugation to remove the insoluble fraction, the soluble fraction was added to 50  $\mu$ L streptavidin agarose resin pre-washed with buffer A and allowed for binding at 4°C for 30 min. The beads were then transferred to an Ultrafree-MC-HV centrifugal filter washed six times with 500  $\mu$ L of buffer A. After last wash to get rid of all remaining buffer, 30  $\mu$ L of 2X sample buffer, diluted from 4X SDS sample buffer containing 200mM Tris-HCl pH 6.8, 8% w/v SDS, 0.4% w/v bromophenol blue, 40% v/v glycerol, was added to the beads and incubated at 28°C for 30 min with agitation for elution twice.

### 2.2.10 In-cell based assay

Transfected cells grown in 60mm TC dishes for 48 hr were washed with ice-cold  $\text{Ca}^{2+}$ - and  $\text{Mg}^{2+}$ -free phosphate-buffered saline (PBS; 137mM NaCl, 10mM Phosphate, 2.6mM KCl, pH 7.4), collected with 1.5 mL per dish of 5 mM EDTA in PBS into microtubes, and washed with serum-free DMEM media without phenol red (SFM) (Sigma-Aldrich) by centrifugation at 500xg at 4°C for 5 min. Cell pellet in each microtube was resuspended in 250  $\mu\text{L}$  of SFM, 50  $\mu\text{L}$  of which was saved for western blot analysis of protein expression, and remaining cells were equilibrated at 15°C for 5 min. NBD-lipids at 1 mg/mL in chloroform were dried in clear glass tubes using a gentle stream of nitrogen gas, solubilized in 95% ethanol and diluted to 10  $\mu\text{M}$  in SFM. For samples without NBD-lipid labeling, 200  $\mu\text{L}$  of SFM was added to each microtube and for those with NBD-lipid treatment, 200  $\mu\text{L}$  of 10  $\mu\text{M}$  NBD-lipid in SFM was added for incubation at 15°C for 2 min. Labeling was stopped by transferring samples onto ice and adding 500  $\mu\text{L}$  of ice-cold 2.5% fatty-acid free BSA (Sigma-Aldrich) in SFM. Cells were centrifuged to discard the supernatant, resuspended in 1 mL of ice-cold BSA in SFM, and incubated on ice for 30 min. After centrifugation and two washes with 1 mL ice-cold PBS, each cell pellet was resuspended in 1 mL PBS thoroughly by pipetting, and 1  $\mu\text{L}$  PI solution was added to each tube immediately before brief vortexing and proceeding to sample acquisition on the BD LSR II flow cytometer (BD Biosciences, San Jose, CA). At least 10,000 cells were analyzed for all samples and three independent experiments were carried out. Data were analyzed using FlowJo data analysis software package (TreeStar, USA).

### **2.2.11 Generation of monoclonal antibodies against ATP9A**

Sequences encoding amino acids 1-33 or 12-44 in the N-terminus and 415-446 in the large cytoplasmic loop containing P and N domains of ATP9A were cloned into pGEX-4T1 vector (GE Healthcare; Chicago, IL) in frame with glutathione S-transferase using BamHI and XhoI restriction sites. GST fusion proteins were purified from *E. coli* on Glutathione Sepharose 4B (GE Healthcare) and injected into BALB/c mice around 10-weeks-old. Serum from a mouse immunized with the antigen GST-ATP9A<sub>415-446</sub> showed the strongest reactivity toward purified recombinant ATP9A proteins on western blots, and the mouse was sacrificed for fusion of myeloma cells with immune spleen cells. Hybridoma cell lines were generated as previously described (Molday & MacKenzie, 1983) and the supernatants were screened for antibodies against ATP9A with western blots. Monoclonal cell line ATP9A-10D1 was subcloned at least three times with confirmed 100% reactivity against ATP9A before expanded into large scale cultures, and the ascites fluid was either collected directly or purified through Protein G PLUS-Agarose (Millipore) matrix and dialyzed against PBS for conjugating to CNBr-activated Sepharose 2B as described previously (Cuatrecasas, 1970; Molday et al., 1990).

### **2.2.12 Expression and purification of GST fusion proteins from *E. coli***

pGEX-4T1 plasmids containing ATP9A peptide sequences were transformed into BL21 competent cells and cells were plated on agar plates with ampicillin. A single colony was picked to grow a 5 mL LB culture at 37°C overnight. This culture was inoculated into 500 mL LB the next day to grow until OD<sub>600</sub> reaches 0.5, and 500 µL of 1M IPTG was added for induction at 37°C for 4 hr. The culture was harvested by centrifugation at 3000 rpm at 4°C for 15 min with a Sorvall SLA-1500 rotor in the Sorvall RC-5B Plus centrifuge. The cell pellet was resuspended in 15 mL of

PBS with 1X Protease Arrest and sonicated while kept on ice for 30 sec three times using the Ultrasonic Sonifier 150 (Branson, Danbury, CT). The lysate was centrifuged at 16,000 rpm at 4°C for 20 min in the Sorvall centrifuge, and the cleared supernatant was incubated with Glutathione Sepharose 4B (GE Healthcare) at 4°C for 1 hr. The beads were washed with 2 mL of PBS four times and the bound proteins were eluted with 0.5 mL of elution buffer containing 10 mM reduced glutathione (Sigma-Aldrich), 50 mM Tris, 3 mM EDTA, and 1X Protease Arrest in PBS, at 4°C for 3 min four times. Concentration of the eluates was calculated from the absorbance at 280 nm.

### **2.2.13 Gene expression by RT-PCR**

RNA was isolated from frozen tissues from 3-month-old BALB/c mice using E.Z.N.A.® Total RNA Kit II (OMEGA; Norcross, GA) according to the manual's instructions. Random primed cDNA was generated with iScript™ cDNA Synthesis Kit (Bio-Rad Laboratories). *Atp9a* gene expression was measured using the following forward and reverse primers: 5'-TGGCCCTGCAGCACTTTG-3' and 5'-TGGACCAGAGCCACCTCATC-3'. Glyceraldehyde-3-phosphate dehydrogenase (*Gapdh*) expression was used as a control and measured with the following forward and reverse primers: 5'-GGAGATTGTTGCCATCAACG-3' and 5'-CACAATGCCAAAGTTGTCATGG-3'. The primers were annealed at 55°C and the PCR was run for 30 cycles using *Taq* polymerase.

### **2.2.14 Isolation of HEK293T membranes**

Transfected HEK293T cells were harvested and resuspended in 0.5 mL per plate of resuspension buffer containing 50 mM HEPES, 150 mM NaCl, 2 mM MgCl<sub>2</sub>, 1 mM DTT, and 1X Protease Arrest while kept on ice. The cell suspension was passed through 22G needle twelve

times throughout a 30 min period, followed by passing through 26G needle right before layering on top of 60% sucrose in resuspension buffer. The sample was centrifuged at 26,000 rpm at 4°C for 30 min in a TLA-55 rotor in the Optima Ultracentrifuge (Beckman Coulter, Brea, CA). The membrane fraction was collected on top of the 60% sucrose layer, washed with resuspension buffer, and centrifuged at 30,000 rpm at 4°C for 15 min in a TLA-110 rotor. The final membrane pellet was resuspended in 5% glycerol in resuspension buffer and kept frozen at -30°C for short-term storage. Concentration of the membrane fractions was determined with Pierce BCA Protein Assay (Thermo Fisher Scientific) by comparing to known concentrations of bovine serum albumin (BSA) as standards.

#### **2.2.15 Isolation of mouse cortical membranes**

Cortices of 3-month-old BALB/c mice were dissected from brains and membranes were prepared as previously described (Cox & Emili, 2006). Briefly, six cortices were minced with sharp scissors, rinsed four times with ice-cold PBS and once with ice-cold 250-STMDPS buffer containing 250 mM sucrose, 50 mM Tris-HCl, pH 7.4, 5 mM MgCl<sub>2</sub>, 1 mM DTT and 1X Protease Arrest. The tissue was homogenized in ice-cold 250-STMDPS buffer in Dounce homogenizer with a tight-fitting Teflon pestle by stroking the pestle up and down until no intact tissue was apparent and then centrifuged at 800xg for 15 min. The supernatant was transferred to a new tube and centrifuged at 6000xg for 15 min to separate the mitochondria in the pellet. The resulting supernatant was then transferred to a new tube and centrifuged at 45,000 rpm in a TLS55 rotor in the Optima Ultracentrifuge, and the pellet was resuspended with 10% glycerol in 250-STMDPS buffer and the protein concentration was quantified by Pierce BCA Protein Assay before storing at -80°C as the cortical membrane fraction.

### **2.2.16 Immunoprecipitation from mouse cortex membranes**

Mouse cortical membranes (3 mg) were solubilized in 1.5 mL of solubilization buffer containing Tris-buffered saline (TBS) (25 mM Tris-HCl, pH 7.4, and 150 mM NaCl), 1 mM EDTA, 1% OGP, and 1X PA. After stirring at 4°C for 30 min, the membranes were centrifuged at 40,000 rpm for 10 min in TLA110 rotor in the Optima Ultracentrifuge. The supernatant was transferred to a new tube for pre-clearing. 20 µL Pierce Protein G Agarose slurry (Thermo Fisher Scientific) per sample was pre-washed three times with the solubilization buffer and incubated with the supernatant for while gently rotating at 4°C for 1 hr for pre-clearing. Another 100 µL of Pierce Protein G Agarose slurry per sample was also pre-washed and incubated with 50 µg of purified ATP9A-10D1 antibody by gently rotating at 4°C for 1 hr. Then, the pre-cleared sample was centrifuged at 3000 rpm and the supernatant was transferred to a new tube containing the antibody-agarose conjugate for binding at 4°C overnight. The sample was centrifuged at 3000 rpm to discard the unbound fraction in the supernatant. The agarose beads were washed three times with the solubilization buffer and the bound proteins were eluted first at 50°C for 10 min with 4X SDS sample buffer without reducing agent and then at 70°C for 10 min with 4X SDS sample buffer with 10% BME. A buffer-only sample that underwent the same immunoprecipitation procedures was included as a negative control.

### **2.2.17 SDS-PAGE and western blots**

Except for the phosphorylation assay, proteins were separated by SDS gel electrophoresis (SDS-PAGE) on 9% polyacrylamide gels followed by Coomassie blue staining or transfer to Immobilon FL membranes (Millipore). SDS-PAGE was carried out in electrophoresis buffer containing 25 mM Tris, pH 8.3, 192 mM glycine, and 0.1% (w/v) SDS, and transfer was in

Towbin semi-dry transfer buffer containing 25 mM Tris, pH 8.3, and 192 mM glycine with 15% methanol added immediately before use. Membranes were blocked with 1% milk in PBS for 30 min and incubated with monoclonal antibodies diluted in PBS for 2 hr. After washing with 0.05% Tween-20 in PBS (PBS/T), membranes were incubated with goat anti-mouse secondary antibody conjugated with IRDye® 680LT and, for double staining, with donkey anti-rabbit secondary antibody conjugated with IRDye® 800CW (LI-COR, Lincoln, NE), diluted 1:20,000 in PBS/T containing 0.5% milk for 1 hr followed by washing with PBS/T. Images were obtained with a LI-COR Odyssey Imaging System. The monoclonal antibodies as ascites fluids were used at the following dilutions: Rho 1D4 at 1:100, ATP9A-10D1 at neat, CDC50A-7F4 at neat. The commercial antibody of  $\beta$ -actin was diluted at 1:1000 and ATP9A-3G2 at 1:200.

### **2.2.18 Statistical Analysis**

At least three individual experiments in triplicate were carried out for each assay. Data was analyzed using GraphPad Prism and statistical significance was determined by t-test (GraphPad Software, In., La Jolla, CA). Error bars are presented as standard error of the mean (SEM), and N equals the number of experimental data points on which the analysis was performed.

## **2.3 Results**

### **2.3.1 Expression and subcellular localization of human ATP9A wildtype and mutants**

To determine if ATP9A wildtype exhibits any functional characteristics, mutations in ATP9A that presumably yield defective proteins were generated for comparison. The conserved glutamate within DGET motif and aspartate within DKTG motif are key residues in the catalysis of dephosphorylation and in phosphorylation, respectively. ATP8A2 harboring mutations at

these two sites have been demonstrated to show undetectable ATPase activity as opposed to the wildtype (Coleman et al., 2012). A mutation that replaces the isoleucine (I376) with methionine in human ATP8A2 causes the disease CAMRQ (Onat et al., 2012). Mutations at the same residue in bovine ATP8A2 have been shown to express at wildtype level but exhibit significantly decreased NBD-PS flippase and ATPase activity (A. L. Vestergaard et al., 2014). Therefore, the corresponding glutamate, aspartate, and isoleucine in human ATP9A were singly mutated in order to observe and compare the ATPase and flippase activity to that of the wildtype.

First, the expression of C-terminally 1D4-tagged human ATP9A wildtype and various mutants in transiently transfected HEK293T cells were tested and compared by solubilizing the cells with SDS or CHAPS. While SDS is a harsh detergent that extracts all the proteins expressed in cells, CHAPS is a much milder detergent that solubilizes proteins that have been properly folded and trafficked to the target membranes. ATP9A wildtype and all the mutants expressed similarly in HEK293T cells as seen with SDS solubilization, but only E195Q, E195A, I345M, and I345S were folded and present on the membranes at comparable levels to that of the wildtype (Figure 2.1A).  $\beta$ -actin was included as a loading control.

The subcellular localization of human ATP9A in transiently transfected HeLa cells has been examined (Takatsu et al., 2011b). ATP9A was shown to be able to exit the ER even in the absence of CDC50 co-expression and was found to localize to the early/recycling endosomes and trans-Golgi network (TGN) but not to late endosomes or cis-Golgi. To examine if exogenously expressed ATP9A proteins in HEK293T cells can also exit the ER, the subcellular distribution of C-terminally 1D4-tagged ATP9A wildtype and different mutants was examined by

immunofluorescence microscopy (Figure 2.1B). Double immunofluorescence labeling with 1D4 antibody for ATP9A and calnexin antibody for the ER showed that the dephosphorylation-deficient mutant E195Q could leave the ER and had a similar expression pattern as the wildtype. In contrast, staining of the phosphorylation-deficient mutant D391N largely overlapped with the ER, suggesting the proteins were misfolded. Partial co-localization with the calnexin staining was observed for I345M and I345S, indicating that some of these mutant proteins were retained in the ER likely due to misfolding. These observations corresponded to the data from the expression analysis.

Since the results indicated that the dephosphorylation-deficient mutant at the conserved glutamate residue (E195Q) was the only fully folded mutant trafficked to the destined membrane compartments, where ATP9A proteins presumably serve their function, E195Q was included in the following functional studies for comparison to the wildtype.

### **2.3.2 Immunoaffinity purification of ATP9A**

Obtaining a sufficient amount of purified  $P_4$ -ATPases was critical for carrying out functional activity assays. Thus, 1D4-tagged ATP8A2 and ATP9A proteins expressed in HEK293T cells were solubilized with CHAPS and purified with Rho 1D4-Sepharose 2B column. The bound proteins were eluted with 0.4 mg/mL 1D4 peptide and visualized on a Coomassie blue-stained gel (Figure 2.2). The  $P_4$ -ATPases were efficiently purified and enriched in the peptide-eluate fractions. ATP8A2 is a well-established  $P_4$ -ATPase known to transport PS and to a lesser extent PE, and it was included in the experiments discussed in this chapter as a positive control.

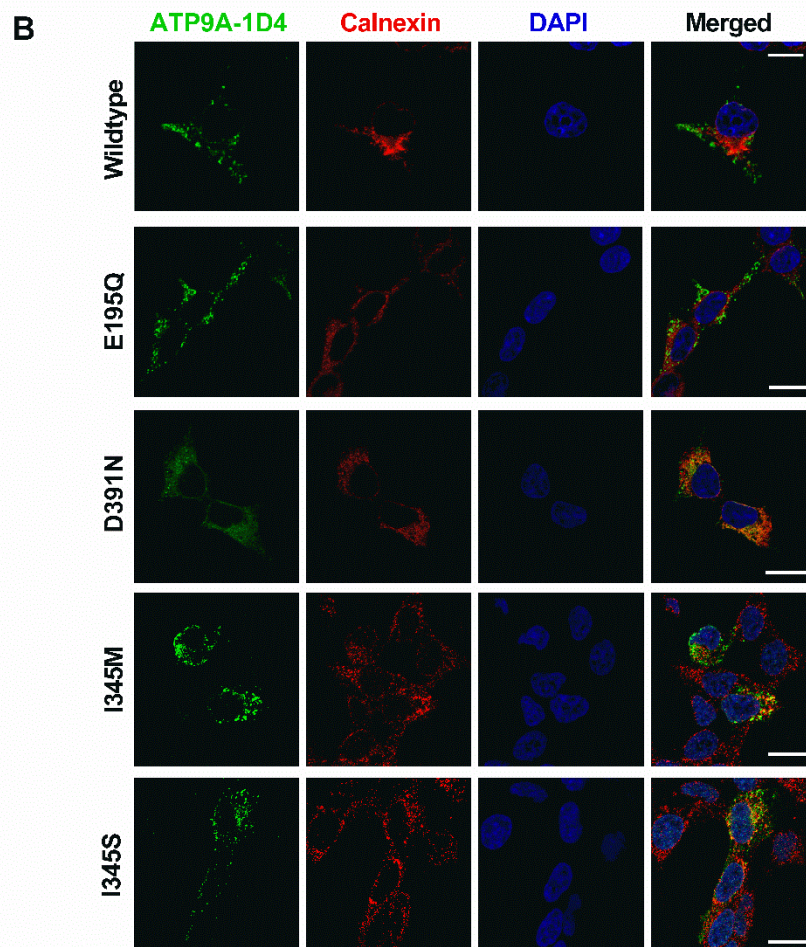
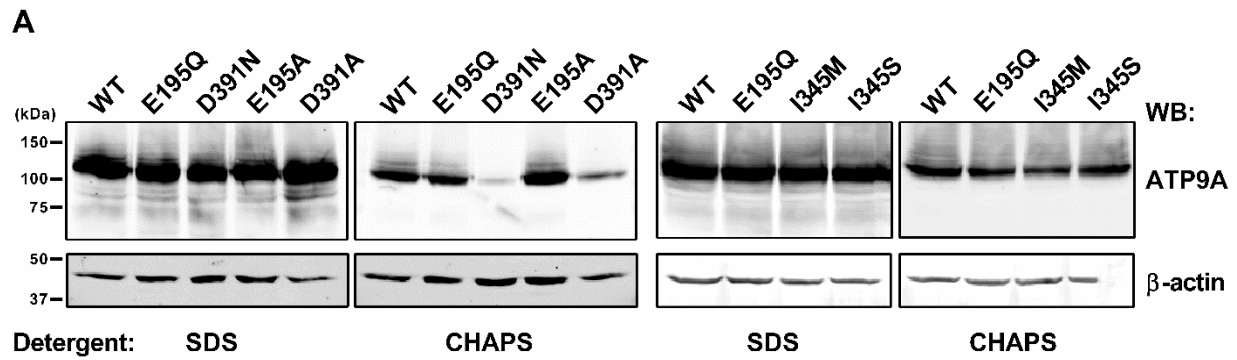


**Figure 2.1 Expression and subcellular distribution of ATP9A expressed in HEK293T cells.**

(A) HEK293T cells expressing 1D4-tagged wildtype (WT) or mutant ATP9A were solubilized with SDS or CHAPS and compared on western blots labeled with Rho 1D4 antibody and  $\beta$ -actin antibody. (B) Wildtype or mutant ATP9A proteins expressed in HEK293T cells were fixed in 4% PFA and doubly labeled with antibodies against 1D4 (green) and calnexin (red) followed by DAPI (blue) staining for fluorescence microscopy. Scale bar, 10  $\mu$ m.

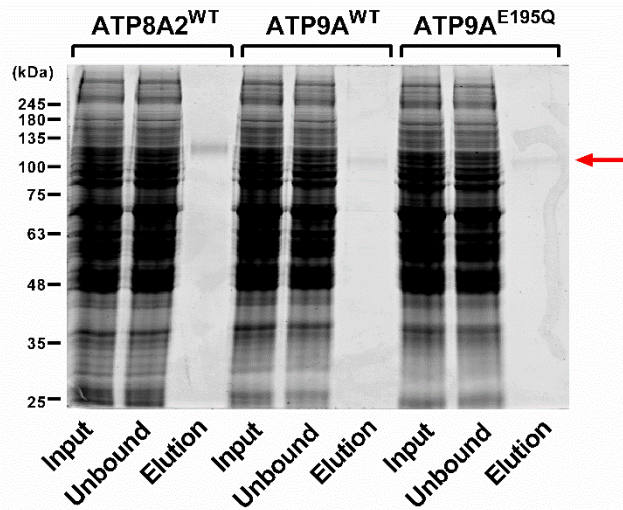


**Figure 2.2 Purification of ATP8A2 and ATP9A from transfected HEK293T cells.**

CHAPS-solubilized HEK293T cell extract (Input) was incubated with Rho 1D4-Sepharose 2B column, and the unbound fraction (Unbound) and the 1D4 peptide-eluted fraction (Elution) were analyzed on SDS-polyacrylamide gel stained with Coomassie blue. The ATP9A band in the elution is pointed by the red arrow.

### 2.3.3 ATPase activity

The first approach to study the function of ATP9A was to test the ability of the purified proteins to hydrolyze ATP. The colourimetric ATPase assay detects activity of the proteins while in the presence of detergent as previously described (Coleman et al., 2009). The Coomassie blue gel and western blot images represent the typical expression level and purity of the P<sub>4</sub>-ATPases used in activity assays (Figure 2.3A). Purified P<sub>4</sub>-ATPases were incubated with reaction cocktails containing ATP and brain polar lipid (BPL), and the amount of free phosphate released from ATP hydrolysis was detected and normalized to the protein levels (Figure 2.3B). BPL is a commercially available total lipid extract from porcine brain that contains a mixture of various naturally occurring lipids including 12.6% PC, 33.1% PE and 18.5% PS. As previously reported, the ATPase activity of ATP8A2 was most highly activated by PS and BPL and to a lower extent by PE (Coleman et al., 2009). In contrast, the ATPase activity of ATP9A wildtype was about 20-fold lower than that of ATP8A2. Also, there was no apparent difference between the activity of ATP9A wildtype and the dephosphorylation-deficient E195Q mutant.

The colourimetric method can detect phosphate ions present in the reactions in the nanomolar range and it is not very sensitive. The second approach was to use the more sensitive ADP-Glo™ Kinase Assay that measures the ADP produced from the hydrolysis of ATP in the picomolar range. This assay requires enough purified proteins to be reconstituted into proteoliposomes. The relative activity of ATP9A to the positive control ATP8A2 was slightly higher than that obtained from the colourimetric assay, but the difference between wildtype and E195Q was still negligible (Figure 2.3C). These results suggested that the activated ATPase activity of the ATP9A wildtype was not elicited in the experimental conditions as described.

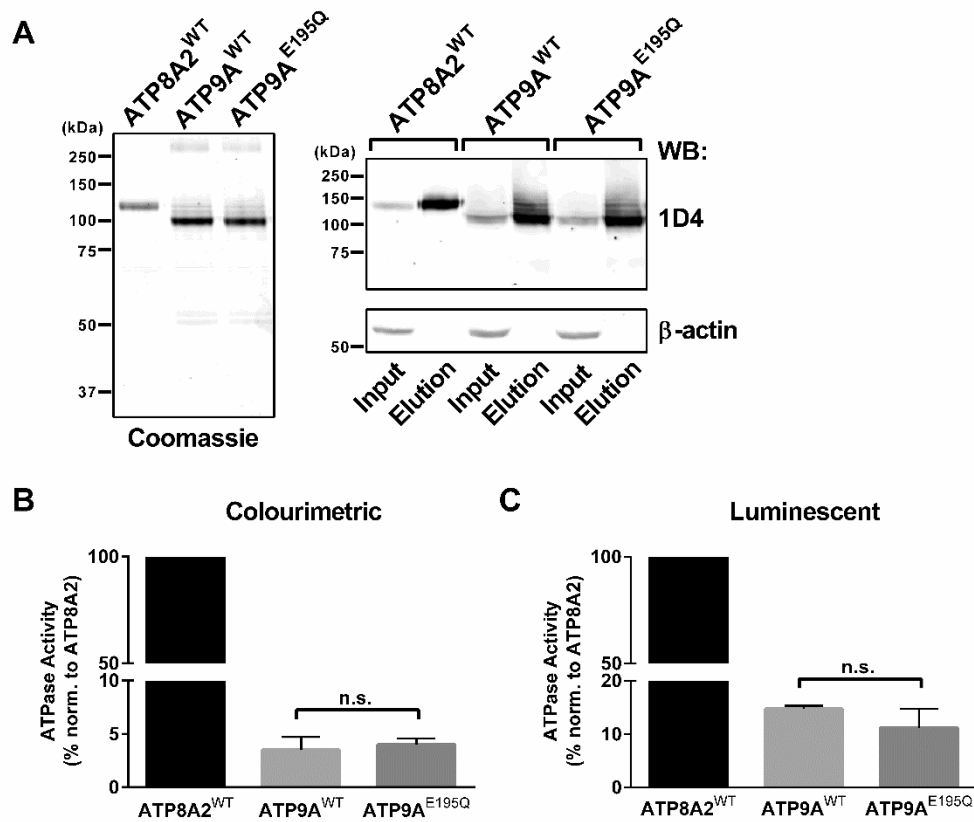


**Figure 2.3 ATP9A shows minimal lipid-activated ATPase activity.**

(A) Wildtype ATP8A2, ATP9A, and mutant ATP9A expressed in HEK293T cells were incubated with Rho 1D4-Sepharose 2B column and eluted with 1D4 peptide to obtain sufficient purified proteins for ATPase activity assays. (B) Typically, 20 ng of purified ATP8A2 or ATP9A was incubated with ATP and brain polar lipids at 37°C for 30 min before the amount of free phosphate released in the reactions were detected by the colourimetric method. Error bars represent SEM (N = 4). (C) For luminescent ATPase activity assay, 200 ng of purified ATP8A2 or ATP9A was reconstituted into proteoliposomes containing brain polar lipids and dialyzed overnight before using the ADP-Glo™ Kinase Kit to measure the amount of ADP formed from ATP hydrolysis. Error bars represent SEM (N = 3). Paired t-test was used to calculate p-values. n.s., not significantly different,  $p > 0.05$ .

### 2.3.4 Phosphorylation assay

The very low ATPase activities of ATP9A proteins prompted us to look at the ability of ATP9A to bind ATP during the catalytic cycle by radioactive  $[\gamma\text{-}^{32}\text{P}]\text{-ATP}$  labeling assay as previously described (Coleman et al., 2012). The aspartyl-phosphate intermediate formed upon ATP binding is a fundamental characteristic of all P-type ATPases and is sensitive to hydroxylamine treatment. Purified and reconstituted ATP8A2 and ATP9A proteins were phosphorylated with  $[\gamma\text{-}^{32}\text{P}]\text{-ATP}$  followed by treatment with or without hydroxylamine (Figure 2.4). The radiograph image showed that, just like ATP8A2, ATP9A was phosphorylated and the aspartyl-phosphate intermediate produced was abolished after treating with hydroxylamine. Results from the ATPase activity assays and phosphorylation assay altogether suggested that ATP9A undergoes autophosphorylation, but fails to dephosphorylate.

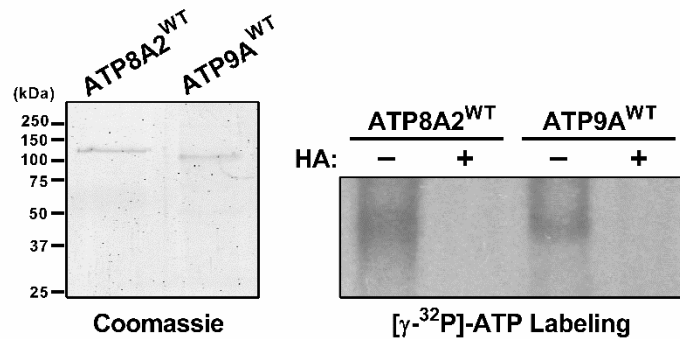


**Figure 2.4 ATP9A binds to ATP and forms an aspartyl-phosphoenzyme, which is sensitive to hydroxylamine.**

Wildtype ATP8A2 and ATP9A expressed in HEK293T cells were purified and reconstituted into proteoliposomes, followed by incubation with  $[\gamma\text{-}^{32}\text{P}]\text{-ATP}$  for phosphorylation assay. The  $[\gamma\text{-}^{32}\text{P}]\text{-ATP}$ -labeled proteins were either untreated (-) or treated (+) with hydroxylamine (HA) and then run on a SDS-polyacrylamide gel for autoradiography.

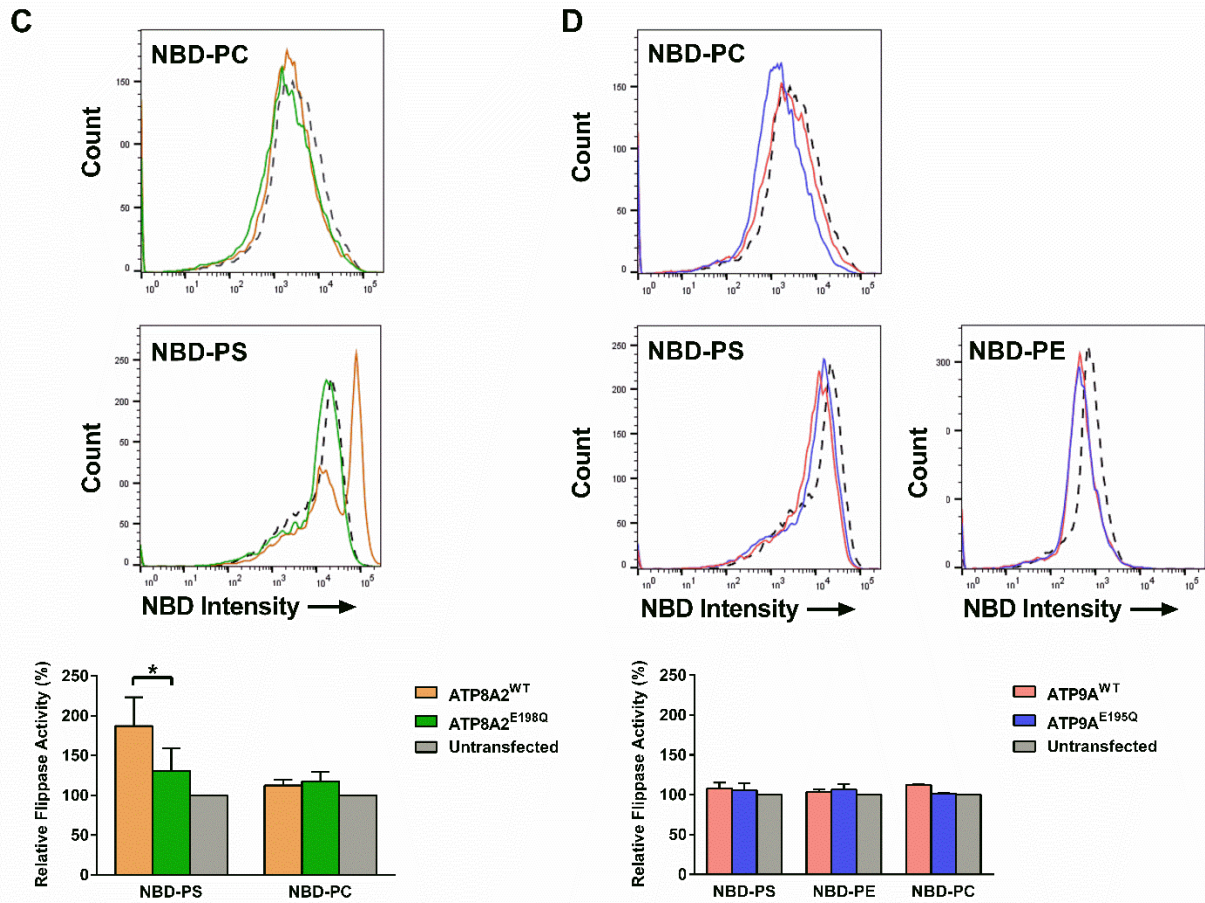
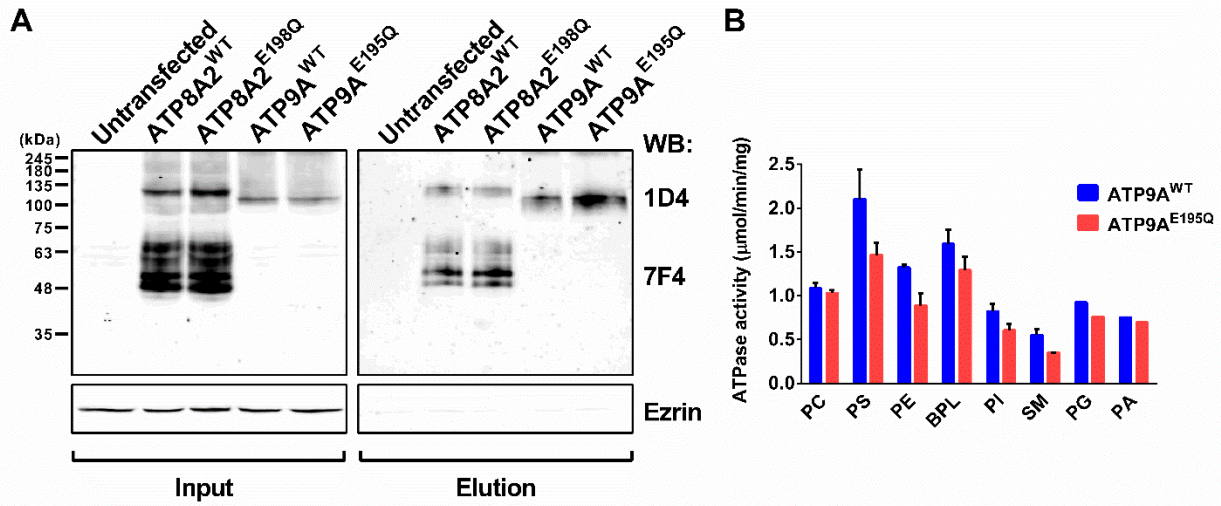
### 2.3.5 Biotinylation and cell-based flippase assay

One possible explanation for the lack of ATPase activity of ATP9A was that the use of detergent during protein solubilization and purification causes some structural changes that block the A domain from performing dephosphorylation, thus rendering the proteins stuck in the E2P state and inactive. To address this possibility, cell-based flippase assay that employs Fluorescence-Activated-Cell-Sorting (FACS) and avoids the use of detergent was carried out as previously described (Jensen et al., 2016; Zhu et al., 2012). Since this assay detects the fluorescent NBD-labeled lipids that have been incubated with cells and incorporated or “flipped” into the cytoplasmic leaflet of cell membrane, a biotinylation experiment was first performed to see if the P<sub>4</sub>-ATPases under study get trafficked to the cell surface. HEK293T cells expressing wildtype and mutant of ATP8A2 and ATP9A were biotinylated, and the proteins bound to streptavidin beads were then eluted (Figure 2.5A). An antibody against ezrin was used as an intracellular marker for western blot. The results indicated that both ATP8A2 and ATP9A were present on the plasma membrane, thereby validating the approach to examine the flippase activity of these P<sub>4</sub>-ATPases using the cell-based method.

Although there is still no direct evidence to show the phospholipid translocase function and substrate specificity of ATP9A to date, a few studies on ATP9A and Neo1p have pointed towards PS and PE as the potential substrates (Tanaka et al., 2016; Wu et al., 2016). In order to determine the substrate specificity of ATP9A for the cell-based flippase assay, a more extensive ATPase activity assay involving a broad range of membrane lipids was done (Figure 2.5B). It was observed that the specific ATPase activity of ATP9A wildtype was the highest for PS, followed by BPL and PE, and the difference between ATP9A wildtype and E195Q was the most apparent for

PS and PE, suggesting that the wildtype proteins were likely activated by these two phospholipids as implicated by the studies mentioned above.

As expected, cells expressing ATP8A2 wildtype displayed significantly increased uptake of NBD-PS, but not NBD-PC, when compared to the untransfected control cells and to the dephosphorylation-deficient mutant E198Q (Figure 2.5C). On the other hand, ATP9A wildtype and E195Q both showed only slightly higher NBD-PS and NBD-PE uptake than the untransfected cells and the differences between them were negligible, suggesting that ATP9A wildtype was not showing flippase activity towards these specific lipids (Figure 2.5D). Even in the absence of detergent and when protein solubilization or purification was not involved in the experimentation, no apparent evidence for the flippase function of ATP9A was observed.



**(Cont.) Figure 2.5 ATP8A2 shows typical flippase activity towards PS, while ATP9A is not activated by PS, PE or PC, despite both P<sub>4</sub>-ATPases get trafficked to the cell surface.**

(A) HEK293T cells expressing the wildtype or mutant of ATP8A2 and ATP9A were biotinylated to detect proteins on the plasma membrane. The cell extracts (Input) were then incubated with streptavidin beads and the bound proteins (Elution) were eluted with 2X SDS sample buffer. Western blots were labeled with the Rho 1D4 antibody for the P<sub>4</sub>-ATPases and 7F4 antibody for the co-expressed CDC50A proteins. Ezrin as an intracellular marker. (B) Purified wildtype or mutant ATP9A proteins were incubated with individual lipids as indicated at 37°C for 30 min, and the specific ATPase activity was determined by normalizing the amount of phosphate ions produced from ATP hydrolysis to the protein levels present in the reactions. Error bars represent SEM (N = 3). (C),(D) Untransfected or transfected HEK293T cells were incubated with fluorescent NBD-lipids (PS, PE or PC) at 15°C for 2 min and unbound lipids were back-extracted with fatty acid-free BSA. The level of NBD fluorescence incorporated into the cells was measured by flow cytometry, and the relative flippase activity of wildtype and mutant ATP8A2 or ATP9A was determined by normalizing to the untransfected samples. Error bars represent SEM (N = 3). Paired t-test was used to calculate p-values. \* p < 0.05.

### 2.3.6 Characterization of the in-house monoclonal antibody ATP9A-10D1

The lack of ATPase and flippase activity of ATP9A expressed in HEK293T cells using both the biochemical and cell-based approaches, despite its proper subcellular localization and protein expression, led to the other possible explanation that ATP9A requires an unidentified associating protein for exerting its function on the membranes. Since there was no commercially available antibodies that were suitable for studying ATP9A proteins in their native context, a monoclonal antibody was generated in the lab in the hope to be used for purification of native ATP9A and identification of its endogenous interacting partners.

GST-fused ATP9A peptides targeting the N-terminal or the large cytoplasmic loop regions were injected to immunize BALB/c mice and the produced antibodies were screened on western blot strips of expressed ATP9A proteins for the most specific and strongest binding monoclonal cell lines. One monoclonal cell line designated as ATP9A-10D1 was chosen for purification and further characterized. On western blots, 10D1 recognized the GST-fused ATP9A<sub>415-446</sub> peptide containing its epitope but not the other ATP9A peptides or purified GST (Figure 2.6A). 10D1 labeled the 1D4-tagged ATP9A proteins in the membranes isolated from transfected HEK293T cells and in the elution of immunoprecipitation with 1D4-Sepharose 2B column, but not the other human P<sub>4</sub>-ATPases including its close family member ATP9B (Figure 2.6B). Also, 10D1-conjugated Sepharose 2B column was tested for its binding affinity to 1D4-tagged ATP9A proteins expressed in HEK293T cells by immunoprecipitation, and the antibody pulled down its target comparably well to the 1D4 column. Furthermore, HEK293T cells expressing 1D4-tagged ATP9A were separately labeled with 1D4 antibody and 10D1 antibody for comparison by fluorescence microscopy (Fig 2.6C). 10D1 staining appeared similar to the

1D4 staining and the stained punctae were not co-localized with the ER marker, suggesting that 10D1 indeed recognized the expressed ATP9A proteins. Therefore, ATP9A-10D1 was extensively tested to show high specificity towards ATP9A and suitability for applications in western blot, immunoprecipitation, and immunofluorescence experiments.

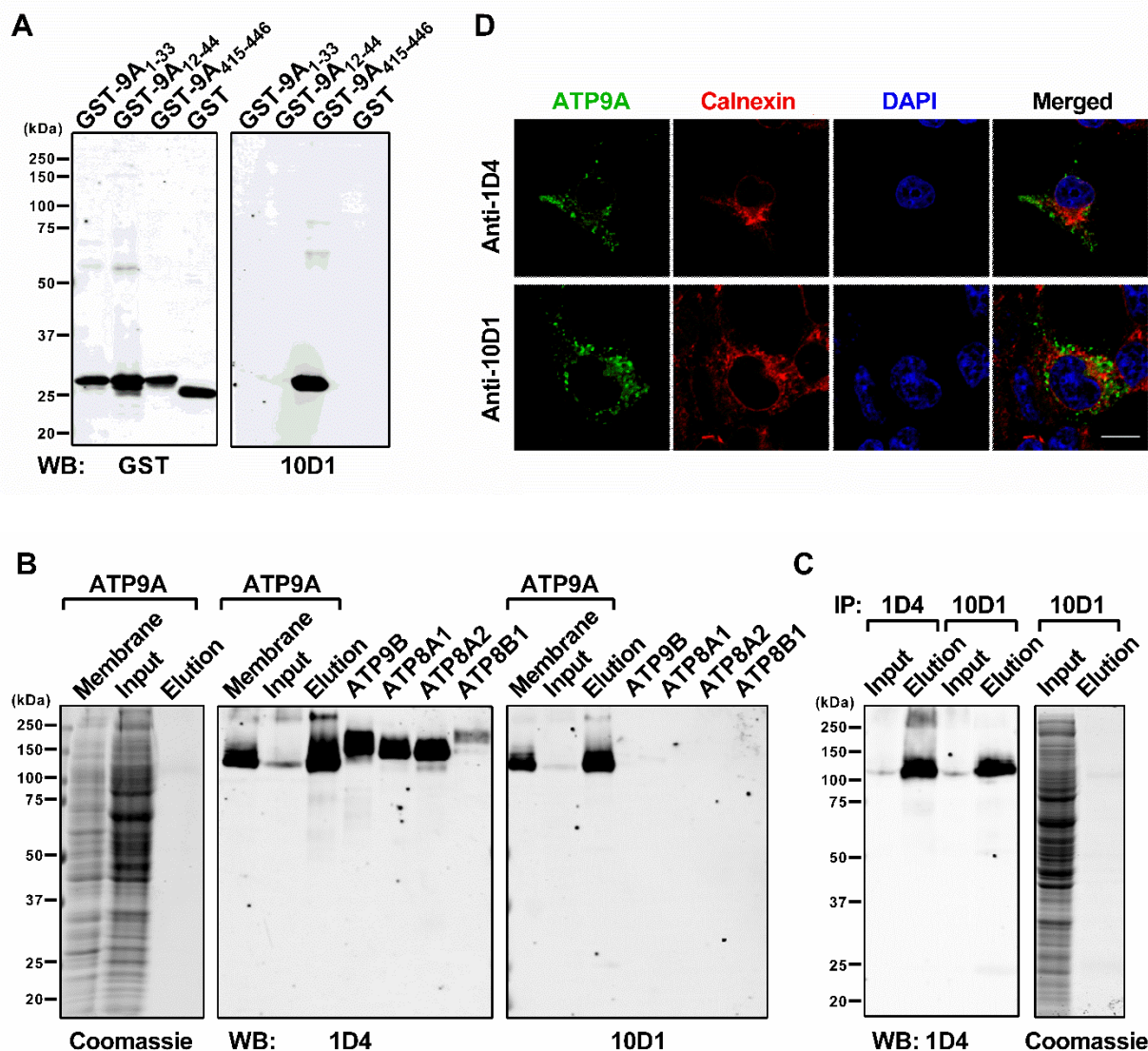


### Figure 2.6 Characterization of ATP9A-10D1 monoclonal antibody.

(A) GST-fused ATP9A peptides or GST expressed in *E. coli* were purified with Glutathione Sepharose 4B column and analyzed by western blot. (B) HEK293T cells expressing 1D4-tagged ATP9A were fractionated to collect membranes (Membrane) or solubilized with CHAPS to obtain cell extracts (Input) and 1D4 peptide-eluted fractions (Elution) from immunoprecipitation using Rho 1D4-Sepharose 2B column. Various human P<sub>4</sub>-ATPases with 1D4 tag were also expressed and purified. SDS-polyacrylamide gels were stained with Coomassie blue or transferred onto PVDF membranes for western blot analysis. (C) 1D4-tagged ATP9A expressed in HEK293T cells were immunoprecipitated with Sepharose 2B beads coupled to 1D4 or 10D1. The cell extracts (Input) and the bound proteins in SDS-eluted fractions (Elution) were analyzed by Coomassie blue staining or western blot with 1D4 antibody. (D) 1D4-tagged ATP9A expressed in HEK293T cells were fixed in 4% PFA and labeled with 1D4 antibody or 10D1 antibody (green) and calnexin (red) followed by DAPI (blue) staining for fluorescence microscopy. Scale bar, 10  $\mu$ m.

### 2.3.7 ATP9A tissue expression

The antigenic peptide used to generate ATP9A-10D1 has a highly conserved sequence throughout species including mouse and rat. In search of mouse tissues enriched in endogenous ATP9A proteins for the purpose of purification and pull-down, the expression of *Atp9a* mRNA in various tissues of 3-month-old BALB/c mice was examined by RT-PCR. Gene-specific primers were amplified a 500-bp fragment of *Atp9a* and *Gapdh*, which was included as a positive control (Figure 2.7A). *Atp9a* expression was high in cortex and testis, but it was undetectable in other neuronal tissues such as retina, hippocampus, and cerebellum and in other tissues as indicated.

Knowing that *Atp9a* is highly expressed in cortex, an attempt to purify native Atp9a proteins from this tissue using the in-house monoclonal antibody ATP9A-10D1 was done next. Mouse cortical membranes were solubilized and incubated with 10D1-conjugated Protein G Agarose beads for binding and the bound fractions were eluted twice with 4X SDS sample buffer due to the lack of 10D1 peptide (Figure 2.7B). A buffer only sample was included in immunoprecipitation as a negative control. A faint band above the 100 kDa marker appeared in the first elution of cortical membrane sample but not in the elution of the buffer only control. Purified 1D4-tagged ATP9A proteins from 1D4 column were run on the same gel as an indicator for the expected band size. Immunoprecipitation of mouse cortical membranes was also attempted by using CNBr-activated Sepharose 2B beads coupled to purified 10D1 antibody, but no signal of Atp9a proteins was observed on western blots (data not shown).

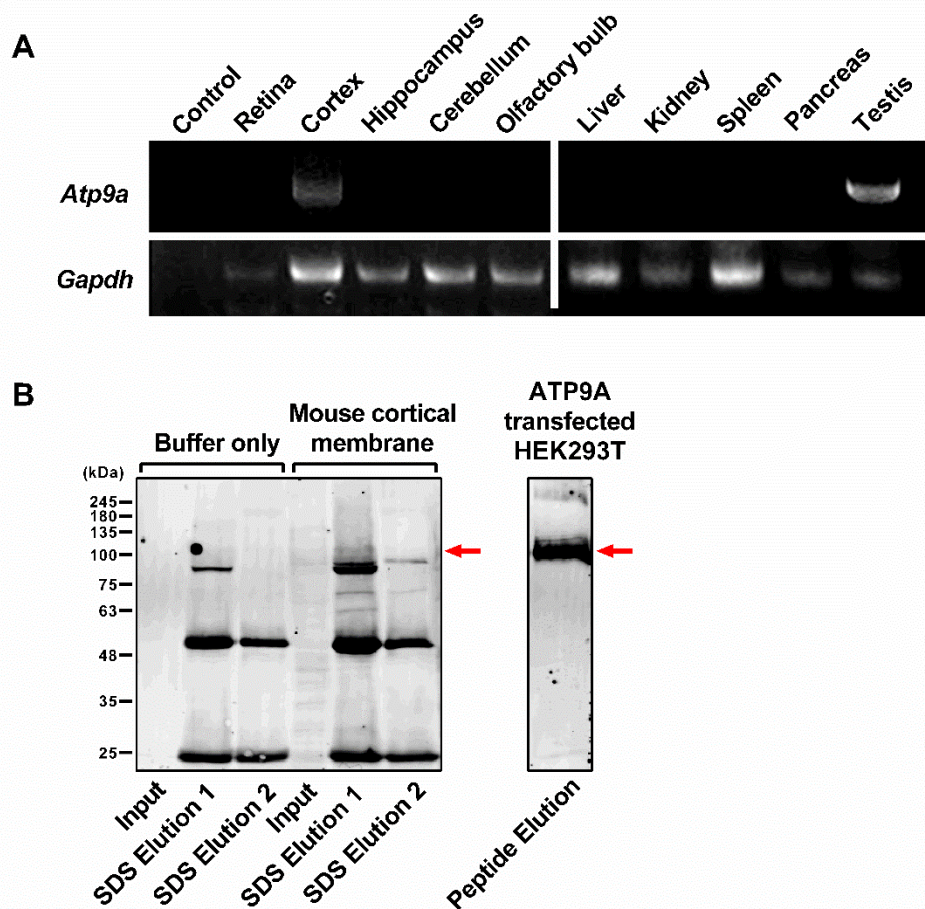


**Figure 2.7 Expression and immunoprecipitation of *Atp9a* in mouse tissues.**

(A) RNA from various mouse tissues was isolated and random primed cDNA was synthesized. Primers specific to mouse *Atp9a* were used to measure gene expression by RT-PCR. *Gapdh* was included as a positive control. (B) Mouse cortical membranes were prepared by fractionation and solubilized with buffer containing 1% octyl- $\beta$ -D-glucopyranoside (OGP) by stirring at 4°C for 30 min. The solubilized fractions were centrifuged and the supernatants (Input) were incubated with 10D1-conjugated Protein G Agarose beads for binding at 4°C overnight. The bound proteins were then eluted twice, first with 4X SDS sample buffer without  $\beta$ -mercaptoethanol (BME) (SDS Elution 1) and second with 5% BME added (SDS Elution 2). 1D4 peptide-eluted ATP9A proteins from transfected HEK293T cells were run on the same SDS-polyacrylamide gel as a marker for the expected band size (red arrows).

### **2.3.8 Comparison of ATP9A-10D1 and the commercial antibody 3G2**

A more recent paper reported that Atp9a is abundant in rat liver subcellular fractions including microsomes and mitochondria by labeling western blots with a commercial antibody 3G2 from Sigma (Chaubey et al., 2016). Since affinity of 10D1 to native Atp9a seemed to be much lower than to expressed ATP9A in HEK293T cells, comparison of the binding affinity and specificity between 10D1 and the commercial 3G2 was carried out to identify the potential limitations to 10D1 antibody. Membrane fractions from empty vector- or ATP9A-transfected HEK293T cells were isolated; some were saved for western blot analysis while the remainder were further solubilized with CHAPS for immunoprecipitation with 1D4 column. Replicates were prepared for Coomassie blue staining as well as western blot analysis by various antibodies as indicated (Figure 2.8). The results showed that ATP9A-10D1 indeed had a significantly higher affinity for labeling ATP9A on western blot as the commercial 3G2 barely detected the proteins.

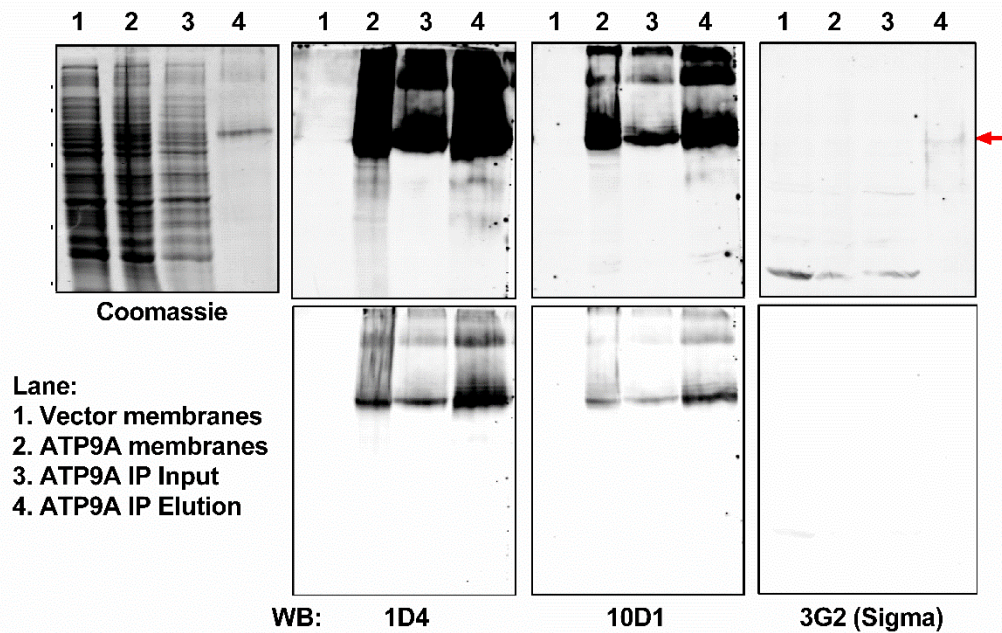


**Figure 2.8 Comparison of ATP9A-10D1 and the commercial antibody 3G2.**

HEK293T cells transfected with an empty vector (Lane 1) or 1D4-tagged ATP9A (Lane 2) were fractionated to collect membranes. Cells expressing 1D4-tagged ATP9A were solubilized with CHAPS and the cell extracts (Lane 3) were loaded onto 1D4-Sepharose 2B column for purifying ATP9A proteins in the peptide-eluates (Lane 4). The four samples were run in replicates on SDS-polyacrylamide gels and analyzed by Coomassie blue staining or western blots labeled with 1D4, 10D1, or 3G2 (Sigma) antibody. The top panel shows the same western blot images as the bottom panel but adjusted with ImageJ for overexposure to reveal a faint band labeled by 3G2 (red arrow).

## 2.4 Discussion

P<sub>4</sub>-ATPases constitute a family of P-type ATPases that utilize energy from ATP hydrolysis to transport a large variety of substrates across cell membranes. There are 14 members in the human P<sub>4</sub>-ATPase family and five in yeast. Numerous studies using cell-based and biochemical approaches have convincingly demonstrated that P<sub>4</sub>-ATPases actively flip phospholipids from the exoplasmic to the cytoplasmic leaflet of cell membrane (Andersen et al., 2016). However, whether the class 2 P<sub>4</sub>-ATPases (ATP9A and ATP9B) transport phospholipids and which lipids serve as their substrates have been poorly investigated. In this study, we have examined the expression, subcellular distribution, and functional activities of ATP9A in transiently transfected HEK293T cells. We have also generated and characterized a monoclonal antibody specific for ATP9A.

To gain a better understanding of the physiological and functional properties of ATP9A, methods that have been used to study the phospholipid flippase activities of well-established P<sub>4</sub>-ATPases such as ATP8A2 were employed (Coleman & Molday, 2011; Coleman et al., 2012). Wildtype and mutant clones of ATP9A with a C-terminal 1D4 tag were first constructed into pcDNA3 vector and transfected in HEK293T cells for analysis of expression and subcellular localization. Our results indicated that all mutants expressed at similar total protein levels to the wildtype, but only some mutants were properly folded and trafficked out of the ER while others were misfolded and co-localized with the ER. Mutations of the conservative glutamate residue within DGET motif and the aspartate residue within DKTG motif presumably yield P<sub>4</sub>-ATPases that are deficient in dephosphorylation and phosphorylation, respectively, and have been commonly used for studying the functional properties along with the wildtype (Coleman et al.,

2012; Takatsu et al., 2014; Takada et al., 2015). The phosphorylation-deficient mutations of D391 in ATP9A produced misfolded proteins that were not able to exit the ER, which was reminiscent of the very low expression and lack of ATPase activity of D416N in ATP8A2 (Coleman et al., 2012). The CAMRQ disease-causing mutation I376M in ATP8A2 resides in a highly conserved C-terminal transmembrane domain and is predicted to change the secondary structure of the protein, thereby interfering with its phospholipid transport activities in the expressing tissues including brain and retina (Onat et al., 2012). In ATP9A, some of the corresponding I345 mutant proteins were misfolded and partially overlapped with the ER, and whether mutations of I345 cause any phenotypes in native tissues requires further *in vivo* studies. In contrast, the dephosphorylation-deficient E195 mutants of ATP9A were completely folded and localized to the same membrane compartments as the wildtype, and thus E195Q was the most appropriate mutant or subsequent functional studies. A similar expression analysis has not been done for other P<sub>4</sub>-ATPases, but our study noted that only the mutants that are properly folded and exhibit a wildtype expression pattern should be used in activity assays for comparison with the wildtype proteins.

Studies in yeast have indicated that Neo1p, the ortholog of ATP9A, plays an important role in establishing PS and PE asymmetry on the plasma membrane (Takar et al., 2016; Wu et al., 2016). On the other hand, ATP9A stably expressed in HeLa cells has been speculated to regulate PS translocation in endosomes but its depletion did not cause any abnormal distribution of PS in the cytoplasmic leaflet (Tanaka et al., 2016). Nonetheless, to date there is no direct evidence to demonstrate the ATP-dependent activities of these P<sub>4</sub>-ATPases. The present study investigated the biochemical properties of purified ATP9A wildtype and E195Q mutant expressed in HEK293T

cells. Our findings indicated that ATP9A undergoes autophosphorylation, but shows minimal lipid-activated ATPase activity and fails to dephosphorylate. Upon incubation with ATP, ATP9A proteins in the reaction cocktails started to bind with and hydrolyze ATP, forming the phosphorylated intermediates E1P and releasing phosphate ions which were detected in the phosphorylation assay. However, subsequent dephosphorylation of the intermediate state was not activated as flipping of lipid substrate did not occur, thereby halting the catalytic cycle and inhibiting further enzymatic reactions of the flippase. This could explain the ATPase activities of both ATP9A wildtype and E195Q mutant that were consistently higher than the background activities of untransfected cells or of ATP9A proteins denatured with 6% SDS before incubation with ATP. Dephosphorylation of E1P might have been hindered in ATP9A due to several factors: 1) the use of detergent causes structural changes that prevent DGET motif from acting as a phosphatase; 2) the lack of accessory proteins required for its flippase function; or 3) the lack of correct substrates. In any case, ATP9A wildtype without activation would yield ATPase activities similar to those of the mutant proteins as we observed.

To address the issue of using detergent in the biochemical purification of ATP9A, we turned to cell-based flippase assay for examining the function of ATP9A. Such cell-based approaches have been increasingly used to demonstrate the flippase activities of various P<sub>4</sub>-ATPases towards specific NBD-labeled lipid substrates, although most studies relied on generating stable cell lines expressing P<sub>4</sub>-ATPases (Segawa et al., 2014; Takada et al., 2015; Takatsu et al., 2014). Indeed, ATP8A2 showed a 50% increase in the uptake of its known substrate NBD-PS compared to the E198Q mutant, and no difference was observed for NBD-PC. ATP9A wildtype and E195Q mutant displayed similar and nearly background levels of NBD-lipid

uptake, indicating that the expressed ATP9A in HEK293T cells did not contribute to the flippase activity towards PS, PE or PC. Therefore, even in the absence of detergent, ATP9A wildtype was not activated by any specific lipid tested in the cell-based assay.

The current as well as previous studies have shown that ATP9A does not need the co-expression of CDC50 proteins to exit the ER and localize to target membranes, and the experiments carried out in this thesis were based on the assumption that the ATP9A proteins trafficked out of the ER were correctly folded and functional. However, it is not unlikely that other unknown associating proteins are required for ATP9A to exert ATP-dependent function on the membranes. The much lower protein expression and ATPase activity of ATP9A in transfected HEK293T cells than that of ATP8A2 with co-transfected CDC50A might have been due to the lack of such an accessory subunit for forming a functional complex and stabilizing the catalytic subunit. Mass spectrometric analysis of the proteins that co-immunoprecipitate with ATP9A from native tissues highly enriched in ATP9A may be useful for identifying potential proteins required for its function. In preparation for this future work, we performed RT-PCR for gene expression analysis in various mouse tissues and found that ATP9A was most abundant in the brain and testis. We also generated and characterized a monoclonal antibody ATP9A-10D1 that showed high specificity and binding affinity for ATP9A. Purification of endogenous ATP9A from mouse brain membranes was attempted using 10D1-Sepharose 2B column, but unfortunately, the bands of anticipated ATP9A often coincided with those of the antibodies co-eluted by SDS. A more recent method named BioID that utilizes biotin ligase fused to a protein of interest to biotinylate proximal endogenous proteins can also be performed to screen for candidate interactors of ATP9A in living cells (Roux et al., 2013). Similar to ATP9A, Neo1p does not require

interaction with either Cdc50p or Lem3p of the yeast CDC50 proteins for ER exit and proper localization (Barbosa et al., 2010; Saito et al., 2004). However, a few studies have pointed out that Neo1p may interact with Dop1p and Ysl2p/Arl1p to modulate vesicle formation and organelle biogenesis in the endosomal system (Barbosa et al., 2010; Wicky et al., 2004). And another paper recently reported a novel membrane protein named Cfs1p to be partially co-localized with Drs2p and Neo1p in endosomal/late Golgi membranes (Yamamoto et al., 2017). These associating partners of Neo1p may be the interesting targets to look for and analyze for ATP9A.

Our results suggested that ATP9A had a slightly higher ATPase activity towards PS and PE than the other common membrane lipids, but the differences between wildtype and E195Q were only subtle, implicating that the activity and substrate specificity of wildtype ATP9A were too low to be characterized. ATP9A and ATP9B have been considered members of the  $P_4$ -ATPase family because they contain conserved sequences that typically serve as structural and functional domains, but whether they transport large lipid substrates, smaller ions, or other molecules remains unclear. The C-terminus of ATP8A2 has been proposed to contain an auto-inhibitor domain and an anti-auto-inhibitor domain, which serve to regulate the protein folding and flippase activity of ATP8A2 (Chalat et al., 2017). While the C-terminal tails of class 2  $P_4$ -ATPases are remarkably shorter than those of the other classes, their N-terminal regions are characteristically longer and have been suggested to contribute to their distinct subcellular localization. Further biochemical and functional characterization of N-terminal truncations of ATP9A and ATP9B will provide more insight into whether the N-terminus plays any regulatory role. Alternatively, they may be the outliers of P-type ATPases and simply do not possess any

ATP-dependent activity or catalyze transport of any kind. Class 2 of the ATP-binding cassette (ABC) transporter superfamily represents the “non-transporters” and are associated with DNA repair, translation, and antibiotic resistance (Davidson et al., 2008). Intriguingly, ATP9A was found to interact with  $\gamma$ -secretase in mouse primary hippocampal neurons and in rat brain membranes, and silencing ATP9A reduced the A $\beta$  levels by less than 20% (Inoue et al., 2015; Teranishi et al., 2015). Therefore, it would not be totally surprising if ATP9A was involved in non-transport-related processes in the brain or testis.

## **Chapter 3: Characterization of Na<sup>+</sup>/K<sup>+</sup>-ATPase (NKA) interactions with retinoschisin (RS1) in retina**

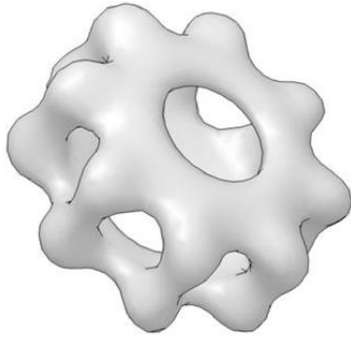
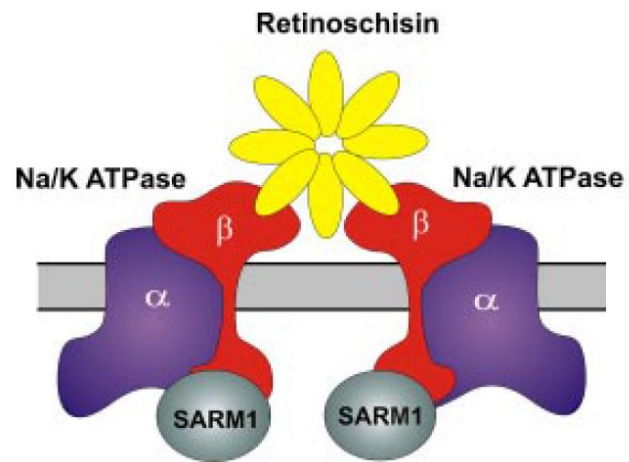
### **3.1 Introduction**

The retina is a light-sensitive tissue in the eye that triggers electrical signals sent to the brain through the optic nerve to ultimately generate vision. It consists of a layer of pigmented epithelial cells (RPE) and three layers of neurons—the photoreceptors, bipolar cells and ganglion cells—interconnected by two synaptic layers (Masland, 2012). The development of this distinct cellular architecture is essential for the efficient conversion of light into nerve impulses in the photoreceptors and the relay of these signals through the underlying neurons to the brain for image perception.

Much remains unknown about the molecular basis for generating the retinal cell organization. However, comparison between healthy and diseased retina indicates that retinoschisin, also known as RS1, serves as an adhesion protein and plays a crucial role in maintaining the cellular and synaptic structure of the retina. RS1 is a discoidin domain-containing protein specifically secreted from photoreceptors and bipolar cells. Over 130 mutations in the gene encoding RS1 are responsible for X-linked retinoschisis (XLRS), an early-onset macular degeneration in males that is characterized by separation of the inner retinal layers and disruption of the photoreceptor–bipolar synaptic signaling, leading to severe loss of vision (Bush et al., 2016; Tolun et al., 2016). RS1 contains a 23-amino acid signal peptide in the N-terminus and a 157-amino acid discoidin domain flanked by a 39-amino acid Rs1 domain and a short 5-amino acid C-terminus. It is assembled as a disulfide-linked homo-octameric complex

and observed under electron microscopy as two stacked rings with each ring resembling a cog-wheel structure with eight projections (Figure 3.1A) (Bush et al., 2016).

RS1 associates with retinal cell surface membranes by interacting with a complex consisting of the  $\alpha 3$  and  $\beta 2$  subunits of sodium-potassium ATPase ( $\text{Na}^+/\text{K}^+$ -ATPase, NKA) and a sterile alpha and TIR motif-containing protein named SARM1 (Figure 3.1B) (Molday et al., 2007). Control experiments further suggest that RS1 is required for the association between NKA and SARM1 and that NKA is the predominant protein for directly anchoring RS1 to the membranes of photoreceptors and bipolar cells.  $\text{Na}^+/\text{K}^+$ -ATPase belongs to Type II of the P-type ATPase superfamily and is an essential enzyme that utilizes energy from ATP hydrolysis to generate and maintain  $\text{Na}^+$  and  $\text{K}^+$  gradients across cellular membranes. It is a heterodimer composed of  $\alpha$  and  $\beta$  subunits that exist in various isoforms. The  $\alpha$  subunit harbours the catalytic site for ATP hydrolysis, and the  $\beta$  subunit is glycosylated and has a crucial role in the maturation and transport of the enzyme (Kathi Geering, 2008). Different  $\alpha/\beta$  combinations exist in specific tissues and cell populations. For example, the  $\alpha 3$  and  $\beta 2$  subunits are highly expressed in photoreceptor and bipolar cells (Wetzel et al., 1999).

**A****B**

**Figure 3.1 3-D reconstruction of RS1 and schematic representation of the RS1-NKA-SARM1 complex.**

(A) Tilted 3-D image of a stacked cog-wheel structure with the two rings interacting primarily at the outer edge. (B) RS1 binds to the  $\beta_2$  subunit of NKA and induces oligomerization of NKA and the recruitment and/or activation of SARM1 to the cytoplasmic region of NKA. Modified from Bush et al., 2016 and Molday et al., 2007.

Previous studies have proposed a model in which RS1 binds to an extracellular site of the Na<sup>+</sup>/K<sup>+</sup>-ATPase β2 subunit and thereby helps to maintain the structure, function and integrity of photoreceptors and bipolar cells. To gain more insights into the structural basis of the RS1-NKA interactions, good molecular tools for a pull-down of all the components of the complex from native tissues are essential. In this chapter of the thesis, a monoclonal antibody specific for the Na/K-ATPase β subunit was generated to achieve this purpose. Using specific antibodies against the β subunit and RS1, we aim to purify the endogenous protein complexes to allow for further functional characterization of the interactions and understanding of the pathogenesis of XLR5.

## **3.2 Materials and Methods**

### **3.2.1 Materials**

Na<sup>+</sup>/K<sup>+</sup>-ATPase α3 isoform (MA3-915) monoclonal antibody was purchased from Abcam (Cambridge, MA) and Na<sup>+</sup>/K<sup>+</sup>-ATPase β2 isoform polyclonal antibody was from Upstate-Millipore. Rho 1D4 monoclonal antibody and the anti-retinoschisin polyclonal antibody were produced in the lab as previously described (Molday et al., 2001; Mackenzie et al., 1984). Bovine rod outer segment (ROS) membranes frozen at -80°C were prepared previously by past members of the Molday Lab (Mackenzie et al., 1984; Wong & Molday, 1986). Additional materials and reagents are described in Chapter 2.2.

### **3.2.2 DNA constructs**

Human cDNA clone of Na<sup>+</sup>/K<sup>+</sup>-ATPase α3 in pENTER vector with a C-terminal Flag and His tag was purchased from ViGene Biosciences (Rockville, MD). Rat Na/K-ATPase α3 and bovine Na/K-ATPase β2 was separately cloned into pcDNA3 vector with a C-terminal 1D4 tag by Ms. Laurie Molday.

### **3.2.3 Immunoprecipitation of 1D4-tagged NKA $\beta$ 2 expressed in HEK293T**

The bovine NKA $\beta$ 2 construct with a C-terminal 1D4 tag was transfected alone or co-transfected with the rat NKA $\alpha$ 3 construct in HEK293T cells, which were solubilized in buffer A containing 50 mM HEPES-NaOH, pH 7.5, 150 mM NaCl, 5 mM MgCl<sub>2</sub>, 1 mM DTT, 20 mM CHAPS, 0.5 mg/mL DOPC, and 1X Protease Arrest, by stirring at 4°C for 30 min. The cell extracts were centrifuged at 40,000 rpm at 4°C for 10 min with a TLA-110 rotor in the Optima Ultracentrifuge. The soluble fraction in the supernatant was then incubated with Rho 1D4-Sepharose 2B beads pre-washed with 10 column volumes of buffer B containing 50 mM HEPES-NaOH, pH 7.5, 150 mM NaCl, 5 mM MgCl<sub>2</sub>, 1 mM DTT, 10 mM CHAPS, 0.5 mg/mL DOPC at 4°C for 2 hr. After binding, the beads were transferred into an Ultrafree-MC-HV centrifugal filter (Millipore, Billerica, MA) and washed six times with 500  $\mu$ L of buffer B. The bound proteins were eluted using 0.4 mg/mL 1D4 peptide in buffer B or 4% SDS in buffer B without DTT, with gentle agitation at 17°C for 1 hr. In the case where 9G9-Sepharose 2B column was used for immunoprecipitation, the bound proteins were eluted with 4% SDS in buffer B without DTT.

### **3.2.4 Generation of monoclonal antibodies against NKA $\beta$ 2**

Sequence encoding amino acids 1-28 in the N-terminus of bovine NKA $\beta$ 2 isoform was cloned into pGEX-4T1 vector (GE Healthcare) in frame with glutathione S-transferase using BamHI and XhoI sites. The coded peptide sequence is also conserved in human, rat and mouse clones of NKA $\beta$ 2. The GST-fused peptides were purified from *E. coli* on Glutathione Sepharose 4B (GE Healthcare) and injected into BALB/c mice around 10-weeks-old. One immunized mouse whose serum showed the strongest reactivity toward native NKA $\beta$ 2 proteins in bovine ROS and retinal membranes as tested on western blots was sacrificed for fusion. Hybridoma cell lines

were generated as previously described (Mackenzie & Molday, 1982) and the supernatants were screened for antibodies against prepared western blots of ROS and retinal membrane fractions. Monoclonal cell line NKA $\beta$ 2-9G9 was subcloned at least three times before expanded for growing large scale cultures, and the ascites fluid was collected as it is or purified through Protein G PLUS-Agarose matrix (Millipore).

### **3.2.5 Expression and purification of GST fusion proteins from *E. coli***

pGEX-4T1 plasmid containing Na<sup>+</sup>/K<sup>+</sup>-ATPase  $\beta$ 2 peptide sequence was transformed into BL21 competent cells and cells were plated on agar plates with ampicillin. A single colony was picked to grow in 5 mL LB at 37°C overnight and inoculated into a 500 mL LB culture the next day. The rest of the procedures for producing and purifying the GST-fused peptides were the same as described in Chapter 2.2.12.

### **3.2.6 Isolation of bovine retinal membranes**

Frozen bovine retinas were moved from -80°C to -30°C freezer overnight and placed on ice for thawing the following day. Ten retinas were homogenized in 6 mL of homogenization buffer containing 20 mM Tris-HCl, pH 7.4, 150 mM NaCl, 1 mM MgCl<sub>2</sub>, 1 mM CaCl<sub>2</sub>, and 1X Protease Arrest, while kept on ice for 20 min by pipetting up and down with a 1 mL tip cut at the end. The homogenized retinas were briefly spun at 3000 rpm for 1 min to collect debris, and the supernatant was transferred to a 50 mL conical tube on ice and passed through 22G needle twelve times. The tissue lysate was layered on top of 50% sucrose in Tris-buffered saline (TBS) and centrifuged at 22,000 rpm at 4°C for 1 hr in a SW28 swinging-bucket rotor in the Optima LE-80K Ultracentrifuge (Beckman Coulter). After the spin, membrane fraction on top of the 50% sucrose was collected and washed with at least five volumes of TBS. The membrane pellet was

resuspended in 500  $\mu$ L of 10% glycerol in resuspension buffer and aliquoted for short-term storage at  $-30^{\circ}\text{C}$ . Concentration of the retinal membrane fraction was determined using Pierce<sup>®</sup> BCA Protein Assay (Thermo Fisher Scientific).

### **3.2.7 Immunoprecipitation of NKA $\beta$ 2 from bovine retinal membranes**

Immunoprecipitation on bovine retinal membranes was carried out as previously described (Molday et al., 2007). Briefly, bovine retinal membranes (6 mg) were solubilized in 3.0 mL of solubilization buffer containing Tris-buffered saline (TBS) (25 mM Tris-HCl, pH 7.4, and 150 mM NaCl), 20 mM CHAPS, and 1X PA. After stirring at  $4^{\circ}\text{C}$  for 20 min, the membranes were centrifuged at 50,000 rpm for 10 min in a TLA110 rotor in the Optima Ultracentrifuge. CNBr-activated Sepharose 2B coupled to the monoclonal antibody 9G9 was pre-washed three times with column buffer containing 10 mM CHAPS in TBS. The supernatant was then incubated with pre-washed 9G9-Sepharose 2B beads by gently rotating at  $4^{\circ}\text{C}$  for 2 hr, and after six washes with the column buffer the bound proteins were eluted with freshly prepared 2% SDS in TBS at room temperature. The unbound fraction was further incubated with new, pre-washed 9G9 beads for binding at  $4^{\circ}\text{C}$  for 16 hours and proteins were eluted again with 2% SDS in TBS. A buffer only sample was included as a negative control. The solubilized membrane extracts and the elution fractions were analyzed on Coomassie blue-stained gels and western blots.

### **3.2.8 SDS-PAGE and western blot**

SDS-PAGE and western blot analysis were carried out as described in Chapter 2.2.17. The monoclonal antibodies as ascites fluids were used at the following dilutions: Rho 1D4 at 1:100 and NKA $\beta$ 2-9G9 at neat. The anti-RS1 polyclonal antibody was diluted at 1:1000. The commercial antibody of NKA $\beta$ 2 was diluted at 1:200 and NKA $\alpha$ 3 at 1:1000.

### 3.3 Results

#### 3.3.1 Expression of NKA $\beta$ 2 in HEK293T and in bovine retina

A plasmid containing NKA $\beta$ 2 with a C-terminal 1D4 tag was expressed with or without another plasmid of NKA $\alpha$ 3 in HEK293T cells to see if sufficient proteins could be immunoprecipitated and detected by western blot. The CHAPS-solubilized cell extracts were incubated with Rho 1D4-Sepharose 2B column and the bound proteins were eluted with 1D4 peptide. A broad and probably heterogeneous band around 50 kDa corresponding to the size of NKA $\beta$ 2 was seen in the elution fraction from both cells with or without the co-expression of NKA $\alpha$ 3, suggesting that NKA $\beta$ 2 was heavily glycosylated (Figure 3.1A). Western blots of the elution were later labeled with 1D4 antibody to serve as positive controls during the process of screening for the in-house monoclonal antibody against NKA $\beta$ 2.

The  $\beta$ 2 and  $\alpha$ 3 subunits of NKA have been reported to express in photoreceptor and bipolar cells in adult mouse and rat, with the highest expression in the inner segment, outer plexiform, and inner nuclear layers and a more moderate level in the outer nuclear and inner plexiform layers (Molday et al., 2007; Wetzell et al., 1999). In order to prepare sufficient amounts of materials for the screening of monoclonal antibodies against NKA $\beta$ 2, membranes of bovine whole retinas or rod outer segment (ROS) were prepared and analyzed on western blots using the commercial NKA $\beta$ 2 antibody (Upstate-Millipore) suitable for labeling. Both  $\beta$ 2 and  $\alpha$ 3 subunits of NKA were more enriched in the retinal membranes than in ROS membranes, whereas rhodopsin as labeled by 1D4 antibody was more abundant in ROS (Figure 3.1B). Therefore, western blot strips of retinal membranes were prepared in large quantities (>2000 strips) for the screening later.

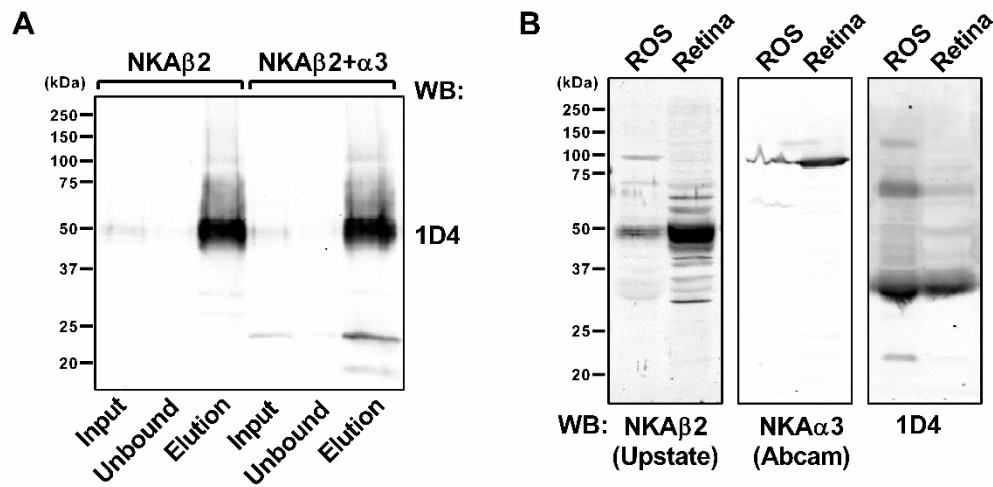


**Figure 3.2 Expression of NKAβ2 in transfected HEK293T cells and bovine retina.**

(A) HEK293T cells expressing 1D4-tagged NKAβ2 alone or with NKAα3 were solubilized with CHAP and immunoprecipitated on Rho 1D4-Sepharose 2B column. The cell extracts (Input), unbound fractions (Unbound), and the bound proteins eluted with 1D4 peptide (Elution) were analyzed on western blots labeled with 1D4 antibody. (B) Membranes were prepared from bovine whole retinas or rod outer segment (ROS) and analyzed on western blots using specific antibodies as indicated. 40 μg of total protein was loaded in each lane.

### 3.3.2 Purification of GST-NKA $\beta$ 2<sub>1-28</sub> peptide from *E. coli*

NKA $\beta$ 2 peptides spanning amino acids 1-28 fused to GST were expressed in *E. coli* and purified using Glutathione Sepharose 4B column. The glutathione-eluted fractions were analyzed on Coomassie blue-stained SDS-polyacrylamide gels to check protein purity and integrity (Figure 3.2). Purified GST was included as a control and the fusion peptides containing NKA $\beta$ 2<sub>1-28</sub> ran slightly above the GST-only band as expected. The peptides were then dialyzed in PBS and stored for immunization of mice.

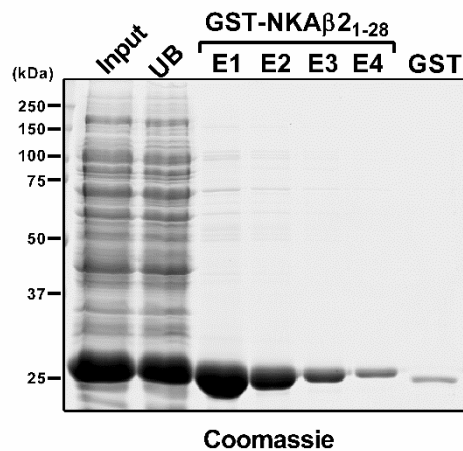


**Figure 3.3 Purification of GST-NKA $\beta$ 2<sub>1-28</sub> from *E. coli*.**

GST-fused NKA $\beta$ 2<sub>1-28</sub> peptides expressed in *E. coli* were extracted by sonication and purified on Glutathione Sepharose 4B column. The peptides were eluted four times consecutively from the column with glutathione. The cell lysates (Input), unbound fraction (UB), elution fractions (E1-E4), and a purified GST only control were analyzed on Coomassie blue-stained gel.

### **3.3.3 Characterization of the in-house monoclonal antibody NKA $\beta$ 2-9G9**

GST-NKA $\beta$ 2<sub>1-28</sub> peptides targeting the cytoplasmic N-terminus were injected to immunize BALB/c mice and the produced antibodies were screened on western blot strips of bovine retinal membranes for the most specific and highest affinity monoclonal cell lines. One monoclonal cell line designated as NKA $\beta$ 2-9G9 was chosen for purification and further characterization. 1D4-tagged NKA $\beta$ 2 in transfected HEK293T cells were solubilized and immunoprecipitated with Sepharose 2B beads coupled to purified 1D4 antibody or 9G9 antibody. On western blots, 9G9 labeled the expressed NKA $\beta$ 2 proteins in cell extracts and in SDS-eluted fractions, although the labeling appeared much less efficient than that of 1D4 antibody for the same amounts of proteins (Figure 3.3). Also, 9G9-Sepharose 2B column was tested for its binding affinity for the 1D4-tagged NKA $\beta$ 2 proteins expressed in HEK293T cells by immunoprecipitation, and the pull-down efficiency of 9G9 column was significantly lower than that of 1D4 column, as many NKA $\beta$ 2 proteins were still detected in the unbound fraction. The in-house 9G9 antibody indeed recognizes and immunoprecipitates the expressed NKA $\beta$ 2 proteins although with a lower binding affinity when compared to 1D4 antibody.

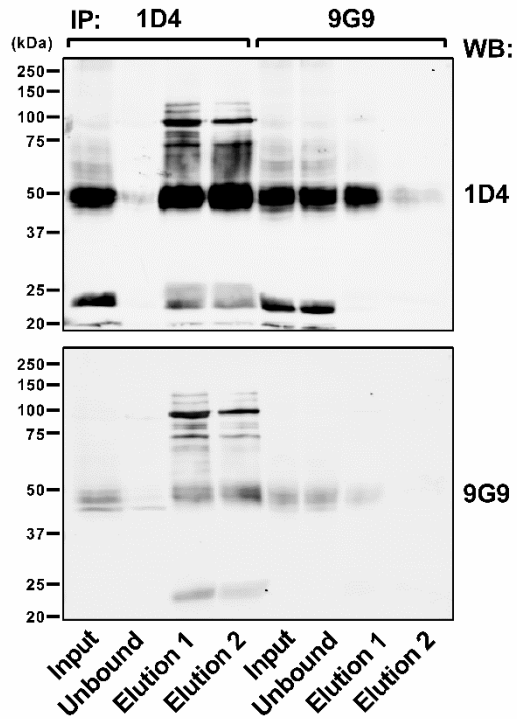


**Figure 3.4 Characterization of the in-house NKA $\beta$ 2-9G9 antibody.**

HEK293T cells expressing 1D4-tagged NKA $\beta$ 2 were solubilized with CHAPS and immunoprecipitated with Sepharose 2B beads coupled to purified 1D4 or 9G9 antibody. The cell extracts (Input), unbound fraction (Unbound), and bound proteins in SDS-eluted fractions (Elution) were analyzed on western blots labeled with 1D4 or 9G9 antibody.

### **3.3.4 Co-immunoprecipitation of the RS1-NKA complex from bovine retina**

Interactions between RS1 and the  $\beta 2$  and  $\alpha 3$  subunits of NKA have been demonstrated in both human and bovine retina using a monoclonal antibody specific for RS1 (3R10) (Molday et al., 2007). To examine the ability of 9G9 antibody to pull-down NKA $\beta 2$  as well as the associating proteins in the complex, bovine retinal membranes were solubilized and immunoprecipitated with Sepharose 2B beads conjugated to 9G9 antibody. Proteins in the bound fractions were eluted from the column with 2% SDS and analyzed by western blot. After binding for 2 hours, NKA $\beta 2$  and  $\alpha 3$  as well as RS1 were all detected in the first elution (Figure 3.4). All interacting proteins were more enriched in the second elution after incubating with 9G9 beads overnight when compared to binding for 2 hours. On Coomassie blue-stained gel, a clean band at 100 kDa around the size NKA $\alpha 3$  was seen in the first elution and in addition, numerous smeary bands around 50 kDa appeared in the second elution, which might correspond to the glycosylated NKA $\beta 2$  also seen at a higher level on the western blot.

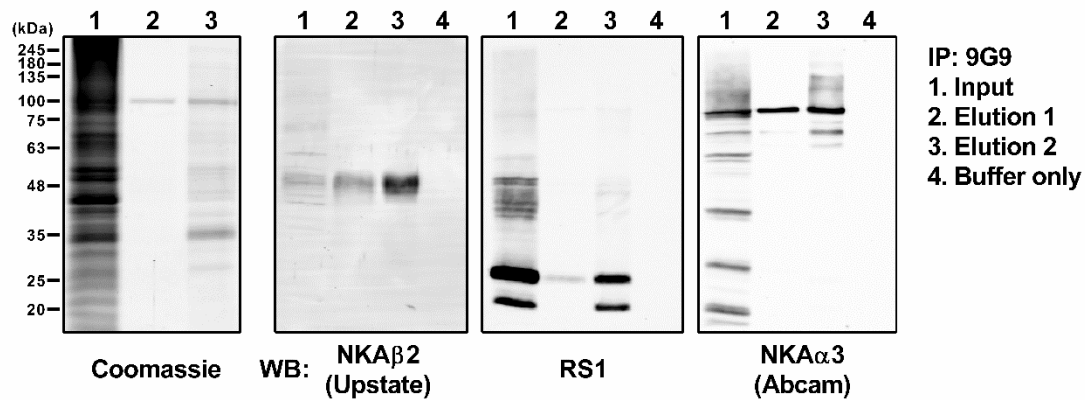


**Figure 3.5 Co-immunoprecipitation of RS1-NKA from bovine retina.**

Bovine retinal membranes were solubilized with CHAPS and the extracts (Lane 1) were incubated with 9G9-Sepharose 2B column for immunoprecipitation. The bound proteins were eluted with 2% SDS after incubation for 2 hours (Lane 2) and subsequently for 16 hours (Lane 3). A buffer only control was included for immunoprecipitation. SDS-polyacrylamide gels were stained with Coomassie blue or transferred onto PVDF membranes for western blot analysis with specific antibodies against NKA $\beta$ 2, RS1, and NKA $\alpha$ 3.

### 3.4 Discussion

Retinoschisin (RS1) is generally believed to serve as a retinal cell adhesion protein that plays a crucial role in maintaining the normal function and structural organization of the retina (Weber et al., 2002). Mice deficient in RS1 display various abnormal phenotypes in the retina, including disorganized retinal structure, disrupted photoreceptor-bipolar synapse, and progressively degenerated rod and cone photoreceptors. RS1 is expressed and secreted from photoreceptors and bipolar cells and associates with the surface of rod and cone photoreceptors (Grayson et al., 2000; Molday et al., 2001; Reid et al., 2003, 1999). The discoidin domain of RS1 implicates its interaction with lipids in the membranes of the photoreceptors; however, previous studies have provided evidence that RS1 is anchored to the surface of these cells through the formation of a protein complex with Na<sup>+</sup>/K<sup>+</sup>-ATPase (NKA) and sterile alpha and TIR motif—containing protein (SARM1) (Molday et al., 2007).  $\alpha 3$  and  $\beta 2$  were the major isoforms of NKA identified in a mass spectrometric analysis using an anti-RS1 immunoaffinity matrix, and their interactions were confirmed by western blot analysis of the co-immunoprecipitated fractions. In addition, immunofluorescence imaging of mouse retinal cryosections labeled with specific antibodies showed the co-localization of NKA $\alpha 3$  with RS1 and SARM1. Further characterization of NKA $\beta 2$  knockout mice has shown that the protein levels of NKA $\alpha 3$  and RS1, but not SARM1, are significantly reduced in crude retinal membranes and that both NKA $\alpha 3$  and  $\beta 2$  are required for the binding of exogenously supplied RS1 to crude membranes, indicating a predominant role of NKA in anchoring RS1 to retinal cell surface (Friedrich et al., 2011).

While RS1 forms a complex with the assembled  $\alpha 3\beta 2$  isoforms of NKA, it mostly likely interacts with the  $\beta 2$  subunit for directly anchoring to the cell surface. The  $\beta 2$  subunit contains up to nine glycosylation sites within its large C-terminal region (E Tokhtaeva et al., 2010). Like other discoidin domain-containing proteins, retinoschisin has an affinity for galactose, which can be used for the biosynthesis of oligosaccharide chains during glycosylation of proteins (Raju et al., 2001; Simpson et al., 1974). In contrast, the  $\alpha 3$  subunit contains much shorter extracellular loops which are less available for binding. Therefore, NKA $\beta 2$  is the prime candidate for direct association with RS1.

In this study, we generated a monoclonal antibody 9G9 specific to NKA $\beta 2$  targeting to amino acid 1-28 of the N-terminus. When compared to an immunoaffinity matrix coupled to Rho 1D4 for immunoprecipitating 1D4-tagged NKA $\beta 2$  expressed in HEK293T cells, the 9G9 antibody showed a binding affinity about half as strong. Nonetheless, 9G9-Sepharose 2B column was used to successfully purify endogenous NKA $\beta 2$  along with its associating proteins NKA $\alpha 3$  and RS1 from bovine retinal membranes. And the efficiency of binding NKA $\beta 2$  was increased when the incubation period was extended to 16 hours. These results were consistent with the reported findings on the interactions between RS1 and NKA in the retina.

Na<sup>+</sup>/K<sup>+</sup>-ATPase activity consumes about 30% of total energy in the body, and approximately 50% of the energy in the retina (Medrano & Fox, 1995; Wetzel et al., 1999). NKA uses energy released from ATP hydrolysis to regulate the Na<sup>+</sup> and K<sup>+</sup> gradients associated with critical retinal processes including the dark current in the photoreceptors, action potentials in the ganglion cells, neurotransmission in Müller cells, and synaptic activity (Murphy & Crewther, 2013). Inhibition of NKA activity by ouabain has been shown to alter the resting potential of the

optic nerve and disrupt the normal morphology of the inner plexiform layer, which then affect the electrophysiological properties of the outer retinal response to a light stimulus (Medrano & Fox, 1995; Van Harreveld & Fikova, 1972). While low concentrations of ouabain selectively damage the cells in inner nuclear layer and ganglion layer, higher ouabain concentrations completely destroy the retina (Fimbel et al., 2007; Maier & Wolburg, 1979; Sherpa et al., 2008). Whether the activity of NKA exists apart from its interaction with RS1 or is in turn modulated by this interaction is unclear and demands a better understanding of the physiological function of RS1. The presence of fluid-filled cystic cavities in mice deficient in RS1 implicates that defective NKA could result in fluid imbalance and the disruption of cellular organization and synaptic integrity of the retina as found in XLRS patients (Xu et al., 2010).

The current and previous studies have provided preliminary analysis of the relationship between components of the RS1-NKA-SARM1 complex in retina. The causative mutations in the RS1-encoding gene emphasize the critical role of functional RS1 as well as its associating proteins in maintaining normal retinal physiology. In order to determine the mechanism underlying the complex formation and to study its significance in the structural and functional basis of healthy and diseased retina, further characterization of the endogenous protein complex from native retinal tissues using highly specific antibodies for each component is necessary.

## Chapter 4: Conclusion and future directions

ATP9A belongs to class 2 of the  $P_4$ -ATPases and is highly expressed in the brain and testis. Although very little is known about ATP9A, the importance of its role in cellular functions and disease is highlighted by the fact that its ortholog Neo1p in yeast is essential for cell growth. Several  $P_4$ -ATPases have been demonstrated to flip phospholipids from the exoplasmic to the cytoplasmic leaflet of cell membranes (Andersen et al., 2016). While ATP9A and Neo1p have been shown to be involved in vesicle trafficking in the Golgi-endosomal system, studies on their ATP-dependent flippase activities have been lacking. On the other hand,  $Na^+/K^+$ -ATPase (NKA) of type 2C of the P-type ATPases is known to have a crucial role in normal retinal function and structure by establishing low intracellular  $Na^+$  and high internal  $K^+$  concentrations across the membranes (Murphy & Crewther, 2013). NKA has also been identified to interact with retinoschisin (RS1), a retinal cell adhesion protein that when mutated can cause X-linked retinoschisis (XLRs) (Molday et al., 2007). XLRs is a macular degeneration that leads to disintegration of the inner retinal layers and progressive loss in vision. RS1 is anchored to the membranes of photoreceptor and bipolar cells mostly likely through direct binding with the  $\beta 2$  subunit and it serves to maintain the structural and function integrity of the retina and the photoreceptor-bipolar synapse.

Chapter 2 of the current thesis described the characterization of human ATP9A expressed in HEK293T cells. First, expression analysis was done on ATP9A wildtype and various mutants which presumably yield impaired ATP9A and have been used in previous studies for comparing the activities with the wildtype. E195Q mutant showed proper protein folding and subcellular localization to target membrane compartments as the wildtype, whereas D391N was

misfolded and co-localized with the ER. Mutations of I345 in ATP9A, corresponding to the CAMRQ disease-causing counterparts in ATP8A2, produced incompletely folded proteins that were retained in the ER. Next, ATPase activities of ATP9A wildtype and E195Q were examined by the colourimetric and luminescent method. Both wildtype and E195Q showed only minimal lipid-activated activities about 10 to 20-fold lower than that of the well-established ATP8A2. Differences between the wildtype and E195Q mutant were negligible, indicating a lack of activation of the wildtype proteins. Subsequently, ATP9A was found to be phosphorylated with radioactive [ $\gamma$ - $^{32}\text{P}$ ]-ATP and the aspartyl phosphoenzyme intermediate was sensitive to hydroxylamine treatment, which is characteristic of all P-type ATPases. These observations indicate that ATP9A undergoes autophosphorylation but fails to dephosphorylate. Further cell-based flippase assay avoiding the use of detergent showed that the activities of ATP9A towards PS, PE, and PC, were similar to the background from untransfected cells. A monoclonal antibody exhibiting high specificity and binding affinity for ATP9A was developed and characterized. Preliminary purification of endogenous ATP9A from mouse brain membranes using this 10D1 antibody was difficult to analyze as the bands of ATP9A and co-eluted antibodies were often very close. To gain more insight into the physiological and functional properties of ATP9A, future work will focus on identifying potential accessory proteins required for the ATP-dependent activity of ATP9A and defining its substrate specificity in native tissues.

In Chapter 3, a monoclonal antibody specific for the  $\beta 2$  subunit of  $\text{Na}^+/\text{K}^+$ -ATPase (NKA) was generated and employed to further characterize the complex formation of NKA with RS1 in the retina. Our study showed that immunoaffinity purification of NKA $\beta 2$  from retinal membranes indeed co-precipitated the  $\alpha 3$  subunit and RS1. Whether RS1 is anchored to the surface of

retinal cells through direct binding with the glycosylated extracellular C-terminus of NKA $\beta$ 2 requires more detailed investigation. It has been implicated that the ion transport activity of NKA may be regulated by its interaction with RS1, the defects of which lead to disrupted cellular organization and function of the retina and the formation of fluid-filled cystic cavities (Weber et al., 2002; Xu et al., 2010). Using monoclonal antibodies specific to each component of the RS1-NKA-SARM1 complex in tandem immunoaffinity purification will hopefully isolate the native protein complex from retinal tissues. Structural properties of the assembly can then be obtained with cryo-electron microscopy (cryo-EM). In addition, careful experimental design will be required for elucidating the relationship between the activity of NKA and the adhesion function of RS1. Studying the mechanism of the protein complex formation will provide basis for understanding the roles of the individual components in maintaining retinal function and integrity as well as in the pathogenesis underlying XLRS.

In summary, this thesis has presented a novel and extensive characterization of ATP9A in terms of its ATPase and flippase activities. Having shown that ATP9A forms the characteristic phosphorylated intermediate E1P, we aim to perform further studies to discover the critical factors and optimal experimental conditions required for its activation. Prospects for developing therapeutic tools for treating individuals affected with XLRS rely on understanding of the effects of the disease-causing RS1 mutants in the retina. Specific antibodies for RS1 and its interacting partners NKA like the one generated in this study will be useful for purifying native intact protein complexes for further functional and structural characterization.

## References

- Andersen, J. P., Vestergaard, A. L., Mikkelsen, S. A., Mogensen, L. S., Chalat, M., & Molday, R. S. (2016). P4-ATPases as phospholipid flippases-structure, function, and enigmas. *Frontiers in Physiology*, *7*(275).
- Ansari, I. U. H., Longacre, M. J., Paulusma, C. C., Stoker, S. W., Kendrick, M. A., & MacDonald, M. J. (2015). Characterization of P4 ATPase phospholipid translocases (flippases) in human and rat pancreatic beta cells: Their gene silencing inhibits insulin secretion. *Journal of Biological Chemistry*, *290*(38), 23110–23123.
- Baldrige, R. D., & Graham, T. R. (2012). Two-gate mechanism for phospholipid selection and transport by type IV P-type ATPases. *Proceedings of the National Academy of Sciences*, *110*(5), E358–E367.
- Barbosa, S., Pratte, D., Schwarz, H., Pipkorn, R., & Singer-Krüger, B. (2010). Oligomeric Dop1p is part of the endosomal Neo1p-Ysl2p-Arl1p membrane remodeling complex. *Traffic*, *11*(8), 1092–106.
- Blanco, G., & Mercer, R. W. (1998). Isozymes of the Na-K-ATPase: heterogeneity in structure, diversity in function. *The American Journal of Physiology, Renal Physiology*, *275*(5 Pt 2), F633–F650.
- Bretscher, M. S. (1972). Asymmetrical lipid bilayer structure for biological membranes. *Nature*, *236*, 11–12.
- Bryde, S., Hennrich, H., Verhulst, P. M., Devaux, P. F., Lenoir, G., & Holthuis, J. C. M. (2010). CDC50 proteins are critical components of the human class-1 P4-ATPase transport machinery. *The Journal of Biological Chemistry*, *285*(52), 40562–72.
- Bublitz, M., Morth, J. P., & Nissen, P. (2011). P-type ATPases at a glance. *Journal of Cell Science*, *124*(22), 3917–3917.
- Bull, L. N., van Eijk, M. J., Pawlikowska, L., DeYoung, J. A., Juijn, J. A., Liao, M., Klomp, L. W., Lomri, N., Berger, R., Scharschmidt, B. F., Knisely, A. S., Houwen, R. H., & Freimer, N. B. (1998). A gene encoding a P-type ATPase mutated in two forms of hereditary cholestasis. *Nature Genetics*, *18*, 219–224.
- Bush, M., Setiapatra, D., Yip, C. K., & Molday, R. S. (2016). Cog-wheel octameric structure of RS1, the discoidin domain containing retinal protein associated with X-linked retinoschisis. *PLoS ONE*, *11*(1), e0147653.
- Cacciagli, P., Haddad, M.-R., Mignon-Ravix, C., El-Waly, B., Moncla, A., Missirian, C., Chabrol, B., & Villard, L. (2010). Disruption of the ATP8A2 gene in a patient with a t(10;13) de novo balanced translocation and a severe neurological phenotype. *European Journal of Human Genetics*, *18*(12), 1360–1363.
- Cai, S. Y., Gautam, S., Nguyen, T., Soroka, C. J., Rahner, C., & Boyer, J. L. (2009). ATP8B1 deficiency

- disrupts the bile canalicular membrane bilayer structure in hepatocytes, but FXR expression and activity are maintained. *Gastroenterology*, 136(3), 1060–1069.
- Chalat, M., Moleschi, K., & Molday, R. S. (2017). C-terminus of the P4-ATPase ATP8A2 functions in protein folding and regulation of phospholipid flippase activity. *Molecular Biology of the Cell*, 28(3), 452–462.
- Chaubey, P. M., Hofstetter, L., Roschitzki, B., & Stieger, B. (2016). Proteomic analysis of the rat canalicular membrane reveals expression of a complex system of P4-ATPases in liver. *PLoS ONE*, 11(6), e0158033.
- Chen, C., & Okayama, H. (1987). High-efficiency transformation of mammalian cells by plasmid DNA. *Molecular and Cellular Biology*, 7(8), 2745–2752.
- Chifflet, S., Torriglia, a., Chiesa, R., & Tolosa, S. (1988). A method for the determination of inorganic phosphate in the presence of labile organic phosphate and high concentrations of protein: Application to lens ATPases. *Analytical Biochemistry*, 168(1), 1–4.
- Coleman, J. A., Kwok, M. C. M., & Molday, R. S. (2009). Localization, purification, and functional reconstitution of the P4-ATPase Atp8a2, a phosphatidylserine Flippase in photoreceptor disc membranes. *Journal of Biological Chemistry*, 284(47), 32670–32679.
- Coleman, J. A., Zhu, X., Djajadi, H. R., Molday, L. L., Smith, R. S., Libby, R. T., John, S. W. M., & Molday, R. S. (2014). Phospholipid flippase ATP8A2 is required for normal visual and auditory function and photoreceptor and spiral ganglion cell survival. *Journal of Cell Science*, 127(5), 1138–1149.
- Coleman, J. a, & Molday, R. S. (2011). Critical role of the beta-subunit CDC50A in the stable expression, assembly, subcellular localization, and lipid transport activity of the P4-ATPase ATP8A2. *The Journal of Biological Chemistry*, 286(19), 17205–16.
- Coleman, J. a, Quazi, F., & Molday, R. S. (2013). Mammalian P4-ATPases and ABC transporters and their role in phospholipid transport. *Biochimica et Biophysica Acta*, 1831(3), 555–74.
- Coleman, J. a, Vestergaard, A. L., Molday, R. S., Vilsen, B., & Andersen, J. P. (2012). Critical role of a transmembrane lysine in aminophospholipid transport by mammalian photoreceptor P4-ATPase ATP8A2. *Proceedings of the National Academy of Sciences of the United States of America*, 109(5), 1449–54.
- Cox, B., & Emili, A. (2006). Tissue subcellular fractionation and protein extraction for use in mass-spectrometry-based proteomics. *Nature Protocols*, 1(4), 1872–1878.
- Cuatrecasas, P. (1970). Protein Purification by Affinity Chromatography. *Journal of Biochemical and Biophysical Methods*, 245(12), 3059–3065.
- Dalton, L. E., Bean, B. D. M., Davey, M., & Conibear, E. (2017). Quantitative high-content imaging identifies novel regulators of Neo1 trafficking at endosomes. *Molecular Biology of the Cell*, 28, mbc.E16-11-0772.
- Davidson, A. L., Dassa, E., Orelle, C., & Chen, J. (2008). Structure, Function, and Evolution of

- Bacterial ATP-Binding Cassette Systems. *Microbiology and Molecular Biology Reviews*, 72(2), 317–364.
- Devaux, P. F. (1991). Static and dynamic lipid asymmetry in cell membranes. *Biochemistry*, 30(5), 1163–1173.
- Dhar, M. S., Sommardahl, C. S., Kirkland, T., Nelson, S., Donnell, R., Johnson, D. K., & Castellani, L. W. (2004). Mice heterozygous for *Atp10c*, a putative amphipath, represent a novel model of obesity and type 2 diabetes. *The Journal of Nutrition*, 134(4), 799–805.
- Dhar, M. S., Yuan, J. S., Elliott, S. B., & Sommardahl, C. (2006). A type IV P-type ATPase affects insulin-mediated glucose uptake in adipose tissue and skeletal muscle in mice. *Journal of Nutritional Biochemistry*, 17(12), 811–820.
- Ding, J., Wu, Z., Crider, B. P., Ma, Y., Li, X., Slaughter, C., Gong, L., & Xie, X. S. (2000). Identification and functional expression of four isoforms of ATPase II, the putative aminophospholipid translocase: Effect of isoform variation on the ATPase activity and phospholipid specificity. *Journal of Biological Chemistry*, 275, 23378–23386.
- Eppens, E. F., Van Mil, S. W. C., De Vree, J. M. L., Mok, K. S., Juijn, J. A., Oude Elferink, R. P. J., Berger, R., Houwen, R. H. J., & Klomp, L. W. J. (2001). FIC1, the protein affected in two forms of hereditary cholestasis, is localized in the cholangiocyte and the canalicular membrane of the hepatocyte. *Journal of Hepatology*, 35(4), 436–443.
- Fimbel, S. M., Montgomery, J. E., Burket, C. T., & Hyde, D. R. (2007). Regeneration of Inner Retinal Neurons after Intravitreal Injection of Ouabain in Zebrafish. *Journal of Neuroscience*, 27(7), 1712–1724.
- Flamant, S., Pescher, P., Lemerrier, B., Clément-Ziza, M., Képès, F., Fellous, M., Milon, G., Marchal, G., & Besmond, C. (2003). Characterization of a putative type IV aminophospholipid transporter P-type ATPase. *Mammalian Genome*, 14(1), 21–30.
- Folmer, D. E., Elferink, R. P. J. O., & Paulusma, C. C. (2009). P4 ATPases - lipid flippases and their role in disease. *Biochimica et Biophysica Acta*, 1791(7), 628–35.
- Folmer, D. E., Van Der Mark, V. A., Ho-Mok, K. S., Oude Elferink, R. P. J., & Paulusma, C. C. (2009). Differential effects of progressive familial intrahepatic cholestasis type 1 and benign recurrent intrahepatic cholestasis type 1 mutations on canalicular localization of ATP8B1. *Hepatology*, 50(5), 1597–1605.
- Friedrich, U., Stöhr, H., Hilfinger, D., Loenhardt, T., Schachner, M., Langmann, T., & Weber, B. H. F. (2011). The Na/K-ATPase is obligatory for membrane anchorage of retinoschisin, the protein involved in the pathogenesis of X-linked juvenile retinoschisis. *Human Molecular Genetics*, 20(6), 1132–42.
- García-Sánchez, S., Sánchez-Cañete, M. P., Gamarro, F., & Castanys, S. (2014). Functional role of evolutionarily highly conserved residues, N-glycosylation level and domains of the *Leishmania* miltefosine transporter-Cdc50 subunit. *The Biochemical Journal*, 459(1), 83–94.

- Geering, K. (2001). The functional role of  $\beta$  subunits in oligomeric P-type ATPases. *Journal of Bioenergetics and Biomembranes*, 33(5), 425–438.
- Geering, K. (2008). Functional roles of Na<sup>+</sup>, K<sup>+</sup>-ATPase subunits. *Current Opinion in Nephrology and Hypertension*, 17, 526–532.
- Gong, E. Y., Park, E., Lee, H. J., & Lee, K. (2009). Expression of Atp8b3 in murine testis and its characterization as a testis specific P-type ATPase. *Reproduction*, 137(2), 345–351.
- González-Romo, P., Sánchez-Nieto, S., & Gavilanes-Ruíz, M. (1992). A modified colorimetric method for the determination of orthophosphate in the presence of high ATP concentrations. *Analytical Biochemistry*, 200(2), 235–238.
- Gordesky, S. E., & Marinetti, G. V. (1973). The asymmetric arrangement of phospholipids in the human erythrocyte membrane. *Biochemical and Biophysical Research Communications*, 50(4), 1027–1031.
- Grayson, C., Reid, S. N., Ellis, J. a, Rutherford, A., Sowden, J. C., Yates, J. R., Farber, D. B., & Trump, D. (2000). Retinoschisin, the X-linked retinoschisis protein, is a secreted photoreceptor protein, and is expressed and released by Weri-Rb1 cells. *Human Molecular Genetics*, 9(12), 1873–1879.
- Halleck, M. S., Pradhan, D., Blackman, C., Berkes, C., Williamson, P., & Schlegel, R. A. (1998). Multiple members of a third subfamily of P-type ATPases identified by genomic sequences and ESTs. *Genome Research*, 8(4), 354–361.
- Hogart, A., Patzel, K. A., & LaSalle, J. M. (2008). Gender influences monoallelic expression of ATP10A in human brain. *Human Genetics*, 124(3), 235–242.
- Hua, Z., Fatheddin, P., & Graham, T. R. (2002). An Essential Subfamily of Drs2p-related P-Type ATPases Is Required for Protein Trafficking between Golgi Complex and Endosomal / Vacuolar System, 13(September), 3162–3177.
- Huang, B. X., Akbar, M., Kevala, K., & Kim, H. Y. (2011). Phosphatidylserine is a critical modulator for Akt activation. *Journal of Cell Biology*, 192(6), 979–992.
- Inoue, M., Hur, J.-Y., Kihara, T., Teranishi, Y., Yamamoto, N. G., Ishikawa, T., Wiehager, B., Winblad, B., Tjernberg, L. O., & Schedin-Weiss, S. (2015). Human brain proteins showing neuron-specific interactions with  $\gamma$ -secretase. *The FEBS Journal*, 282(14), 2587–99.
- Jensen, M. S., Costa, S., Günther-pomorski, T., & López-marqués, R. L. (2016). Cell-based lipid flippase assay employing fluorescent lipid derivatives, 1377, 371–382.
- Jørgensen, P. L. (1986). Structure, function and regulation of Na,K-ATPase in the kidney. *Kidney International*, 29(1), 10–20.
- Kato, U., Inadome, H., Yamamoto, M., Emoto, K., Kobayashi, T., & Umeda, M. (2013). Role for phospholipid flippase complex of ATP8A1 and CDC50A proteins in cell migration. *Journal of Biological Chemistry*, 288, 4922–4934.

- Kühlbrandt, W. (2004). Biology, structure and mechanism of P-type ATPases. *Nature Reviews. Molecular Cell Biology*, 5(4), 282–95.
- Lee, S., Uchida, Y., Wang, J., Matsudaira, T., Nakagawa, T., Kishimoto, T., Mukai, K., Inaba, T., Kobayashi, T., Molday, R. S., Taguchi, T., & Arai, H. (2015). Transport through recycling endosomes requires EHD 1 recruitment by a phosphatidylserine translocase, 34(5), 669–688.
- Lenoir, G., Williamson, P., Puts, C. F., & Holthuis, J. C. M. (2009). Cdc50p plays a vital role in the ATPase reaction cycle of the putative aminophospholipid transporter Drs2p. *The Journal of Biological Chemistry*, 284(27), 17956–67.
- Levano, K., Punia, V., Raghunath, M., Debata, P. R., Curcio, G. M., Mogha, A., Purkayastha, S., McCloskey, D., Fata, J., & Banerjee, P. (2012). Atp8a1 deficiency is associated with phosphatidylserine externalization in hippocampus and delayed hippocampus-dependent learning. *Journal of Neurochemistry*, 120(2), 302–13.
- Li, H., Wetten, S., Li, L., St. Jean, P. L., Upmanyu, R., Surh, L., Hosford, D., Barnes, M. R., Briley, J. D., Borrie, M., Coletta, N., Delisle, R., Dhalla, D., Ehm, M. G., Feldman, H. H., Fornazzari, L., Gauthier, S., ... Roses, A. D. (2008). Candidate Single-Nucleotide Polymorphisms From a Genomewide Association Study of Alzheimer Disease. *Archives of Neurology*, 65(1), 45–53.
- Longo, P. A., Kavran, J. M., Kim, M. S., & Leahy, D. J. (2013). Transient mammalian cell transfection with polyethylenimine (PEI). *Methods in Enzymology*, 529, 227–240.
- López-Marqués, R. L., Poulsen, L. R., Hanisch, S., Meffert, K., Buch-Pedersen, M. J., Jakobsen, M. K., Pomorski, T. G., & Palmgren, M. G. (2010). Intracellular targeting signals and lipid specificity determinants of the ALA/ALIS P4-ATPase complex reside in the catalytic ALA alpha-subunit. *Molecular Biology of the Cell*, 21, 791–801.
- Lopez-Marques, R. L., Theorin, L., Palmgren, M. G., & Pomorski, T. G. (2014). P4-ATPases: lipid flippases in cell membranes. *Pflügers Archiv: European Journal of Physiology*, 466(7), 1227–40.
- Machnicka, B., Czogalla, A., Hryniewicz-Jankowska, A., Bogusławska, D. M., Grochowalska, R., Heger, E., & Sikorski, A. F. (2014). Spectrins: A structural platform for stabilization and activation of membrane channels, receptors and transporters. *Biochimica et Biophysica Acta - Biomembranes*, 1838(2), 620–634.
- Mackenzie, D., Arendt, A., Hargrave, P., Mcdowell, J. H., & Molday, R. S. (1984). Localization of Binding Sites for Carboxyl Terminal Specific Anti-Rhodopsin Monoclonal Antibodies Using Synthetic Peptides<sup>1</sup>, (1982), 6544–6549.
- Mackenzie, D., & Molday, R. S. (1982). Organization of Rhodopsin and a High Molecular Weight , Glycoprotein. *Biological Chemistry*, (12), 7100–7105.
- Maier, W., & Wolburg, H. (1979). Regeneration of the goldfish retina after exposure to different doses of ouabain. *Cell and Tissue Research*, 202(1), 99–118.

- Masland, R. H. (2012). The Neuronal Organization of the Retina. *Neuron*.
- Medrano, C. J., & Fox, D. A. (1995). Oxygen consumption in the rat outer and inner retina: Light- and pharmacologically-induced inhibition. *Experimental Eye Research*, 61(3), 273–284.
- Meguro, M., Kashiwagi, A., Mitsuya, K., Nakao, M., Kondo, I., Saitoh, S., & Oshimura, M. (2001). A novel maternally expressed gene, ATP10C, encodes a putative aminophospholipid translocase associated with Angelman syndrome. *Nature Genetics*, 28(1), 19–20.
- Miyoshi, N., Ishii, H., Mimori, K., Tanaka, F., Nagai, K., Uemura, M., Sekimoto, M., Doki, Y., & Mori, M. (2010). ATP11A is a novel predictive marker for metachronous metastasis of colorectal cancer. *Oncology Reports*, 23(7), 505–510.
- Molday, L. L., Cook, N. J., Kaupp, U. B., & Molday, R. S. (1990). The cGMP-gated cation channel of bovine rod photoreceptor cells is associated with a 240-kDa protein exhibiting immunochemical cross-reactivity with spectrin. *Journal of Biological Chemistry*, 265(30), 18690–18695.
- Molday, L. L., Hicks, D., Sauer, C. G., Weber, B. H. F., & Molday, R. S. (2001). Expression of X-linked retinoschisis protein RS1 in photoreceptor and bipolar cells. *Investigative Ophthalmology and Visual Science*, 42(3), 816–825.
- Molday, L. L., Wu, W. W. H., & Molday, R. S. (2007a). Retinoschisin (RS1), the Protein Encoded by the X-linked Retinoschisis Gene, Is Anchored to the Surface of Retinal Photoreceptor and Bipolar Cells through Its Interactions with a Na / K ATPase-SARM1 Complex \*, 282(45), 32792–32801.
- Molday, L. L., Wu, W. W. H., & Molday, R. S. (2007b). Retinoschisin (RS1), the protein encoded by the X-linked retinoschisis gene, is anchored to the surface of retinal photoreceptor and bipolar cells through its interactions with a Na/K ATPase-SARM1 complex. *The Journal of Biological Chemistry*, 282(45), 32792–801.
- Molday, R. S., & MacKenzie, D. (1983). Monoclonal antibodies to rhodopsin: characterization, cross-reactivity, and application as structural probes. *Biochemistry*, 22(3), 653–660.
- Morth, J. P., Pedersen, B. P., Buch-pedersen, M. J., Andersen, J. P., Vilsen, B., Palmgren, M. G., & Nissen, P. (2011). REVIEWS A structural overview of the plasma membrane Na<sup>+</sup>, K<sup>+</sup> - ATPase and H<sup>+</sup> -ATPase ion pumps. *Nature Publishing Group*, 12(1), 60–70.
- Mouro, I., Halleck, M. S., Schlegel, R. A., Genevie, M., Williamson, P., Zachowski, A., Devaux, P., Cartron, J., & Colin, Y. (1999). Cloning, Expression, and Chromosomal Mapping of a Human ATPase II Gene, Member of the Third Subfamily of P-Type ATPases and Orthologous to the Presumed Bovine and Murine Aminophospholipid Translocase, 339, 333–339.
- Murphy, M. J., & Crewther, S. G. (2013). Ouabain inhibition of Na/K-ATPase across the retina prevents signed refractive compensation to lens-induced defocus, but not default ocular growth in young chicks. *F1000Research*, (0), 1–12.

- Naito, T., Takatsu, H., Miyano, R., Takada, N., Nakayama, K., & Shin, H.-W. (2015). Phospholipid flippase ATP10A translocates phosphatidylcholine and is involved in plasma membrane dynamics. *The Journal of Biological Chemistry*, *290*(24), 15004–17.
- Newton, A. C., & Keranen, L. M. (1994). Phosphatidyl-L-serine is necessary for protein kinase C's high-affinity interaction with diacylglycerol-containing membranes. *Biochemistry*, *33*(21), 6651–6658.
- Onat, O. E., Gulsuner, S., Bilguvar, K., Basak, A. N., Topaloglu, H., Tan, M., Tan, U., Gunel, M., & Ozcelik, T. (2012). Missense mutation in the ATPase, aminophospholipid transporter protein ATP8A2 is associated with cerebellar atrophy and quadrupedal locomotion. *PLoS One*, *7*(3), 281–285.
- Osada, N., Hashimoto, K., Hirai, M., & Kusuda, J. (2007). Aberrant termination of reproduction-related TMEM30C transcripts in the hominoids. *Gene*, *392*, 151–156.
- Palmgren, M. G., & Nissen, P. (2011). P-Type ATPases. *Annual Review of Biophysics*, *40*, 243–266.
- Paterson, J. K., Renkema, K., Burden, L., Halleck, M. S., Schlegel, R. A., Williamson, P., & Daleke, D. L. (2006). Lipid Specific Activation of the Murine P 4 -ATPase Atp8a1 (ATPase II) †, 1(ATPase II), 5367–5376.
- Paulusma, C. C., & Elferink, R. P. J. O. (2010). P4 ATPases--the physiological relevance of lipid flipping transporters. *FEBS Letters*, *584*(13), 2708–16.
- Paulusma, C. C., Folmer, D. E., Ho-Mok, K. S., de Waart, D. R., Hilarius, P. M., Verhoeven, A. J., & Oude Elferink, R. P. J. (2008). ATP8B1 requires an accessory protein for endoplasmic reticulum exit and plasma membrane lipid flippase activity. *Hepatology (Baltimore, Md.)*, *47*(1), 268–78.
- Paulusma, C. C., Groen, A., Kunne, C., Ho-Mok, K. S., Spijkerboer, A. L., Rudi De Waart, D., Hoek, F. J., Vreeling, H., Hoeben, K. A., Van Marle, J., Pawlikowska, L., Bull, L. N., Hofmann, A. F., Knisely, A. S., & Oude Elferink, R. P. J. (2006). Atp8b1 deficiency in mice reduces resistance of the canalicular membrane to hydrophobic bile salts and impairs bile salt transport. *Hepatology*, *44*(1), 195–204.
- Prezant, T. R., Chaltraw, W. E., & Fischel-Ghodsian, N. (1996). Identification of an overexpressed yeast gene which prevents aminoglycoside toxicity. *Microbiology*, *142*(12), 3407–3414.
- Puts, C. F., & Holthuis, J. C. M. (2009). Mechanism and significance of P4 ATPase-catalyzed lipid transport: lessons from a Na<sup>+</sup>/K<sup>+</sup>-pump. *Biochimica et Biophysica Acta*, *1791*(7), 603–11.
- Raju, T. S., Briggs, J. B., Chamow, S. M., Winkler, M. E., & Jones, A. J. S. (2001). Glycoengineering of Therapeutic Glycoproteins: In Vitro Galactosylation and Sialylation of Glycoproteins with Terminal N -Acetylglucosamine and Galactose Residues, 8868–8876.
- Ray, N. B., Durairaj, L., Chen, B. B., McVerry, B. J., Ryan, A. J., Donahoe, M., Waltenbaugh, A. K., O'Donnell, C. P., Henderson, F. C., Etscheidt, C. A., McCoy, D. M., Agassandian, M., Hayes-Rowan, E. C., Coon, T. A., Butler, P. L., Gakhar, L., Mathur, S. N., ... Mallampalli, R. K. (2010).

- Dynamic regulation of cardiolipin by the lipid pump Atp8b1 determines the severity of lung injury in experimental pneumonia. *Nature Medicine*, 16(10), 1120–1127.
- Reid, S. N. M., Akhmedov, N. B., Piriev, N. I., Kozak, C. A., Danciger, M., & Farber, D. B. (1999). The mouse X-linked juvenile retinoschisis cDNA: Expression in photoreceptors. *Gene*, 227(2), 257–266.
- Reid, S. N. M., Yamashita, C., & Farber, D. B. (2003). Retinoschisin, a photoreceptor-secreted protein, and its interaction with bipolar and muller cells. *The Journal of Neuroscience: The Official Journal of the Society for Neuroscience*, 23(14), 6030–6040.
- Roux, K. J., Kim, D. I., & Burke, B. (2013). BioID: A screen for protein-protein interactions. *Current Protocols in Protein Science*, 74, 19.23.1–19.23.14.
- Saito, K., Fujimura-kamada, K., Furuta, N., Kato, U., Umeda, M., & Tanaka, K. (2004). Cdc50p , a Protein Required for Polarized Growth , Associates with the Drs2p P-Type ATPase Implicated in Phospholipid Translocation in *Saccharomyces cerevisiae*, 15(July), 3418–3432.
- Sauer, C. G., Gehrig, A., Warneke-Wittstock, R., Marquardt, A., Ewing, C. C., Gibson, A., Lorenz, B., Jurklies, B., & Weber, B. H. (1997). Positional cloning of the gene associated with X-linked juvenile retinoschisis. *Nature Genetics*, 17(2), 164–70.
- Sebastian, T. T., Baldrige, R. D., Xu, P., & Graham, T. R. (2012). Phospholipid flippases: Building asymmetric membranes and transport vesicles. *Biochimica et Biophysica Acta - Molecular and Cell Biology of Lipids*.
- Segawa, K., Kurata, S., & Nagata, S. (2016). Human Type IV P-type ATPases That Work as Plasma Membrane Phospholipid Flippases and Their Regulation by Caspase and Calcium \*, 291(2), 762–772.
- Segawa, K., Kurata, S., Yanagihashi, Y., Brummelkamp, T. R., Matsuda, F., & Nagata, S. (2014). Caspase-mediated cleavage of phospholipid flippase for apoptotic phosphatidylserine exposure, (January), 2–7.
- Sharom, F. J. (2011). Flipping and flopping--lipids on the move. *IUBMB Life*, 63(9), 736–46.
- Sherpa, T., Fimbel, S. M., Mallory, D. E., Maaswinkel, H., Spritzer, S. D., Sand, J. A., Li, L., Hyde, D. R., & Stenkamp, D. L. (2008). Ganglion cell regeneration following whole-retina destruction in zebrafish. *Developmental Neurobiology*, 68(2), 166–181.
- Siggs, O. M., Arnold, C. N., Huber, C., Pirie, E., Xia, Y., Lin, P., Nemazee, D., & Beutler, B. (2011). The P4-type ATPase ATP11C is essential for B lymphopoiesis in adult bone marrow. *Nature Immunology*, 12(5), 434–440.
- Siggs, O. M., Schnabl, B., Webb, B., & Beutler, B. (2011). X-linked cholestasis in mouse due to mutations of the P4-ATPase ATP11C. *Proceedings of the National Academy of Sciences*, 108(19), 7890–7895.
- Simpson, Rosen, & Barondes. (1974). Discoidin, a developmentally regulated carbohydrate binding protein from *Dictyostelium discoideum*. Purification and characterization.

*Biochemistry*, 13(17), 3487–3493.

- Soupene, E., & Kuypers, F. A. (2006). Identification of an erythroid ATP-dependent aminophospholipid transporter. *British Journal of Haematology*, 133(4), 436–438.
- Stapelbroek, J. M., Peters, T. A., van Beurden, D. H. A., Curfs, J. H. A. J., Joosten, A., Beynon, A. J., van Leeuwen, B. M., van der Velden, L. M., Bull, L., Oude Elferink, R. P., van Zanten, B. A., Klomp, L. W. J., & Houwen, R. H. J. (2009). ATP8B1 is essential for maintaining normal hearing. *Proceedings of the National Academy of Sciences of the United States of America*, 106(24), 9709–14.
- Strautnieks, S. S., Bull, L. N., Knisely, a S., Kocoshis, S. a, Dahl, N., Arnell, H., Sokal, E., Dahan, K., Childs, S., Ling, V., Tanner, M. S., Kagalwalla, a F., Németh, a, Pawlowska, J., Baker, a, Mieli-Vergani, G., Freimer, N. B., ... Thompson, R. J. (1998). A gene encoding a liver-specific ABC transporter is mutated in progressive familial intrahepatic cholestasis. *Nature Genetics*, 20(3), 233–238.
- Takada, N., Takatsu, H., Miyano, R., Nakayama, K., & Shin, H.-W. (2015). ATP11C mutation is responsible for the defect in phosphatidylserine uptake in UPS-1 cells. *Journal of Lipid Research*, 56(11), 2151–7.
- Takar, M., Wu, Y., & Graham, T. R. (2016). The Essential Neo1 Protein from Budding Yeast Plays a Role in Establishing Aminophospholipid Asymmetry of the Plasma, 291(30), 15727–15739.
- Takatsu, H., Baba, K., Shima, T., Umino, H., Kato, U., Umeda, M., Nakayama, K., & Shin, H.-W. (2011a). ATP9B, a P4-ATPase (a putative aminophospholipid translocase), localizes to the trans-Golgi network in a CDC50 protein-independent manner. *The Journal of Biological Chemistry*, 286(44), 38159–67.
- Takatsu, H., Baba, K., Shima, T., Umino, H., Kato, U., Umeda, M., Nakayama, K., & Shin, H.-W. (2011b). ATP9B, a P4-ATPase (a putative aminophospholipid translocase), localizes to the trans-Golgi network in a CDC50 protein-independent manner. *The Journal of Biological Chemistry*, 286(44), 38159–67.
- Takatsu, H., Tanaka, G., Segawa, K., Suzuki, J., Nagata, S., Nakayama, K., & Shin, H. (2014). Phospholipid Flippase Activities and Substrate Specificities of Human Type IV P-type ATPases Localized to the Plasma, 289(48), 33543–33556.
- Tanaka, Y., Ono, N., Shima, T., Tanaka, G., Katoh, Y., Nakayama, K., Takatsu, H., & Shin, H.-W. (2016). The phospholipid flippase ATP9A is required for the recycling pathway from the endosomes to the plasma membrane. *Molecular Biology of the Cell*, 27(24), 3883–3893.
- Tang, X., Halleck, M. S., Schlegel, R. a, & Williamson, P. (1996). A subfamily of P-type ATPases with aminophospholipid transporting activity. *Science (New York, N.Y.)*, 272(5267), 1495–7.
- Teranishi, Y., Inoue, M., Yamamoto, N. G., Kihara, T., Wiehager, B., Ishikawa, T., Winblad, B., Schedin-Weiss, S., Frykman, S., & Tjernberg, L. O. (2015). Proton myo-inositol cotransporter is a novel  $\gamma$ -secretase associated protein that regulates A $\beta$  production without affecting Notch cleavage. *The FEBS Journal*, 282(17), 3438–51.

- Tokhtaeva, E., Clifford, R. J., Kaplan, J. H., Sachs, G., & Vagin, O. (2012). Subunit isoform selectivity in assembly of Na,K-ATPase  $\alpha$ - $\beta$  heterodimers. *Journal of Biological Chemistry*, *287*(31), 26115–26125.
- Tokhtaeva, E., Sachs, G., & Vagin, O. (2010). Diverse pathways for maturation of the Na,K-ATPase beta1 and beta2 subunits in the endoplasmic reticulum of Madin-Darby canine kidney cells. *J Biol Chem*, *285*(50), 39289–39302.
- Tolun, G., Vijayasathy, C., Huang, R., Zeng, Y., Li, Y., & Steven, A. C. (2016). Paired octamer rings of retinoschisin suggest a junctional model for cell – cell adhesion in the retina, *113*(19), 5287–5292.
- Toyoshima, C. (2009). How Ca<sup>2+</sup>-ATPase pumps ions across the sarcoplasmic reticulum membrane. *Biochimica et Biophysica Acta - Molecular Cell Research*.
- van der Mark, V. a, Elferink, R. P. J. O., & Paulusma, C. C. (2013). P4 ATPases: Flippases in Health and Disease. *International Journal of Molecular Sciences*, *14*(4), 7897–922.
- van der Velden, L. M., Wichers, C. G. K., van Breevoort, A. E. D., Coleman, J. a, Molday, R. S., Berger, R., Klomp, L. W. J., & van de Graaf, S. F. J. (2010). Heteromeric interactions required for abundance and subcellular localization of human CDC50 proteins and class 1 P4-ATPases. *The Journal of Biological Chemistry*, *285*(51), 40088–96.
- Van Harreveld, A., & Fifkova, E. (1972). Effects of metabolic inhibitors on the release of glutamate from the retina. *J.Neurochem.*, *19*, 1439–1450.
- van Meer, G., & de Kroon, A. I. P. M. (2011). Lipid map of the mammalian cell. *Journal of Cell Science*, *124*(Pt 1), 5–8.
- Vestergaard, A. L., Coleman, J. A., Lemmin, T., Mikkelsen, S. A., Molday, L. L., Vilsen, B., Molday, R. S., Dal Peraro, M., & Andersen, J. P. (2014). Critical roles of isoleucine-364 and adjacent residues in a hydrophobic gate control of phospholipid transport by the mammalian P4-ATPase ATP8A2. *Proceedings of the National Academy of Sciences*, *111*, E1334–E1343.
- Vestergaard, A. L. et al. (2014). Critical roles of isoleucine-364 and adjacent residues in a hydrophobic gate control of phospholipid transport by the mammalian P4-ATPase ATP8A2, *111*(28).
- Wang, L., Beserra, C., & Garbers, D. L. (2004). A novel aminophospholipid transporter exclusively expressed in spermatozoa is required for membrane lipid asymmetry and normal fertilization. *Developmental Biology*, *267*(1), 203–15.
- Weber, B. H. F., Schrewe, H., Molday, L. L., Gehrig, A., White, K. L., Seeliger, M. W., Jaissle, G. B., Friedburg, C., Tamm, E., & Molday, R. S. (2002). Inactivation of the murine X-linked juvenile retinoschisis gene, Rs1h, suggests a role of retinoschisin in retinal cell layer organization and synaptic structure. *Proceedings of the National Academy of Sciences of the United States of America*, *99*(9), 6222–7.
- Wetzel, R. K., Arystarkhova, E., & Sweadner, K. J. (1999). Cellular and Subcellular Specification of

- Na<sup>+</sup>, K-ATPase  $\alpha$  and  $\beta$  Isoforms in the Postnatal Development of Mouse Retina, *19*(22), 9878–9889.
- Wicky, S., Schwarz, H., & Singer-kru, B. (2004). Molecular Interactions of Yeast Neo1p, an Essential Member of the Drs2 Family of Aminophospholipid Translocases, and Its Role in Membrane Trafficking within the Endomembrane System, *24*(17), 7402–7418.
- Williamson, P. (2015). Phospholipid Scramblases. *Lipid Insights*, *8*(S1), 41–44.
- Wong, S., & Molday, R. S. (1986). A Spectrin-like Protein in Retinal Rod Outer Segments<sup>1</sup>. *Biochemical Society Transactions*, *25*, 6294–6300.
- Wu, Y., Takar, M., Cuentas-condori, A. A., Graham, T. R., Wu, Y., Takar, M., Cuentas-condori, A. A., Wu, F. Y., Takar, M., Cuentas-condori, A. A., & Graham, T. R. (2016). Neo1 and phosphatidylethanolamine contribute to vacuole membrane fusion in *Saccharomyces cerevisiae*. *Cellular Logistics*, *6*(3), e1228791.
- Xu, J., Gu, H., Ma, K., Liu, X., Snellingen, T., Sun, E., Wang, N., & Liu, N. (2010). R213W mutation in the retinoschisis 1 gene causes X-linked juvenile retinoschisis in a large Chinese family. *Molecular Vision*, *16*(March), 1593–1600.
- Xu, P., Baldridge, R. D., Chi, R. J., Burd, C. G., & Graham, T. R. (2013). Phosphatidylserine flipping enhances membrane curvature and negative charge required for vesicular transport. *Journal of Cell Biology*, *202*(6), 875–886.
- Xu, P., & Ding, X. (2007). Characterization and expression of mouse Cdc50c during spermatogenesis. *Acta Biochimica et Biophysica Sinica*, *39*, 739–744.
- Xu, P., Okkeri, J., Hanisch, S., Hu, R.-Y., Xu, Q., Pomorski, T. G., & Ding, X.-Y. (2009). Identification of a novel mouse P4-ATPase family member highly expressed during spermatogenesis. *Journal of Cell Science*, *122*(Pt 16), 2866–76.
- Xu, Q., Yang, G.-Y., Liu, N., Xu, P., Chen, Y.-L., Zhou, Z., Luo, Z.-G., & Ding, X. (2012). P4-ATPase ATP8A2 acts in synergy with CDC50A to enhance neurite outgrowth. *FEBS Letters*, *586*(13), 1803–12.
- Yabas, M., Coupland, L. A., Cromer, D., Winterberg, M., Teoh, N. C., D'rozario, J., Kirk, K., Bröer, S., Parish, C. R., & Enders, A. (2014). Mice deficient in the putative phospholipid flippase Atp11c exhibit altered erythrocyte shape, anemia, and reduced erythrocyte life span. *Journal of Biological Chemistry*, *289*(28), 19531–19537.
- Yabas, M., Jing, W., Shafik, S., Bröer, S., & Enders, A. (2016). ATP11C facilitates phospholipid translocation across the plasma membrane of all leukocytes. *PLoS ONE*, *11*(1).
- Yabas, M., Teh, C. E., Frankenreiter, S., Lal, D., Roots, C. M., Whittle, B., Andrews, D. T., Zhang, Y., Teoh, N. C., Sprent, J., Tze, L. E., Kucharska, E. M., Kofler, J., Farrell, G. C., Bröer, S., Goodnow, C. C., & Enders, A. (2011). ATP11C is critical for the internalization of phosphatidylserine and differentiation of B lymphocytes. *Nature Immunology*, *12*(5), 441–449.
- Yamamoto, T., Fujimura-Kamada, K., Shioji, E., Suzuki, R., & Tanaka, K. (2017). Cfs1p, a Novel

Membrane Protein in the PQ-Loop Family, Is Involved in Phospholipid Flippase Functions in Yeast. *G3 (Bethesda)*, 7(1), 179–192.

Zhou, X., & Graham, T. R. (2009). Reconstitution of phospholipid translocase activity with purified Drs2p, a type-IV P-type ATPase from budding yeast. *PNAS*, 106(39), 16586–16591.

Zhou, X., Sebastian, T. T., & Graham, T. R. (2013). Auto-inhibition of Drs2p, a Yeast Phospholipid Flippase, by Its Carboxyl-terminal Tail. *J Biol Chem*, 288(44), 31807–31815.

Zhu, X., Libby, R. T., de Vries, W. N., Smith, R. S., Wright, D. L., Bronson, R. T., Seburn, K. L., & John, S. W. M. (2012). Mutations in a P-Type ATPase Gene Cause Axonal Degeneration. *PLoS Genetics*, 8(8), e1002853.